Optical Outflows associated with Herbig Ae/Be Stars

by

David Corcoran B.Sc. (Hons.)

A thesis submitted for the degree of
Doctor of Philosophy

Supervisors: Prof. T.P. Ray,
Prof. D.M. Heffernan.

School of Physical Sciences,
Dublin City University,
Dublin 9,
September 1993.

DECLARATION

I hereby certify that this material, which I now submit for assessment on the programme of study leading to the award of Doctor of Philosophy is entirely my own work and has not been taken from the work of others save and to the extent that such work has been cited and acknowledged within the text of my work.

Signed: David Corcoran Date: Sept. 20th 93

David Corcoran

Contents

Abstract

Optical outflows (HH objects and jets) have only recently been found to be associated with high luminosity sources ($> 50\,L_{\odot}$) such as the Herbig Ae/Be stars. In this thesis, using deep narrow band CCD imaging, the regions about three Herbig Ae/Be stars, V380 Ori, LkHα 198 and V376 Cas, together with one high luminosity embedded infrared source Cepheus A, have been examined in detail. In most cases, these young stellar objects, have been known or have been suspected in the past to be associated with HH objects. However, each of these regions is found to be considerably more complex than previously thought with the detection of at least twenty new HH objects, many of which are examined by spectroscopy. For LkHα 198, a bright HH knot previously thought to be associated with it, is in fact, not related. This object appears to be part of an optical outflow, the source of which is a newly discovered star located 5" to the northeast. A jet is seen to emanate from LkHα 198 and the presence of these two outflows in close proximity not only explains many of the existing observations such as polarimetric measurements, but draws into question previous interpretations of the molecular outflow source and the presence of a far infrared halo about LkHα 198. For V376 Cas, a number of nearby HH emission knots are reported some of which may be associated. Perhaps one of the most remarkable discoveries, is that of a HH "loop" to the east of Cepheus A. Taken together with GGD 37, it is argued that one observes here a bipolar poorly collimated wind, orientated East–West in the plane of the sky. A similar emission line "loop" structure is also observed to the west of V380 Ori, and while it is clear that this "loop" and the molecular outflow to the east, delineate a bipolar poorly collimated wind, it is unclear whether the more distant components of the "loop" are HH or HII emission. Importantly, the presence of LiIλ6708 in the spectrum of V380 Ori, suggests that it is not a Herbig Ae/Be star but is in fact a T-Tauri star. The high luminosity of the star and the HH emission seen nearest to it, is taken as evidence of a variable poorly collimated wind, which emanates from V380 Ori and is interacting with a cavity left over from some previous outburst. A poorly collimated HH component is also seen for LkHα 198, and using all the observations made here and those collected from existing data, *it seems increasingly more obvious that optical outflows are more poorly collimated from higher rather than lower luminosity sources (e.g. the T-Tauri stars).*

Chapter 1

Introduction

1.1 Historical Background

It has been over 3 decades since Herbig proposed that a subgroup of Ae/Be stars might be young pre–main–sequence (PMS) objects. In his seminal paper, Herbig (1960) suggested that these, later to be called Herbig Ae/Be stars (henceforth referred to as HAEBESs) might be the intermediate mass counterparts of the better known T-Tauri stars. By analogy with the latter, Herbig (1960) laid down criteria by which HAEBESs might be distinguished:

1) they should have a spectral type earlier than F0,

2) they should have strong emission line spectra,

3) they should be associated with an obscured region,

4) and lastly they should illuminate nebulosity in their immediate vicinity.

Based on these criteria, Herbig (1960) originally selected 26 candidates, which was extended to 57 in the catalogue of Finkenzeller and Mundt (1984). These surveys are far from complete even in terms of sky coverage. Moreover, additional evidence for further

candidates has been found for example in the recent IRAS study of Hu *et al.* (1989).

Over two decades elapsed since Herbig's initial work with little attention being paid to these stars. What work was carried out, was largely devoted to determining whether they were genuine PMS objects. Strom *et al.* (1972) investigated by spectrophotometry a large number of these stars and found that their surface gravities were lower than those of the ZAMS and hence lay above it. This result was later confirmed by Cohen and Kuhi (1979) but challenged by Herbst *et al.* (1982) who suggested, that the location of the HAEBESs (in the Hertsprung–Russell diagram) might be better explained by young main–sequence stars rotating close to their breakup velocity. Such rotation for example was thought to place classical Be stars above the ZAMS (Collins and Sonneborn 1977). However, Finkenzeller (1985) showed that while the rotational velocities of HAEBESs were faster than T-Tauri stars, they were still significantly smaller than the breakup velocities. Moreover, it was possible from the distribution of the rotational velocities to distinguish them from both the classical Be and main-sequence A and B type stars. Finkenzeller (1985) concluded that their rotational velocities were thus further evidence of the PMS nature of the HAEBESs.

Like the T-Tauri stars, HAEBESs have infrared excesses (Cohen 1973, 1975, 1980). Such excesses can be explained through the reprocessing of stellar light by dust (Finkenzeller and Mundt 1984), although an alternative explanation in terms of free–free emission by analogy with the classical Be stars has been proposed (e.g. Lorenzetti *et al.* 1983). Finkenzeller and Mundt (1984) point out however, that in a two colour plot (H–K, K–L), there is a clear separation between the location of classical Be stars and the HAEBESs, indicating that such a process is probably not responsible for the excess in the latter. The alternative explanation, that the excess is due to dust seems more likely. As mentioned above, one of the selection criteria for HAEBESs is that they are still associated with their parent molecular cloud, as verified, for example, by the radial velocity measurements of Finkenzeller and Jankovics (1984). Moreover, given the detection in many of their near–infrared spectra of a silicate dust feature (9.7μm) (Cohen 1980), a dust origin for the infrared excesses would seem indisputable.

In brief, the location of these stars above the ZAMS, their rotational velocities, and their association with dust, make it clear that HAEBESs are indeed PMS objects as originally proposed by Herbig (1960). In the following, after considering some theoretical aspects of their evolution, it is shown that their activity probably does not derive from the star itself but more likely from accretion. For the remainder of the Introduction, two intimately related phenomena are examined i.e. both the evidence for circumstellar (c.s.) disks and outflows near HAEBESs. In addition, a review is given of what is presently known about optical outflows in general.

1.2 The Evolution of Intermediate Mass Stars: A Theoretical Perspective

Before beginning the theoretical examination of HAEBESs it is important to distinguish between two stages in their evolution namely, the protostellar and the later PMS phases. The essential difference is that the young stellar object (YSO) is only observable in the visible for the later PMS phase; the earlier protostar is surrounded by placental material which absorbs and reemits the light in the infrared. A comprehensive review of both stages of evolution is beyond the scope of this work, instead only some of the more relevant points are considered. Based upon these considerations, the possible causes of activity in the HAEBESs is then examined.

1.2.1 Stellar Evolution of HAEBESs

In the classical approach to stellar evolution, modeling of the protostar was neglected (see Stahler and Walter 1993 for a recent review). YSOs of all masses were assumed to begin life as fully convective objects contracting homologously along their Hayashi tracks. The neglect of the protostellar phase had however severe ramifications. For example the classical theory assumed that during the protostellar collapse little energy was radiated away. As a result the initial radius of the PMS star was expected to be quite large e.g. $50\,R_{\odot}$ for a $1\,M_{\odot}$ star (Hayashi 1966). This assumption has however proved to be incorrect: it is now realised that the clouds from which protostars form, contract non–homologously (Larson 1969). Consequently, the inner parts of the cloud collapse first, forming a small core which later becomes the PMS star. Material from the outer regions of the cloud, free–falls onto the core, forming a spherical radiative shock front i.e. contrary to what was originally assumed the protostar is *strongly radiative.* Indeed, numerical modeling later showed that the initial PMS stellar radius would in fact be much smaller than that assumed by classical theory e.g. $5\,R_{\odot}$ for a $1\,M_{\odot}$ star (Stahler *et al.* 1980).

An even more apparent problem with the early protostellar evolution models was their failure to predict the existence of HAEBESs. In particular the numerical collapse calculations of Larson (1972) predicted that the onset of hydrogen burning would occur in PMS stars of $> 3\,M_{\odot}$. The implication of this result was that one would not expect to see intermediate mass PMS stars above this limit. They would essentially evolve along the Main Sequence while still accreting matter. Such a result is of course completely contradicted by the observations of HAEBESs. Recently this problem appears to have been resolved, since early calculations neglected deuterium burning in the protostellar/PMS phase (Palla and Stahler 1990,1991,1992). Deuterium burning requires temperatures of 10^6K, but these temperatures can be easily achieved in the core region of the protostellar collapse (Stahler *et al.* 1980). Initially, deuterium is fed into this region through either a spherical shock front (Palla and Stahler 1991) or through an accretion disk (Palla and Stahler 1992). In either case, the temperature eventually rises to the point where the deuterium ignites and convection rapidly takes over. The mass radius relation taken from Palla and Stahler (1990) is shown in Fig. 1.1.

Palla and Stahler (1990,1991), have pointed out that at low masses ($< 1\,M_{\odot}$), the YSO radius remains small until the onset of deuterium ignition where it increases rapidly (first circle). It continues to increase as more material is deposited. Convective eddies then bring this material to the inner regions of the YSO where they ignite. At some point, gravity begins to dominate causing a contraction of the YSO radius. At the same time the inner region of the YSO becomes substantially hotter and optically thinner. At the minimum radius (second circle), this region becomes radiatively stable, initially as a subsurface layer, and then the entire region as any remaining deuterium is burned. Convection is then effectively stopped. Outside this layer, deuterium burning may also stop for a while until sufficient new material is accreted to start re-ignition. With re-ignition, deuterium burning is now confined to an outer subsurface shell with resultant convection and a swelling of the YSO. This subsurface layer then recedes towards the surface. Eventually, because of the additional mass; gravity causes the YSO to collapse until the temperature is hot enough for hydrogen to burn (third circle).

From these results the lower mass limit expected for PMS stars from earlier theories is wrong. A higher mass limit is simply a consequence of deuterium shell burning in

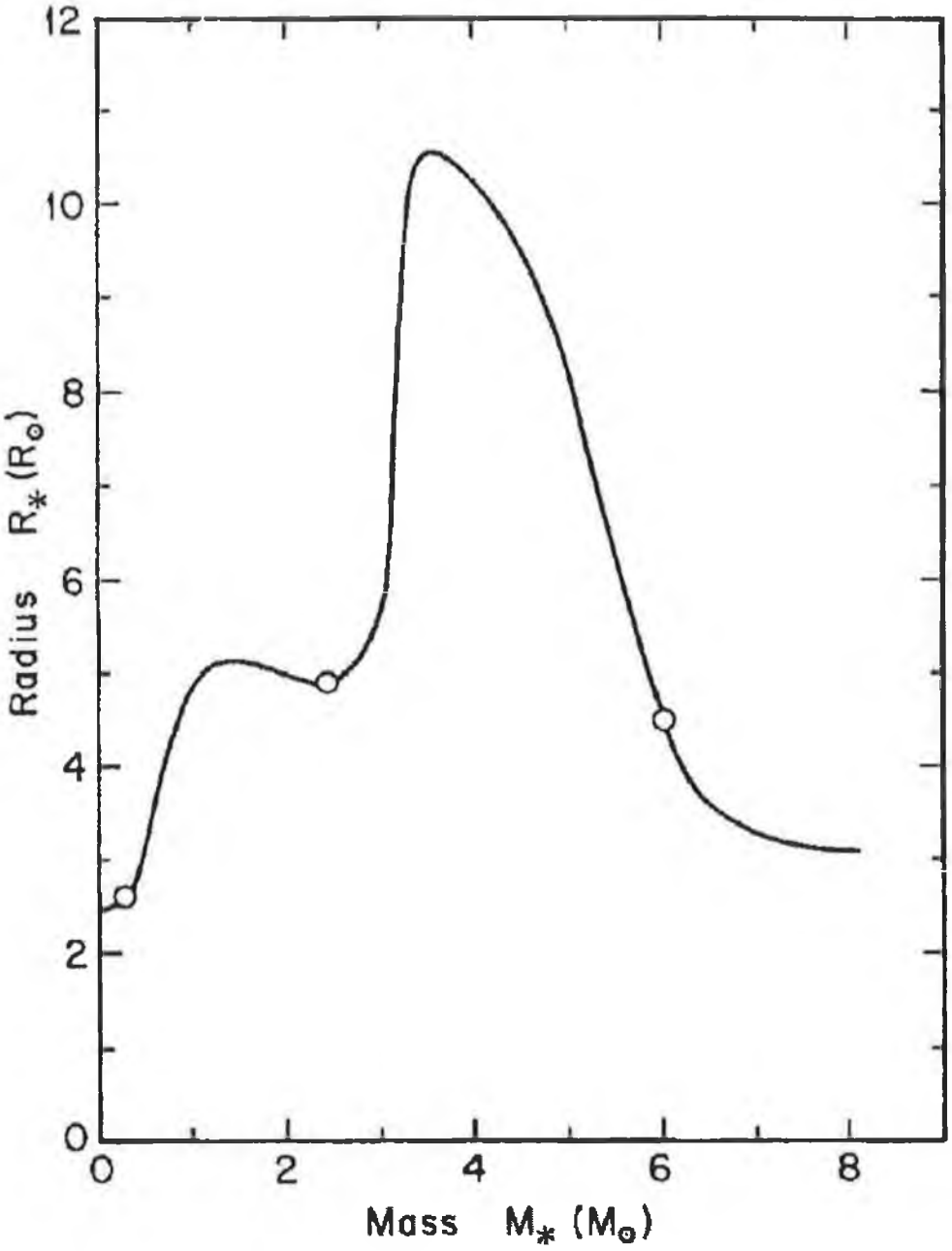

Figure 1.1: The evolution of the radius in an accreting protostar shown as a function of its mass, (taken from Palla and Stahler 1990). See text for details.

the YSO (Palla and Stahler 1991). The swelling in its radius lowers the temperature of the inner core region, and thereby allows accretion to higher masses to take place before hydrogen ignites. The most important result of the work of Palla and Stahler (1990,1991,1992) however, is that by combining their mass-radius relationship with existing evolutionary tracks (taken from Iben 1965), it was possible for the authors to determine a stellar birthline for HAEBESs. This is shown in Fig. 1.2(a), and one sees clearly that it provides an excellent upper envelope to these stars. Another consequence of this work is that the birthline joins the main sequence for a stellar mass of $8\,M_{\odot}$. This means that any protostar larger than this will never be seen as a PMS star, rather it will appear only as a main-sequence or post main-sequence object.

In their most recent contribution, Palla and Stahler (1993) have determined the evolutionary tracks of the intermediate mass stars. In particular, they only determine those portions of the tracks where the star is in its PMS stage. To consider the evolution they first define two quantities:

$$L_{rad} = L_o \times \left(\frac{M_*}{M_\odot}\right)^{11/2} \left(\frac{R_*}{R_\odot}\right)^{-1/2}$$

and

$$L_{surf} = 4\pi R_*^2 \sigma T_{eff}^4$$

The first quantity L_{rad} is a measure of the radiative energy per unit time carried by the star (here L_o is a measure of the detailed structure in the star $\approx 1\,L_\odot$), while the second quantity L_{surf} is the amount of energy a star with effective temperature T_{eff} radiates into space. Interestingly, for lower mass PMS stars L_{rad} will be lower than L_{surf}, which implies that the star loses more energy from its surface than can be supplied radiatively. As a consequence the additional energy must be supplied by convection L_{con}. For the intermediate mass PMS stars however, because of the dependence of L_{rad} on M_*, for reasonable mass values, L_{rad} will exceed that radiated from its surface. As a result the additional energy is supplied to heat a surface layer and the star is said to go through non-homologous quasi-static contraction. A further requirement that this is the case is that $L_{rad} < L_{acc}$ i.e. the accretion luminosity. The latter simply states that the Kelvin–Helmholtz time scale is greater than the accretion time scale so that the star has not

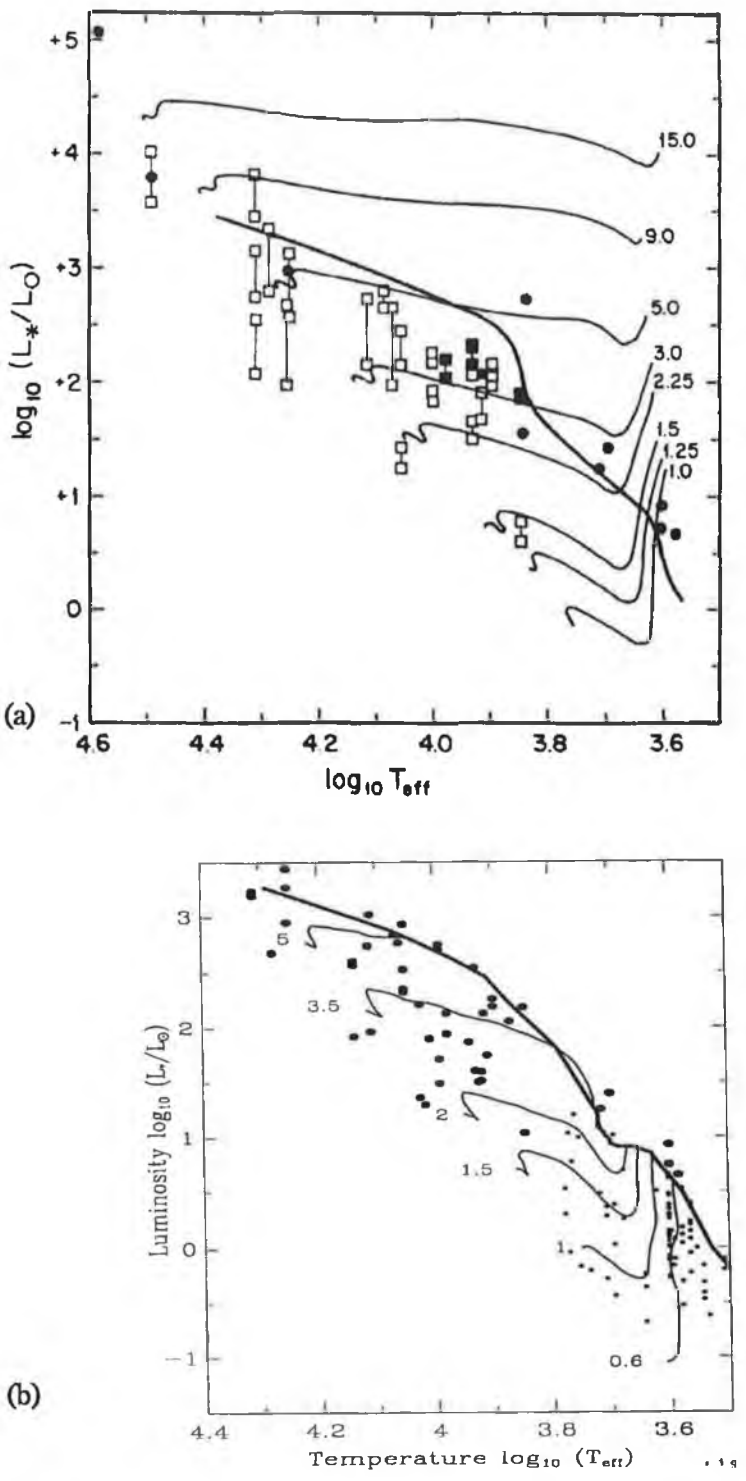

Figure 1.2: Evolutionary tracks and the location of the stellar birthline. (a) The birthline is seen to traverse the evolutionary tracks of Iben (1965). The squares represent HAEBESs and the filled symbols are molecular outflow sources (diagram taken from Palla and Stahler 1990). Note the agreement of the upper envelope of stars with the birthline. (b) The calculated evolutionary tracks of Palla and Stahler (1993). The large circles represent HAEBESs, while the smaller circles denote CTTSs.

had time to thermally relax from its accreted state. It is important to note however, that since L_{rad} depends so critically on M_*, a higher mass PMS star will violate the second condition. At this point the star will contract homologously. Such criteria set limits for the PMS stars in which convection, non-holmolguos contraction (i.e. partially convective, partially radiative) and fully radiative objects apply. The values determined for a $\dot{M}_{acc} = 10^{-5}\,M_\odot$/year model imply that:

1) PMS objects in the range $< 2\,M_\odot$ are convective,

2) PMS objects in the range between 2 and 4 $M_\odot$ are partially convective,

3) PMS objects in the range > 4 $M_\odot$ are fully radiative.

The main difference between the calculated tracks of Palla and Stahler (1993), and those of the classical theory of Iben (1965) (see Figs. 1.2(b) and (a) respectively), is that the PMS evolutionary times are shorter for the former. This is a consequence of the reduced initial PMS stellar radii (as mentioned above). Other differences are to be found in the evolution of the fully and partially convective PMS stars. While the fully convective objects essentially follow a Hayashi track to start with, those stars with mass about $2\,M_\odot$ are close to the region where a radiative core forms in the mass–radius relation of Fig. 1.1. In fact Palla and Stahler (1993) predict that a radiative core forms only after some 10^4 years, with a subsequent swelling of the star. For the partially convective stars, these start immediately in the non-homologous contraction phase, then swelling in luminosity, until after some 10^6 years they have reached a standard radiative or Henyey track.

1.2.2 Activity in HAEBESs

As will be seen here, the theoretical work of Palla and Stahler (1993) has also important implications for the line emitting regions in HAEBESs, which are a signature of their intense activity. Perhaps the best studied class of HAEBESs are those which exhibit P-Cygni profiles in one or more spectral lines. Finkenzeller and Mundt (1984) found that 20% of their sample exhibited such a property. In particular, Catala (1989) has

proposed that the similarities in the spectral lines of this P-Cygni class as a whole, allow a single star to be taken as representative of this class. The star selected was AB Aur, for which earlier modeling (Catala *et al.* 1984, Catala *et al.* 1987) implied the presence of an extended chromosphere in addition to its stellar wind.

Palla and Stahler (1990,1991) originally hypothesised that deuterium shell burning, a source of convection, might be responsible for the stellar activity in stars like AB Aur. However, Palla and Stahler (1993) now point out from their examination of the HAEBES evolution that this cannot be the case. Although surface convection lasts a substantial fraction of the PMS phase, the surface temperature during this time is simply too cool for the star to have an A or B type spectrum. This is illustrated in Fig 1.3 (taken from Palla and Stahler 1993) for a $2\,M_{\odot}$ star. In this figure, ΔM_{con} is the mass of the convective region and one sees that when ΔM_{con} is a substantial fraction of M*, T_{eff} is in the range 4000–5000K. Such temperatures would correspond to a G or K rather than an A or B spectral type. Thus, stellar evolutionary theory does not support convection as a source of activity in these stars. The question which must now be asked, is that if convection is not responsible for the observed activity in the majority of HAEBESs, what type of mechanism is?

Rotation is one possible source of energy, HAEBESs are known to rotate with intermediate velocities ($\approx 100\,km\ s^{-1}$, see Finkenzeller 1985), but as yet, it is unclear how this energy could be tapped to produce the observed activity (see Catala 1989). An increasingly more popular idea, is that magnetic activity from these stars may be responsible. Praderie *et al.* (1986) first discovered a temporal modulation of the (P-Cygni) Mg II lines in the spectrum of AB Aur. On examination, they found that this modulation was periodic with a period of 45 hours consistent with the rotation period of the star. Praderie *et al.* (1986) suggested that one was observing a rotational modulation of the stellar wind, analogous to the type that occurs in the sun. In this way, the wind from AB Aur would be governed by its magnetic field, fast streams of wind would occur along open field lines, slow streams along closed field lines (Catala 1989). Similar, rotational modulations have also been detected in HD 163296 (Catala *et al.* 1989) and HD 250550 (Catala *et al.* 1991) and explained in a similar manner.

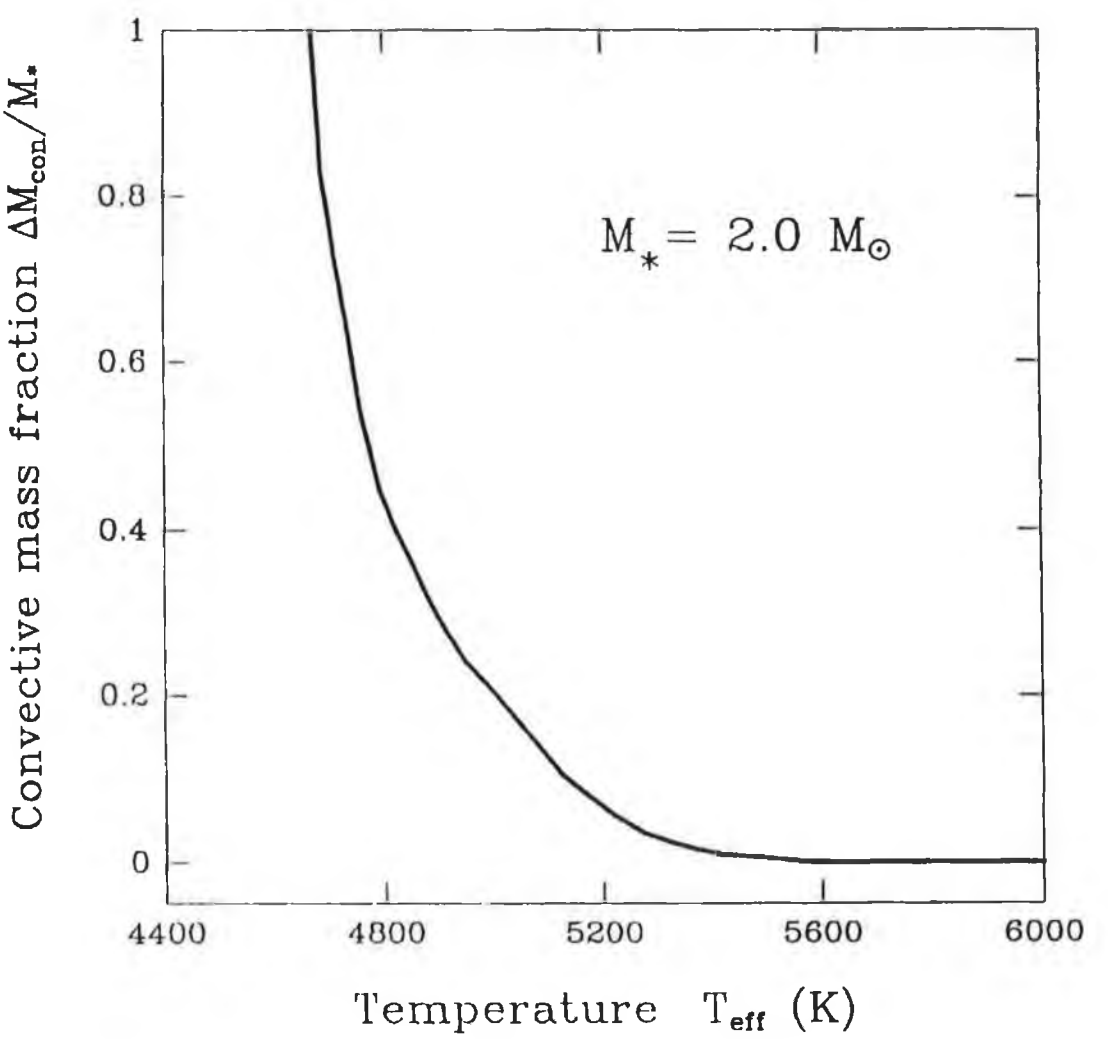

Figure 1.3: Retreat of convection for a $2\,M_\odot$ star (taken from Palla and Stahler 1990). The mass in the convection zone ΔM_{con} is seen only to be a large fraction of the stellar mass at low effective temperatures.

It is not possible as yet, to detect magnetic fields directly in stars such as the HAEBESs, rather one must rely on indirect evidence. One such indirect method is radio observations. If the radio continuum has a negative spectral index (α < -0.1 where $S_\nu = \nu^\alpha$) than its origin is almost certainly synchrotron emission. The latter process is of course directly dependent on the presence of a magnetic field. From the three stars for which rotational modulation has been observed, only one has any evidence for the presence of a non thermal radio component, namely AB Aur (Güdel *et al.* 1989). Both HD 250050 and HD 163296 are not detected (Skinner *et al.* 1993; lower limit of the detections about 0.1 mJky). Even for AB Aur, the inference of a non-thermal component is by no means certain, the spectral index derived by Güdel *et al.* (1989) is α = -0.1 ($\pm$0.7). Indeed, the results of the latest radio survey for the HAEBESs, covering a sample of 57 stars, reveals that only one of these has a definite non–thermal component (Skinner *et al.* 1993). The presence of magnetic fields is clearly not supported by the radio data for almost all HAEBESs. Moreover, contemporary theory on the origin of stellar magnetic fields requires the presence of a convective zone which, as pointed out above also seems unlikely.

With the evidence available, one sees that there are extreme difficulties in interpreting the observed activity in HAEBESs in terms of the stars themselves. One might conclude, that the responsible mechanism is either still unknown, or ultimately that it is linked to the accretion process (discussed in the next section). The problem with a global interpretation of the HAEBESs phenomenon, in terms of any one model is that it probably does not exist. This is clearly indicated by the diverse spectral emission line properties of these stars (see Hamann and Persson 1992a; henceforth HPa) and is further supported by evolutionary models (Palla and Stahler 1993). While CTTSs essentially start their PMS phase as fully convective objects, HAEBESs can begin as fully convective, partially convective or fully radiative.

1.3 Have Herbig Ae/Be Stars Circumstellar Disks?

Many of the recent studies of HAEBESs concentrate on the nature of the surrounding c.s. material. In particular, as will be shown here, there is much controversy as to whether this material is distributed in a disk, a spherical envelope, or a combination of both. Indeed, it will be shown later that even if a c.s. disk is more appropriate, there is still some question as to whether this disk is passive, i.e. that it is simply reprocessing stellar photons, or whether it is active, in that viscous accretion is taking place. The idea that c.s. disks surround HAEBESs is particularly appealing: as the higher mass analog of CTTSs, one might expect them simply to be scaled up versions of the latter, in which the presence of c.s. disks is generally accepted (see Basri and Bertout 1993).

That HAEBESs have c.s. disks similar to those surrounding CTTSs has recently been invoked by Hillenbrand *et al.* (1992) (henceforth referred to as HSVK). The principle reason for this suggestion is that both groups of stars share many characteristics, principally their spectral properties and their continuum excesses (from infrared to millimetre wavelengths). HSVK also advocates the same reasoning as originally suggested for the existence of c.s. disks about CTTSs (e.g. Myers *et al.* 1987); since the HAEBESs are generally optically visible, one can only reconcile this with their large infrared excesses if the dust responsible for the infrared excess is distributed in a disk.

The emission line properties of HAEBESs in the optical and near infrared range have been investigated by HPa. In general, the stars do appear to have hotter line emitting envelopes[1], for example, neutral species such as FeI or CaI are either very weak in intensity, or in most cases absent from their spectra. Also, the presence of NI emission is clearly indicative of a hotter type envelope, as it is generally observed in B or earlier type stars. HPa do however, point out that there are many spectral similarities between this group of stars and the CTTSs. For example, the presence of the CaIIλ8556 triplet emission is seen in over 84% of the HAEBESs, and while this is almost always seen in CTTSs it occurs less frequently in the classical Be stars (20%).

[1]The idea of a line emitting envelope which is distinct from the star was proposed by Hamann and Persson (1992b) to explain many of the broader spectral features observed in CTTSs.

The strongest similarities between HAEBESs and CTTSs spectra are found for a subgroup of HAEBESs which comprises over 30% of the total sample. HPa designate these the "outflow" sources, since they have T-Tauri like properties of outflow activity, for example, P-Cygni shaped profiles or blueshifted forbidden line emission. The similarities do not end here, both classes of stars also exhibit NaI and KI doublet emission and in addition single peaked profiles in the CaII triplet lines are frequently observed. Moreover, a peculiar pattern originally noted by HPb for the CTTSs, in the CaII triplet lines, is also seen in several of these HAEBESs. This pattern suggests particular velocity and temperature conditions common to both types of star. HPa also note that the optically thicker lines of the outflow sources e.g. Hα, generally appear widest. Although often seen in CTTSs (Hamann and Persson 1992b; henceforth HPb) this is contrary to what one finds for classical Be stars (HPa). Based on the spectral similarities, and the earlier work on CTTSs (HPb), HPa have suggested that the emission line activity of many HAEBESs is a direct result of accretion at a star/disk boundary.

The continuum excesses of the HAEBESs have been examined by HSVK, who classified the spectral energy distributions (SEDs) of these stars into one of three classes. Group I sources exhibit a decreasing slope ($\lambda F_\lambda \propto \lambda^{-3/4}$) (e.g. Fig. 1.4(a)) and comprise over 60% of their sample. HSVK found that group I sources were indeed, well modeled with the assumption of a geometrically thin but optically thick c.s. disk. However, such a model requires the presence of a hole or optically thin region in the disk, extending from the star to distances between 3 and 25R_*. Such a region is necessary to explain an absorption dip between 1 and 2μm seen in almost all of the Group I SEDs and its existence has been recently criticised (see Hartmann *et al.* 1993 for details). To check for possible reprocessing disks and to determine the accretion rate ($\dot{M}$), HSVK identified the contribution of accretion to the SEDs. They found that out of their sample of 30 Group I sources, 23 showed evidence of active rather than passive disks. Comparing the derived values of $\dot{M}$ for the HAEBESs with those derived from existing data on CTTSs, HSVK found that the values of $\dot{M}$ were about two orders of magnitude greater than in CTTSs (typically $10^{-5}\,M_\odot/yr$). More importantly however, they found that the accretion rate increased linearly with the stellar mass i.e. $\dot{M} \propto M_*$ (see Fig. 1.5). Thus it appears that the T-Tauri disk accretion phenomena, is simply scaled up in HAEBESs.

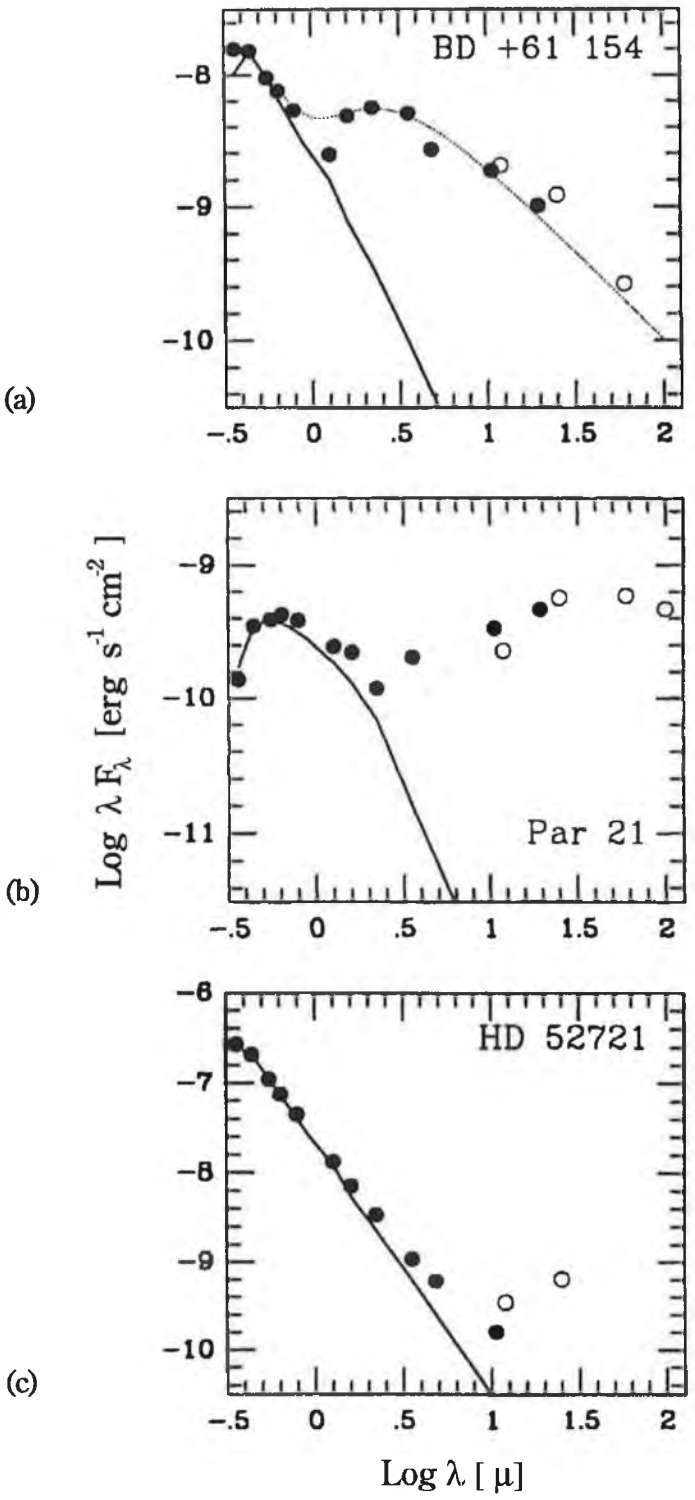

Figure 1.4: The classification scheme of HSVK for the reddening-corrected SEDs of HAEBESs. Examples are given of the (a) Group I (b) Group II and (c) Group III type sources. The meaning of the symbols and lines are as follows: solid circles are ground based observations; open circles IRAS PSC data; the solid line is the scaled SED appropriate to a corresponding main sequence star of identical spectral type; and the dashed line shown in (a) represents the best fit disk model (see text).

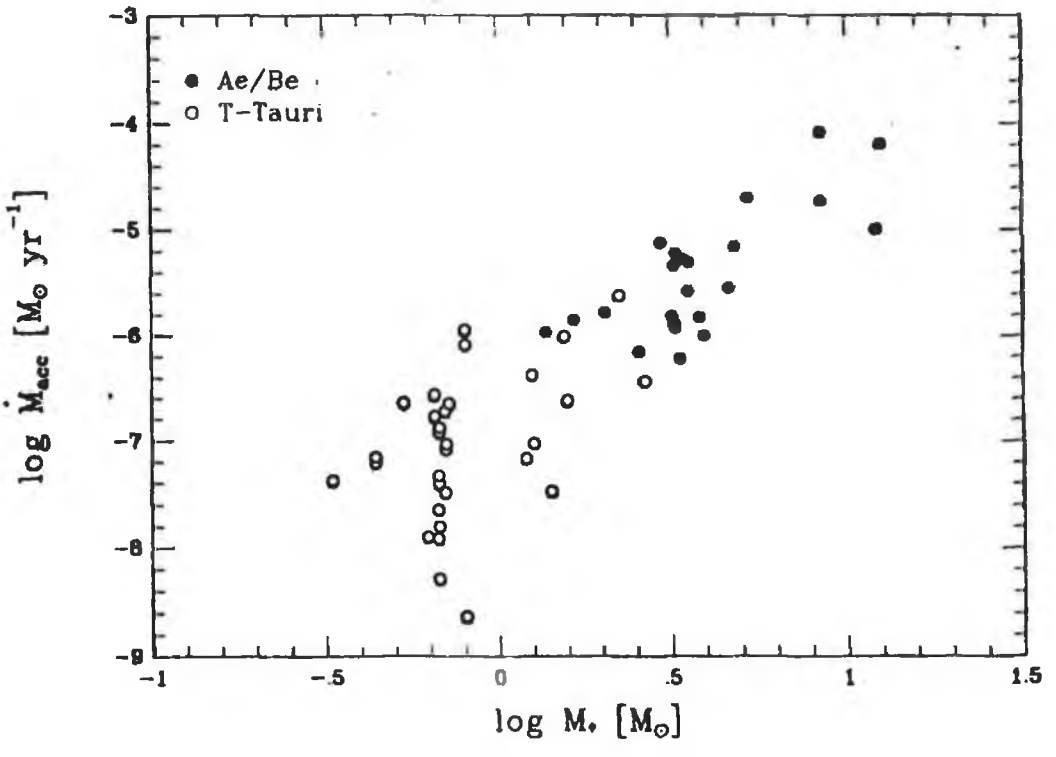

Figure 1.5: Mass accretion rate as a function of stellar mass for HAEBESs and T-Tauri stars (taken from HSVK), which indicates that accretion rates are higher among disks surrounding higher mass stars.

The Group II sources envisioned by HSVK, comprise some 11 stars or approximately 25% of their sample. These are thought to be a much less homogenous set of objects compared to Group I, and are generally characterised by a flat or steeply rising infrared spectrum (see Fig. 1.4(b)). Both HSVK and a study of similar objects by Hamann and Persson (1992c) (henceforth HPc), have suggested that many of these sources are not observed directly but viewed through scattered light. This is most apparent in the way that many Group II sources lie *below* the ZAMS in a H–R diagram, i.e. the derived stellar luminosity is too low as the extinction correction for these stars has been underestimated (see HPc). The additional extinction must then arise from a local envelope of material. Evidence for the presence of surrounding material can be found from the higher intrinsic polarisations of Group II objects; these are much larger (>5%) when compared to Group I objects (P< 2%) where the star is expected to be observed directly (HSVK). A Group II spectrum may also be incorrectly assigned to a HAEBES if there is a nearby heavily obscured infrared companion (HSVK, HPc). This, as will be shown in the course of this work, bears particular relevance to the Group II object LkHα 198 (see Chapter 4).

Natta *et al.* (1992) and Natta *et al.* (1993) (henceforth NPBEH) have examined independently sources, where the SED in the infrared is flat or rising i.e. Group II objects. To model the SED of these sources the presence of a surrounding envelope of material is invoked. This is necessary to interpret the resolved and apparently spherical distributions of far–infrared emission (50 and 100μm), in addition to the shape and magnitude of the far–infrared excess in the SED. However, although an envelope distribution of material provides a good fit to the far infrared excess, it fails in the near–infrared regime (see Natta *et al.* 1992). To fit the near infrared excess, NPBEH require the presence of a c.s. disk. Thus, a model seems necessary, where in addition to a star/disk system there is also the presence of a surrounding spherical c.s. envelope. Such a model was also proposed by HSVK for these sources.

For both Group I and Group II objects the presence of a disk seems plausible. A question which must be raised however, is what fraction if any of the infrared luminosity is derived from accretion. It has already been mentioned that HSVK estimated that at least 23 out of the 30 Group I objects possess active accretion disks. Contradicting this,

HPc have suggested that almost all HAEBESs, have in fact reprocessing disks. These diverging views arise from the different choices of the maximum possible contribution of reprocessed stellar light to the infrared excess. Only an infrared excess substantially above this maximum would be likely to have an accretion origin. HSVK adopt a maximum contribution for the reprocessed stellar light of $0.25L_*$ which corresponds to the observation of a pole on reprocessing disk (Adams *et al.* 1987). A more cautious view is taken by HPc, who allow for the possibility of flared disks (Kenyon and Hartmann 1987). For such a disk, viewed pole on, the fraction of reprocessed stellar light could in fact be $0.86L_*$.

Unless the geometry of the disk is known it is not possible to determine whether accretion or reprocessing is more likely. NPBEH are unsure for similar reasons on the origin of the near–infrared excess in the disks of Group II objects. In principle, they suggest that if L_* is well known it would be possible to distinguish whether reprocessing or accretion is responsible. However, L_* depends on the spectral type and extinction which in most cases is not well known (see Hartmann *et al.* 1993 for example). Indeed, a comparison between HSVK and HPc reveals that their estimates of L_* can vary by orders of magnitude. NPBEH conclude that until accurate estimates of L_* are available it will not be possible to determine whether disks around HAEBESs are active or passive.

Lastly, one must mention the Group III sources of HSVK, which show only small infrared excesses (see Fig. 1.4(c)), and which the authors suggest maybe the HAEBE analog of the weak line T-Tauri stars (WTTSs) (Bertout 1989). In number, group III objects are only six or 10% of the total HSVK sample. Two of these, HD 52721 and HD 53367, are attributed by HPa, to have spectral properties most like those of the classical Be stars. In particular, they are both early B type stars, with the absence of lower ionisation species like FeI, NaI, and weak or absent CaII triplet emission. Indeed in HPc, the small infrared excesses are suggested to be the result of ionised disks typical of classical Be stars and a similar conclusion is drawn by HSVK. However, not all of the Group III objects are likely to be classical Be stars owing to their association with molecular clouds and reflection nebulosities.

1.4 Outflows

Nearly 3 decades ago, it was found that many young stars lose a substantial amount of their mass through energetic winds. Kuhi (1964) inferred the presence of these winds on the basis of P-Cygni profiles in several CTTSs. Assuming that the winds are spherical, he estimated the mass loss rates to be between 10^{-7} and 10^{-9} $M_{\odot}$/year with velocities of several hundred kilometres/second. Although, the contemporary work of Herbig (1960) also revealed the presence of P-Cygni profiles in the HAEBESs, it was more than ten years later before their mass loss rates were estimated (between 10^{-6} and $10^{-8}\,M_{\odot}$/year by Garrison 1978). Such a delay probably reflects the historical bias towards interest in the CTTSs (a point that will be returned to again).

Further manifestations of the outflow phenomenon amongst young stars, were found in the subsequent studies of wind/environment interactions. These interactions, which often occur on dimensions comparable to the molecular cloud, can be seen for example in the large scale molecular outflows (Bachiller and Gómez-González 1992) and illuminated reflection nebulae (Neckel and Staude 1990). Of interest here however, is the visually remarkable Herbig–Haro (HH) objects and jets, also referred to as optical outflows. These outflows are generally regarded as tracing the highest collimated component of the stellar wind (see Edwards *et al.* 1993 for example) and in the following, an overview is given of their observational properties and current theoretical explanations. In particular, one of the most recent discoveries is considered, in that optical outflows are not only associated with lower luminosity sources ($L_{*} \leq 100\,L_{\odot}$), but also with their higher luminosity counterparts (typically $L_{*} \geq 1000\,L_{\odot}$).

1.4.1 Observational Properties of Optical Outflows: Herbig–Haro objects and Jets

It was over 40 years ago, while surveying Hα emission line stars in Orion, that a chance detection of some nebulous condensations led to the discovery of the first HH objects, (Herbig 1951 and Haro 1952). Although it was quickly realised that these objects were associated with star formation, their origin was not understood. A major clue was the

discovery that their emission line spectra were similar to those of supernova remnants. It was this similarity that led Schwartz (1975) to suggest that HH objects would arise from shock excitation, due to the interaction of a supersonic stellar wind with its surroundings. Nowadays, it is well established that the origin of HH emission is indeed radiative shocks, although the exact details of this mechanism are still being considered. In principle there are four different scenarios; 1) the cavity type model (Canto 1980), 2) the shocked cloudlet model (Schwartz 1978), 3) the interstellar bullet model (Norman and Silk 1979) and 4) the jet model (Mundt 1985). Which of these models is most applicable depends of course on the observational properties of the HH objects, but as HH emission is just shocked emission no unique model *need* apply.

Properties: Morphology of HH objects

The morphology of the HH objects are in general wide and varied, from the complex structure of knots and condensations comprising HH 2 (Herbig and Jones 1981), to the rather isolated and diffuse features of HH 64 (Reipurth and Graham 1988). Yet, from early on it was recognised that many HH objects form in close associations indicating a directed outflow e.g. HH 7–11 (Herbig 1974). Such associations were later to become more obvious with the advent of CCD imaging (Mundt *et al.* 1983) and were interpreted in terms of jet models. Indeed, it was found that in many cases, what had originally been considered as an isolated HH object was in fact just the brightest knot in a jet (Mundt *et al.* 1984 and Ray 1987). In addition to these jets, there are also collimated outflows (Mundt *et al.* 1988). In both cases, they possess a knotty elongated structure with a HH spectrum, but the distinguishing factor is their length to diameter ratio: for jets L/D $\geq$ 5 while collimated outflows have 2 $\geq$ L/D $\leq$ 5. Good examples of each are the HH 34 Jet (see Fig. 1.6(a) and (b)) and the collimated outflow from DG Tau (see Fig. 1.7). In the following however, because of their many similarities, no distinction will be drawn between these two phenomena and the terms jet and collimated outflow will be used interchangeably.

It is possible to use HH 34 to highlight some of the more common properties attributed to collimated outflows (see Mundt 1988 and Edwards *et al.* 1993). Many are known

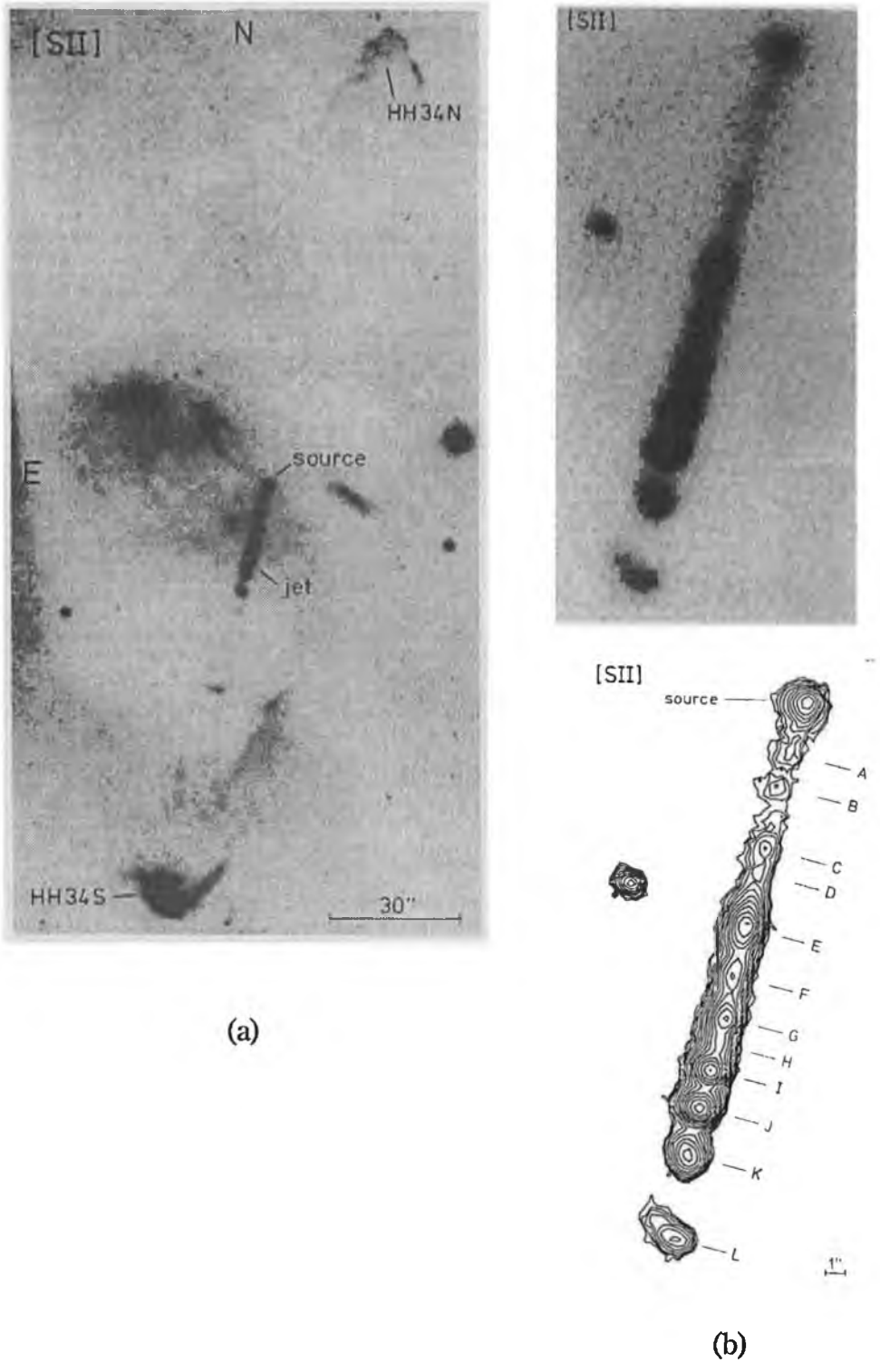

Figure 1.6: (a) A [SII] image of the HH 34 region (taken from Mundt 1988). A knotty jet points towards HH 34S and both this object and HH 34N are bow shaped. (b) A [SII] image and contour plot revealing in greater detail the HH 34 jet. Note its linearity and the quasi-periodic spacing of its knots.

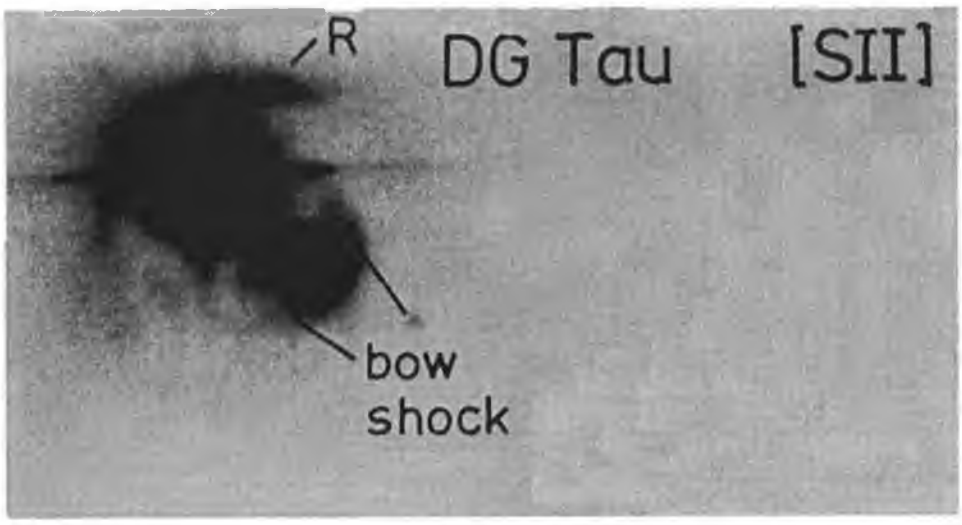

Figure 1.7: A [SII] image of DG Tau (taken from Mundt 1988), which is an example of a collimated optical outflow.

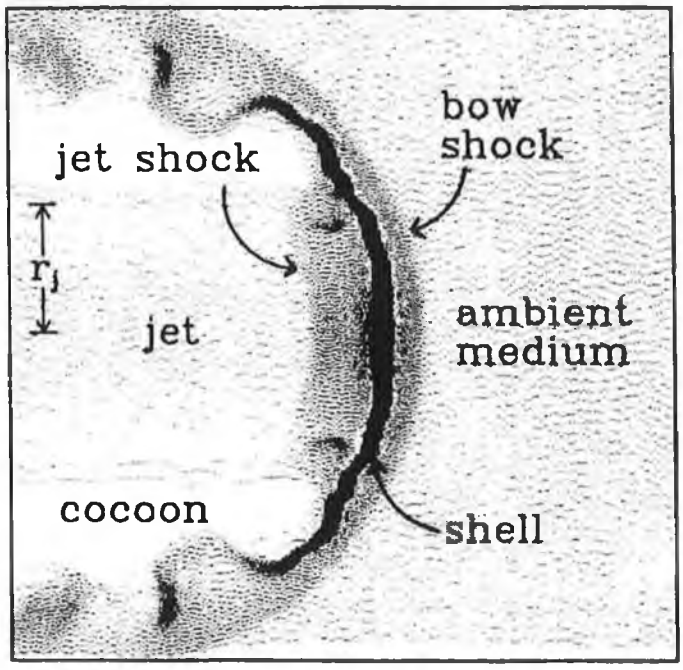

Figure 1.8: The working surface of a radiatively cooled jet (Blondin *et al.* 1989).

to terminate in bow-shaped objects, good examples of which are HH 34S and HH 34N (see Fig. 1.6(a)). The HH 34 outflow is clearly bipolar as are almost half of all known optical outflows from YSOs. Where only one component is seen, it is the blueshifted side which is normally observed. Moreover, although the HH 34 outflow is bipolar, a jet is only seen to one side and as expected it is blueshifted. The most probable reason the redshifted or receding part of an outflow is not observed is because of obscuration by the surrounding cloud. Another interesting property of the HH 34 jet is the almost collinear quasi-periodic spacing of its knots (see Fig. 1.6(b)). Some jets wiggle from side to side e.g. HH 46/47 (Raga and Mateo 1987), and the knot spacing can be irregular e.g. RN0 43N (Ray 1987). Lastly, if one examines the opening angle of the HH 34 jet it is found to be only some 2° (Mundt *et al.* 1988). In contrast, Raga *et al.* (1991) and Mundt *et al.* (1991) have shown that for a sample of 15 YSOs, the "initial" opening angle close to the source ($\approx$ 100 A.U.) is usually much larger (several tens of degrees); only further from the source ($\approx$ 1000 A.U) does the degree of collimation increase. This suggests that the large scale local environment plays a part in the collimation of optical outflows.

Properties: Kinematics and Excitation

While the emphasis has so far been on the morphological properties of HH objects and jets one must also consider the origin of the shocked emission. Before doing this it should be remarked that HH emission can be distinguished from HII emission in a relatively straightforward manner. In general for those HH objects associated with low luminosity sources (1–100 $L_\odot$), it is unlikely that any HII regions will be present. Moreover, a comparison of the shock excited and HII emission spectra, reveals the presence of substantially lower ionisation species in the former. For example, while [OI]$\lambda\lambda$6300,6363 is often seen in HH objects, oxygen exists almost entirely in its first ionisation level in a HII region. One must also distinguish between two broad classes of shocked HH emission, namely those of high excitation and low excitation. A good indicator, is the ratio of the Hα and the [SII]$\lambda\lambda$6716,6731 line strengths i.e. Hα/[SII]λ6716+6731. For a typical low excitation shock this ratio is 0.5, while for a high excitation shock a value of 2.5 is more appropriate (see Schwartz 1983). That different excitations exist is a result of

varying shock velocities, with high excitations found for high shock velocities and vice versa for low excitations (for example Raymond 1979). Another important quantity is the [SII]λ6716/[SII]λ6731 line ratio, from this one can determine the electron densities in the postshock cooling region (typical values 400–2000cm^{-3}). Such a diagnostic is necessary to calculate parameters for the optical outflows, such as mass loss rates (0.05–2×10^{-8} $M_\odot$/year; but see below), kinetic luminosities (0.01–0.2 $L_\odot$) and also to look for density changes in the outflow (see Mundt *et al.* 1987).

Comparing the kinematics of the HH objects with the properties of the shocked emission leads to some important conclusions for HH objects and their associated optical outflows. In particular, Mundt *et al.* (1988) has shown from statistical arguments for low luminosity sources, that the mean radial velocities of the optical outflows are in the range of 100–150 km s^{-1}. The flow speeds are closer to 200–400 km s^{-1}, a result which has been recently confirmed by proper motion studies (Eislöffel and Mundt 1993). It is particularly interesting therefore that with such high flow velocities, the emission line spectra of many knots in the jet are characteristic of low excitation shocks (Edwards *et al.* 1993). Indeed, the small velocity dispersions typically found for these knots (10–100 km s^{-1}) are also indicative of low shock velocities (Mundt 1988). Such a result implies that the shock fronts cannot be perpendicular to the flow direction, but must instead be oblique (Mundt 1988, Edwards *et al.* 1993). In contrast, the characteristics of the bow–shocks are considerably more complex. In particular a range of excitation values are found, with high excitations detected towards the apex and lower excitations both in the wings and the bow-shock tail. A good example of this is HH 34S (Bührke *et al.* 1988). Moreover, the velocity dispersions for the bow shock are generally much broader than those of the knots in the optical outflow (100–200 km s^{-1}).

1.4.2 Theoretical Aspects of Optical Outflows

Understanding the Bow shock

The bow shock, is part of what Blandford and Rees (1974) termed the "working surface" of a jet (Raga 1989, Ray 1993 and see also Fig. 1.8). Here, two main shocks are formed;

the bow shock where the ambient medium is accelerated, and the jet shock or Mach disk where the jet material is decelerated. Which of these shocks is most likely to be observed optically has been investigated by Hartigan *et al.* (1989). They find that the surface brightness of both shocks are likely to be comparable unless there are orders of magnitude differences in the jet and ambient density. In fact, many jets are denser than their surrounding medium, but only by factors of 1–4 (Mundt *et al.* 1988). Thus, one expects and indeed sees, both the Mach disk and bow shock in a number of cases e.g. HH 34S (Reipurth and Heathcote 1991, Morse *et al.* 1992, Eislöffel and Mundt 1992). Up to recently, in modeling radiative bow shocks it has been assumed they are driven by solid bodies, an idea similar to the earlier interstellar bullet model of Norman and Silk (1979). Examples where this rigid body approximation are used include, HH 1 (Raga and Böhm 1985;1986;1987), HH 32, GGD 37 (Hartigan *et al.* 1987) and HH 2A' (Raymond *et al.* 1988). While this approach is useful, it is nevertheless limited and numerical simulations (see below) with variable jet densities seem closer to reality.

The wide variations of excitation in a bow shock, are easiest to understand in terms of its shape (see for example Hartigan *et al.* 1987). In particular, near the head of the object, the shock front will be virtually perpendicular to the ambient material entering it, hence a high shock velocity and high excitation will result. Towards the wings, material will enter the bow surface at oblique angles giving rise to much lower shock velocities and excitations. Lower excitations will also be found behind the apex of the bow shock as the shocked gas cools. As bow shocks are optically thin, Hartigan *et al.* (1987) have shown that their spectral linewidths are a measure of their velocity. Given typical flow speeds, and that the jet is usually denser than its ambient medium, large linewidths are expected. As to the bow-shaped HH objects which are often seen to be comprised of several subcondensations, e.g. HH 1; these condensations are perhaps due to thermal instabilities or inhomogeneities in the local environment (Raga and Böhm 1987). Numerical simulations of the head of a nonadiabatic supersonic jet have been carried out by Blondin *et al.* (1989). A cool shell of material is formed behind the bow shock causing the onset of Rayleigh–Taylor instabilities. Thus, Blondin *et al.* (1989) suggest that dynamic instabilities may be responsible for the observed condensations in bow shocks.

Interpreting the Optical Outflows

In contrast, to the present understanding of bow shocks, the physics of YSO jets is far from being understood. One of the earliest models was proposed by Cantó (1980). In this, the combination of the stellar wind and a local pressure gradient resulted in the formation of a cavity. The observed jet was then simply the projection onto the sky of the shocked flow along the cavity walls. A bright shock was expected at the termination point of the jet, since the flows along the walls would eventually be forced to meet in a bright shock at the cavity apex. An extension of this model, was later proposed by Cantó *et al.* (1988). Instead of the flow terminating at the apex, the bright shock would instead collimate the flow into an over–pressurised jet (w.r.t. the ambient medium). Following this the knot structure in the flow would be formed by a series of incident and reflected (bi-conical) shocks, in a manner akin to that described by Falle *et al.* (1987). To see how this occurs one notes that the overpressurised jet initially expands to try and reduce its internal pressure to that of the ambient medium. However, in the process, it overshoots, falling below the external pressure. A shock ensues, (the incident shock) forcing the jet back towards its axis. The flow would then be reflected off the axis forming the reflected shock, and once again the flow would be recollimated into an overpressurised jet. The entire process is then repeated until pressure equilibrium is reached. In this case, each incident/reflected shock pair is associated with a knot in the jet. However, as was noted by Bührke *et al.* (1988), the predicted knot spacing from the model of Falle *et al.* (1987) is over a magnitude too large compared with observations. More importantly however, the series of incident/reflected shocks would form a stationary configuration, yet it is now known that knots within optical outflows move with velocities comparable to the jet flow speed (e.g. Eislöffel and Mundt 1992).

One of the more recent models to explain knots in jets takes account of the suspected temporal variability of optical outflows. Mundt *et al.* (1988) suggested such variability to explain the apparently short dynamical timescales (200–3000yr) of YSO jets compared to their statistically derived lifetimes ($\approx 10^4$ years). In the recent models of Raga *et al.* (1990) and Falle and Raga (1992), variability is also proposed to explain the knots in collimated outflows. Put simply if the flow speed in a jet increases to V_n, an

internal working surface arises, where the new and old flows meet. Provided V_n is not substantially greater than the old flow speed V_o, the internal shock velocity is small. Thus low excitation internal shocks can be naturally explained without the necessity of invoking oblique geometries. Moreover, the newly formed internal working surface would move with essentially the flow speed. However, while such a mechanism may explain the multiple bow shocks seen in flows like HH 111 (Reipurth 1989b) it is unclear whether it can explain the knots in all collimated outflows. Certainly, the recent proper motion studies of Eislöffel (1992) suggest that the knots do not all move at the flow speed as is required in the above model (see also Ray and Mundt 1993, and Ray 1993 for further details), in fact many only move at a fraction of this velocity (between 20 and 100%).

Another model which has achieved much attention, is the formation of knots through Kelvin–Helmholtz (KH) instabilities. Although, originally proposed for extragalactic radio jets, the model might also be applicable to stellar jets (Bührke *et al.* 1988). KH instabilities occur at the interface between flows of differing velocities and take various forms, including pinching and helical modes (Ray 1981). For supersonic flows, additional "reflecting modes" occur due to the jet acting as a type of acoustic waveguide. Cohn (1983) found that for a jet of sufficiently high Mach number (as is the case for most stellar jets) the fundamental longitudinal mode is essentially unimportant to its structure. Instead, the dominant instability is the non linear growth of higher order, reflection type modes which for pinching instabilities gives rise to bi-conical shocks along the outflow (see e.g. Payne and Cohn 1985). Such KH driven shocks have been observed in the numerical simulations of Norman *et al.* (1984) and the results agree well with both observations of knot spacings and their velocities. In particular, a range of velocities are predicted for the knots, between approximately 10 and 70% of the flow speed. However there are problems with the instability model, not least in that the growth of reflection modes might be expected to lead to an increase in knot brightness with distance from the source, contradicted for example by the observations of the HH 34 jet (Bührke *et al.* 1988). The solution may be that reflection modes rather than continually growing, saturate at some point and then decay radiatively losing large proportions of their energy to the environment (see Ray and Mundt 1993 for further details).

Origin of the Jet

An important question which must be addressed, is how do jets or highly collimated outflows originate. In particular, there is some uncertainty as to whether the star or possibly some external agent (such as c.s. disks) plays the key role. One considers first the convectively stellar wind driven models of for example Lago (1984). Indeed such models predict mass loss rates which are similar to those found for jets (see Königl and Ruden 1993, and references therein). There is however, a problem: *jets are only detected for CTTSs and not for WTTSs.* In fact, the winds from WTTSs are several orders of magnitude smaller than those of CTTSs. Since both groups of stars are regarded as being similar in their convective properties, convectively driven winds seem an unlikley source of CTTSs activity. Instead, Edwards *et al.* (1993) argue the presence of energetic winds and indeed jets are always coupled to an optically thick c.s. disk close to the star.

One must now ask, how is the disk capable of producing energetic winds and in particular optical outflows? The answer is still uncertain, but it does seem likely that it depends on viscous accretion. The observed correlation between the strength of the wind generated [OI] emission, and the near infrared excess (Cabrit *et al.* 1990) demonstrates that there is a causal relationship between the outflowing stellar wind and the mass inflow or accretion rate. This interpretation is further strengthened by the lack of correlation between the luminosities of the [OI] lines and the corresponding photospheric luminosities of the stars. Cabrit *et al.* (1990) also found that Hα and the accretion luminosities were correlated. Although, Hα is usually interpreted as a wind diagnostic, it has recently been suggested that the origin of this line may be better described as due to inflowing rather than outflowing material (Basri and Bertout 1989). In either case, accretion through a c.s. disk still seems to play a dominant role.

Finally, a few models are mentioned which describe the formation of energetic winds from accretion disks. In general, magnetic forces are thought to play a dominant role as indicated perhaps by the alignment of many optical outflows along the expected field direction (Strom *et al.* 1986). Many models invoke the presence of a shear boundary layer between a slowly rotating stellar surface and a keplerian disk (Lynden-Bell and Pringle 1974). In these cases, either thermal or magnetic forces within the shear region, drive the

stellar wind (Torbett 1984, Pringle 1989). Uchida and Shibata (1985) suggest a model similar to that of Pringle (1989) in which a winding of the magnetic field, produces a "spring–like" force normal to the disk . In both these models the magnetic fields are predominantly toroidal, other examples incorporate poloidal fields. One of these is the centrifugally driven wind (CDW) model (see Ray and Mundt 1993 and references therein). According to this scenario, magneto–gravitational contraction, results in a disk threaded by an hour glass magnetic field. Ionised material in the disk, produced by either turbulent viscosity, ambipolar diffusion, or ohmic heating, is flung out by the disk rotation but forced to move along the field lines. Safier and Königl (1992) have recently found that a CDW with an ionisation of some 10% can be maintained by ambipolar diffusion. Overall, one must remark that the abundance of existing models serves mostly to illustrate the uncertainties in the exact mechanism producing energetic winds.

1.4.3 Outflows from High Luminosity Sources

Most of the known sources of HH outflows and HH–like jets (see, for example, the catalogue of von Hippel *et al.* 1988) are either classical T Tauri stars (CTTSs) or embedded infra-red sources (EIRS) of comparable luminosity. To a large degree this is to be expected on the basis of the much longer evolutionary timescales of T Tauri stars, as compared to their higher mass counterparts. But the bias towards lower mass stars is also due to a combination of other factors, not the least being a historical concentration of observations in nearby low mass star formation regions (e.g. Taurus-Auriga, Chameleon and Lupus). In addition there are difficulties in observing HH objects in areas where intermediate mass stars form: often there are problems with background HII emission (e.g. Ray *et al.* 1990 or Poetzel *et al.* 1992) and also one has to contend with the large distances to these sources.

Despite the difficulties with such observations several optical outflows are known to be associated with high luminosity sources. Examples in the literature include V645 Cyg (Goodrich 1986, Hamann and Persson 1989; Zou 1989), R Mon (Brugel *et al.* 1984), Cepheus A (Lenzen 1988) and HH 80/81 (Rodríguez and Reipurth 1989; Reipurth

Source	Sp. Type.	L $1000\,L_{\odot}$	Dist Kpc	Proj. Length pc	$\mid V_{rad,max} \mid$ km s^{-1}	$\dot{M}$ $10^{-8}\,M_{\odot}/yr$
AFGL 2591	?	90	2.0	0.29(b)	500	40
Cepheus A	?	25	0.7	0.44(b)	475	?
				0.37(r)	80	?
AFGL 4029	?	> 20	2.2	0.14(b)	500	300
HH 80/81	?	> 18	1.7	2.4(r)	≤ 600	?
MWC 1080	B0	17	2.2	0.24(b)	300	50
R Mon	B0?	0.7	0.8	1.6(b)	75	≤ 4.3
LkHα 234	B6	1.3	1.0	0.19(b)	200	2–3
V645 Cyg	A0	50	3.5	?	450	?
HK Ori	A4	0.3	0.5	?	?	?
ZCMa	F5	3.5	1.2	1.6(b)	620	2
					345	

Table 1.1: Table of HH outflows in the literature associated with intermediate and high luminosity young stars, based on the work of Poetzel *et al.* (1992) while spectral types are taken from HPc. Notation: (b) blueshifted, (r) redshifted, and a question mark signifies uncertainty in some quantity.

1989b). In recent years two notable surveys have been undertaken of optical outflows from high luminosity YSOs. In the first which included both EIRS and the optically visible HAEBESs, several new outflows were discovered. These include AFGL 2591 and MWC 1080 (Poetzel *et al.* 1992), and jets from LkHα 234, AFGL 4029 (Ray *et al.* 1990) and ZCMa (Poetzel *et al.* 1989). The second survey was conducted by Goodrich (1993) and consists exclusively of HAEBESs, with the detection of four possible new HH objects in the near vicinity of the stars, HK Ori, BD +46 3471, BD +41 3731 and LkHα 198. Aside from LkHα 198 (see chapter 4) only one of these objects has been confirmed as a HH object, namely that associated with HK Ori. Interestingly, of the other objects it is noted that the source BD +41 3731 is quite distinctively a Group III source in the classification of HSVK. In fact its SED is characteristic of a classical Be star, a point which has previously been suggested (Herbig and Bell 1988). The association of a HH object with this star is thus extremely unlikely.

The number of high luminosity sources which are well described, and have confirmed HH emission in the literature, totals about 10 objects so far (see table 1.1). Of this sample four are EIRS, and these should not be confused with the protostars discussed earlier, rather they are most likely optically obscured HAEBESs. Of the remainder at least one, ZCMa, is in fact an FU Orionis type star (Hartmann *et al.* 1989), while the classification of R Mons is extremely uncertain due to the absence of absorption features in its spectrum (Catala *et al.* 1989). Indeed, as has been pointed out previously, there is a large uncertainty in the spectral classification of almost all HAEBESs. Nevertheless, it is worth noting that excluding ZCMa, the spectral classes range from A0 to B0 i.e. they cover the full spectral range of HAEBESs. It is also particularly interesting that excluding ZCMa, all the remaining sources are also associated with CO molecular outflows.

In section §1.4.1 a descriptions was given of the characteristics of jets and collimated outflows from the lower luminosity sources only, namely the CTTSs and their corresponding EIRS. One must now consider whether there are differences in the optical outflows between these and their higher luminosity counterparts. As expected the maximum radial velocities are some 2–3 times greater (450–600 km s^{-1} in most cases; see Poetzel *et al.* 1992 and table 1.1). Indeed, even for those exceptions which exhibit low radial velocities, namely Cepheus A, R Mon and LkHα 234; these can be attributed to projection effects resulting from motion close to the plane of the sky. Certainly this appears to be the case in LKHα 234 (Ray *et al.* 1990), and the proper motions of the associated HH object of R Mon (HH 39) are also quite high at 300 km s^{-1} (Herbig and Jones 1983). For Cepheus A see Chapter 3. In those cases where P-Cygni profiles are seen the derived wind velocities are even higher, e.g. 900 km s^{-1} for V645 Cyg (Hamann and Persson 1989).

As to their morphology, common to both the high and low luminosity outflows, are the appearance of isolated HH objects e.g in HK Ori (Goodrich 1993), jets e.g. in LkHα 234 (as mentioned above) and bow shocks e.g. in ZCMa (Poetzel *et al.* 1989). However, there is some evidence to suggest that poorer collimation may be more frequent in optical outflows emanating from higher luminosity sources. The classic example is GGD 37, a large HH complex located to the west of Cepheus A. GGD 37 which has

an arc-shaped structure is comprised of several subcondensations many of which can be interpreted as bow shocks (Hartigan *et al.* 1987). Since these individual objects cover a wide range of opening angles with respect to their presumed source, the optical outflow must be poorly collimated (see also Chapter 3). Evidence of poor collimation has also been detected in the shocked H_2 emission of AFGL 2591, (Poetzel *et al.* 1992), and for the optical outflows of V645 Cyg (Goodrich 1986) and MWC 1080 (Poetzel *et al.* 1992).

One now considers whether the same mechanism which is responsible for the optical outflows from low luminosity sources also holds for high luminosity sources. In this respect, Ray *et al.* (1991) have shown that the mass loss rate of optical outflows ($\dot{M}_{opt}$) increases with the luminosity of the YSO $L_{YSO}^{-0.6}$, over several decades from 0.1 to $2\times10^4\,L_\odot$ (see Fig. 1.9). Edwards *et al.* (1993), take this to infer a universal origin for optical outflows. Moreover, since they suggest that the source of the optical outflow is accretion for low luminosity sources, the implication is, that disk accretion is responsible for driving the optical outflows of high luminosity sources as well.

Finally one considers the relationship of optical outflows to one other large scale tracer of energetic winds namely, CO molecular outflows. Levreault (1988) found that the mass loss rate inferred from the molecular outflow data ($\dot{M}_{co}$), increased with the bolometric luminosity as $L_{BOL}^{-0.6}$, i.e in exactly the same manner as $\dot{M}_{opt}$. Edwards *et al.* (1993) have suggested that this result implies the same mechanism responsible for driving optical outflows is also responsible for driving molecular outflows[2]. An important point which must be made however, is that $\dot{M}_{opt}$ is typically some 30 times smaller than $\dot{M}_{co}$. Indeed, in this respect, Mundt *et al.* (1987) have previously compared the momentum flux of optical jets from low luminosity stars ($\dot{M}_j v_j$) and found that these were between 10–100 times smaller than the momentum rates of molecular outflows. Such a result implied that the molecular outflows could not be momentum driven by the jets but perhaps instead by neutral winds from the YSO (Lizano *et al.* 1988). In this situation the jet is only one component in a predominantly neutral wind. However, the values of $\dot{M}_j v_j$ derived by Mundt *et al.* (1987) have been questioned, and they may in fact be greatly underestimated (see Ray and Mundt 1993).

[2]It is interesting that the derived ionisation mass loss rates determined from the radio observations of Skinner *et al.* (1993) also scale in a similar manner ($\dot{M}_{ion} \propto L_{BOL}^{-0.6}$).

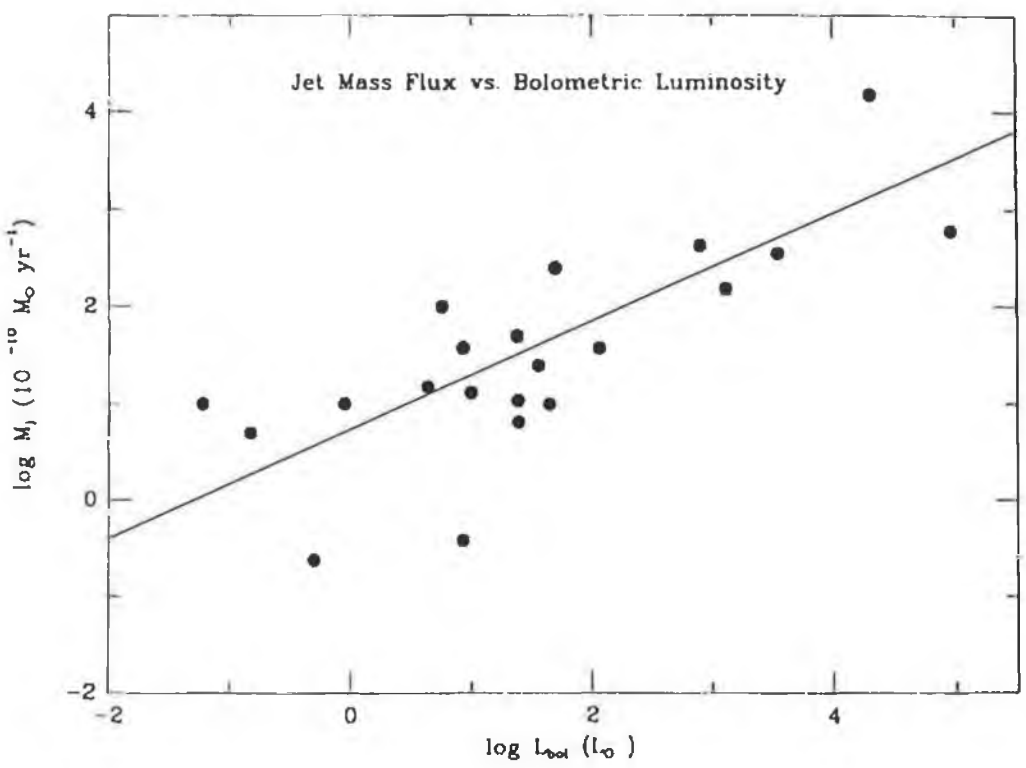

Figure 1.9: A log-plot of jet mass flux versus bolometric luminosity of the jet source. A power law of $\dot{M}_j \propto L_{BOL}^{-0.6}$ is derived from this plot (Edwards *et al.* 1993).

1.4.4 Forward

The sample of known optical outflows from high luminosity sources although increasing in number is still statistically small. Moreover, although some of their general properties such as their higher flow velocities seem to be well substantiated, other features such as poorer collimation are, at this stage only suggested by the data. In this thesis, the optical outflows in the vicinity of four high luminosity sources are examined in detail. The sample contains three HAEBESs, namely, V380 Ori, LkHα 198 and V376 Cas, and one EIRS, Cepheus A. For most of these sources possible HH emission has been suspected or known in the past. However, with the aid of deep narrow band CCD imaging, and the use of a differentiation technique for finding HH objects, one will see that each of these regions is considerably more complex than previously thought. In particular, over twenty new HH objects are detected, many of which have been studied here spectroscopically. Moreover, the morphology of the HH emission, in the case of Cepheus A, and V380 Ori shows a "loop-shaped" geometry. This geometry, it is argued reveals the presence of a poorly collimated wind. In particular, the interaction of this wind with its environment is studied in great detail in terms of existing models in Chapter 2 for V380 Ori.

For each source, an attempt is made to explain not only the observations made here, but to interpret them in terms of existing multi-wavelength studies. Indeed, for one particular case Cepheus A, which has been well-studied for almost two decades, there is still considerable controversy not least regarding the number of outflows present and their orientation. Comparison will also be made of the optical outflows from the high luminosity sources here and existing studies on low luminosity sources. In particular, one addresses such questions as whether alignments of the optical outflows occur with the magnetic field (see above), or whether one finds close associations of optical outflows as e.g. in HL Tau (Mundt *et al.* 1988). As will be seen these bear particular relevance to the HAEBESs, LkHα 198 and V376 Cas.

The layout is as follows, the outflows from individual regions are discussed separately (Chapters 2 to 4; for V380 Ori, Cepheus A, and LkHα 198/V376 Cas, respectively) and, as will be shown, many of the observed features are readily understood in terms of a poorly collimated wind. For each chapter the order is similar to a paper, starting with

an introduction to the individual objects and a description of the observations made; following this the observations are studied and finally discussed. A summary of the results is then presented in Chapter 5, together with a brief look at possible future work.

Chapter 2

The V380 Orion Region

2.1 Introduction

V380 Ori, originally listed by Herbig (1960) as a candidate intermediate mass young star, lies at a distance of 460pc and is associated with the nebulosity NGC 1999. This nebula is one of the brightest in the Lynds 1641 complex, a cloud that also contains the well known HH 1/HH 2 outflow. Herbig (1960) classified the star as having a spectral type between A0 and A2, although, he did suggest that its emission line features were more characteristic of an "advanced" T-Tauri star. More recent classifications put its spectral type anywhere between B8–A2e (see Finkenzeller and Mundt 1984, Strom *et al.* 1989, HSVK and references therein).

The total luminosity of V380 Ori has been estimated at 300 $L_\odot$ and its effective temperature at about 10^4 K (Strom *et al.* 1989). These values are however poorly known due to uncertainties in A_v and spectral type (see Hartmann *et al.* 1993). Thus for example, Berilli *et al.* (1993) suggest a value for the total luminosity of V380 Ori to be within the range 80–140 $L_\odot$. Like many young stars, V380 Ori is variable, not only in its optical luminosity (for example, Herbig (1960) refers to changes in its visual magnitude from $m_v = 9.7$ to 10.1), but also in its Hα equivalent width (Finkenzeller and Mundt 1984, and see also §2.3.4), in the near-infrared (Strom *et al.* 1989), and at X-ray

wavelengths (Mereghetti and Garilli 1987). In Fig. 2.1 an overview of the V380 Ori region is given, including most of the sources and outflows considered in this chapter.

2.1.1 NGC 1999 and its source

The reflection nebula NGC 1999 is almost symmetrically distributed about V380 Ori (see Fig. 2.1), but interestingly, located just to the west at a distance of 20", is a dark nebular patch. This dark region is triangular in shape and results in an "arc-like" appearance of the nebula at high intensities (Herbig 1960). The object has been identified as a Bok globule (see Brück 1974 and references therein). Furthermore, in the polarisation studies by Warren-Smith *et al.* (1980), there is only a marginal decrease in the polarisation of the nebula at the globule's position, which is clear evidence of their association.

It was shown by Herbig (1960), that V380 Ori is part of the NGC 1999 nebulosity for the following reasons: firstly, the spectrum of the star itself is seen reflected in the nebula, except for some minor variations in the CaII lines; secondly, the radial velocity of the HI molecular cloud (24 km s^{-1}) is close to the V380 Ori observed emission line velocity (22km s^{-1}). The latter result has been subsequently confirmed by the work of Finkenzeller and Mundt (1984) who measured the radial velocities of the hydrogen lines. In the particular case of V380 Ori, the differences between these velocities and those of the molecular cloud were small (less than 6 km s^{-1}).

Further evidence of the illumination of NGC 1999 by V380 Ori is found from the photometric observations by Brück (1974). These revealed that NGC 1999 is bluer than the central star, a characteristic of a reflection nebulosity of significant optical depth. In addition, the polarisation observations of NGC 1999 (Warren-Smith *et al.* 1980) reveal a centrosymmetric pattern, the E-vectors being aligned perpendicular to the radial directions from V380 Ori. Such a centrosymmetric pattern can be understood in terms of single scattering from an optically thin dust region about the central source (Bastien and Ménard 1988). Warren-Smith *et al.* (1980) and Warren-Smith (1983) have modeled this region and find that its polarisation pattern is consistent with V380 Ori being embedded about 0.11pc within the cloud, the surface of which is tilted by 15°.

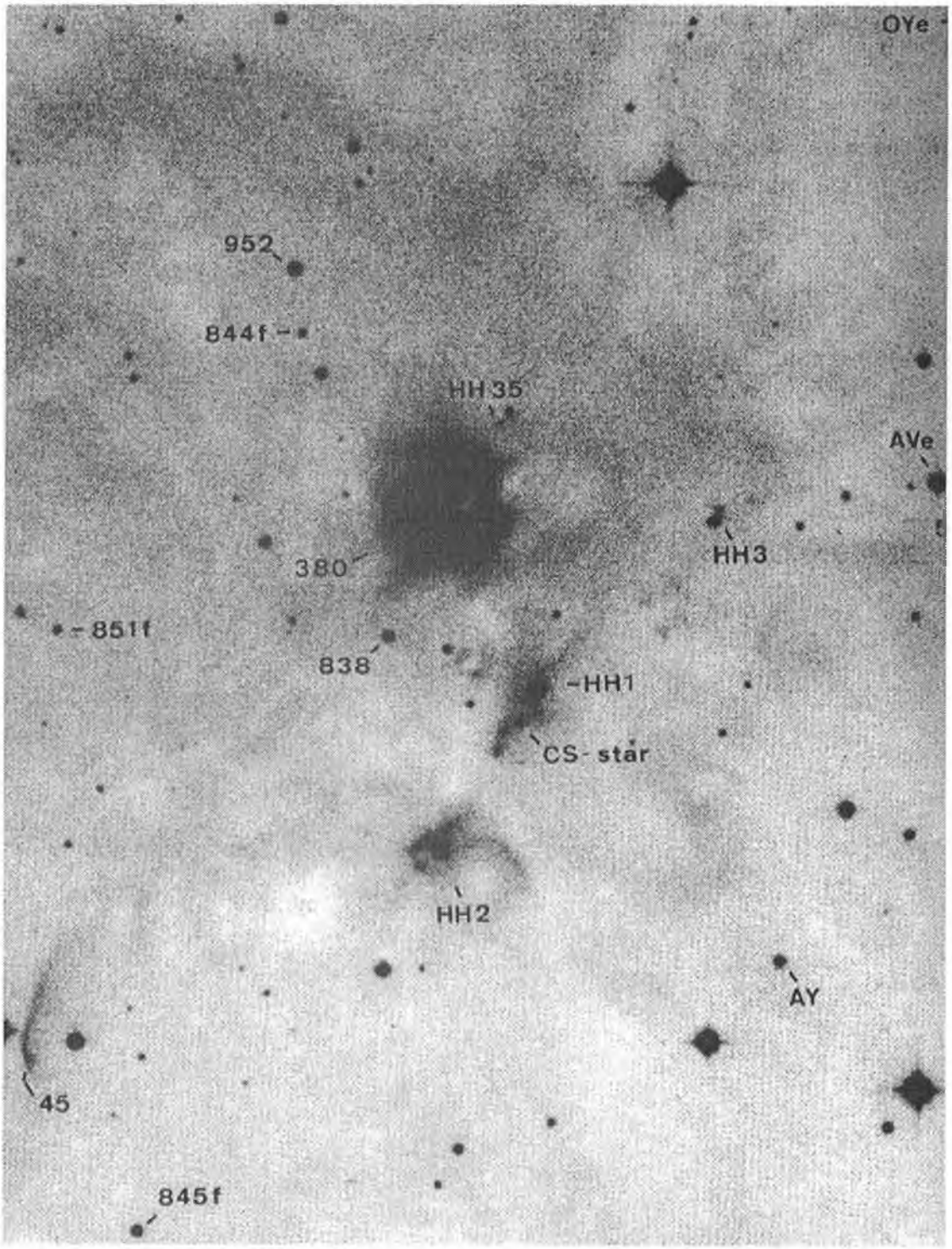

Figure 2.1: A scanned image of a deep red Schmidt–plate covering the region about V380 Ori (taken from Reipurth 1985).

2.1.2 The Spectral Energy Distribution of V380 Ori

A good review of all the photometry, from the visible to the far infrared of the V380 Ori region, can be found in Strom *et al.* (1989). The purpose of the latter was to compose SED curves for the pre-main-sequence stars in the Lynds 1641 cloud. In so doing, they grouped the stars into one of three SED types (IRAS-Classes) and these were interpreted as describing various stages of stellar evolution. For V380 Ori the SED curve is Class II i.e. it exhibits a slope which is somewhat between a flat and a blackbody curve. Strom *et al.* (1989) propose that for such an object, the star has reached the stage where it is optically visible. This is because the circumstellar envelope has been blown away, most probably, in the case of a star like V380 Ori, by a stellar wind. The luminosity of V380 Ori is then assumed to come from the photosphere at visible wavelengths (i.e. it is essentially blackbody radiation) and in the NIR to the FIR, from a disk. The luminosity of the disk will be produced by both reprocessing of stellar photons and thermal heating from accretion, although, the relative contributions of the two is uncertain. Thus, although, the total apparent luminosity calculated by Strom *et al.* (1989) for V380 Ori is $300\,L_{\odot}$, they suggest that only $125\,L_{\odot}$ is due to the star itself, the remainder arising from the disk. Indeed, in the classification of HSVK, V380 Ori is a Group I type object, i.e. best modeled by a star/disk system (see §1.1 for further details).

2.1.3 The Outflow of V380 Ori

V380 Ori is historically one of the first HAEBESs to be tentatively associated with an optical outflow. To the northeast of the star lies a bright knot of shocked emission, HH 35 (Herbig 1974) which has an extended 5" tail in the direction of the NGC 1999 nebula (see Fig. 2.1). Strom *et al.* (1985) noted that the PA of this object (with respect to V380 Ori), was close to the direction of the local magnetic field. Indeed, Reipurth (1989a) suggested that there could be a physical link between HH35 and V380 Ori because of the elongation of HH35 towards the star and their proximity. Reipurth also noted the alignment with the magnetic field. He further pointed out that this was only one of several outflows in the same region having a similar alignment, including e.g. the well known HH 1/HH 2 system.

The only other evidence of HH emission, believed to be associated with V380 Ori was discovered by Strom *et al.* (1985). This consisted of three low intensity knots located at a PA of 56° (with respect to V380 Ori) i.e. approximately at right angles to the large scale magnetic field. By tilting the interference filter, through which the objects were observed, he determined that they were all redshifted in velocity. The objects appeared brightest, when the peak transmission wavelength of the filter corresponded to a V_{LSR} of +40km s^{-1}.

In addition to the optical outflows in the region about V380 Ori, molecular outflows have also been found. The first report of such a molecular outflow was made by Edwards and Snell (1983) who detected the presence of low intensity wings in their ^{12}CO observations. These occurred at the locations of both HH 35 and HH 2 (see the next section) and they were interpreted as indicating the presence of a low velocity molecular outflow. A map revealing the overall spatial distribution of the outflow was published in a subsequent paper (Edwards and Snell 1984). An interesting feature of this map was the quantity of redshifted emission. Though blueshifted features were apparent towards the NE, and in an L-shaped structure, just south of NGC 1999, these features were much smaller in spatial extent than their redshifted counterparts. In particular, however, it was unclear whether one or more outflows were present as a result of the low sampling rate employed in producing the map.

Using a higher sampling rate, Levreault (1988) remapped the same region and found that there were at least three outflows present. In the case of V380 Ori, the molecular outflow consisted of a symmetric redshifted lobe centered on the star, indeed, most of the low velocity emission in this region was redshifted. Levreault commented that this might be expected if the outflows occurred near the edge of the molecular cloud. The most recent observations in ^{12}CO have been carried out by Morgan *et al.* (1991). In the case of V380 Ori, his results mirror those of Levreault (1988). He points out, however, that in the ^{13}CO intensity map of Bally *et al.* (1987), V380 Ori apparently coincides with a high density core.

2.1.4 Other Outflows near V380 Ori

Located to the southwest of V380 Ori (see Fig. 2.1), lies the well known optical outflow HH 1 and HH 2, which are amongst the brightest HH objects known and were discovered independently by Herbig (1951) and Haro (1952). HH 1 lies to the northeast and HH 2 to the southwest of what was once thought to be their source, the Cohen-Schwartz star (Cohen and Schwartz 1979). Herbig and Jones (1981) measured their proper motions and found they were moving in almost exactly opposite directions at high tangential velocities $\leq 350\,\mathrm{km\ s^{-1}}$. These measurements, coupled with their known low radial velocities (see for example Mundt *et al.* 1987), indicate that the HH 1/HH 2 optical outflow is almost in the plane of the sky.

Reports of any other optical outflows in the immediate vicinity of V380 Ori are quite small. In Fig. 2.1 HH 3 is apparent, (see Ray 1987) but it is not within the observations made here and is omitted from further discussion. Also apparent but not labelled is HH 36, it is situated less than 1' northeast from a star listed as V851f by Reipurth (1985). Herbig (1974) describes it as having a bow shaped structure, with its northern tip being the brightest feature. The remaining object is Reipurth 45. In Fig. 2.1 this object appears as an arc-shaped feature which he suggests could be two jets originating from a common point. The HH nature of this object has been confirmed by Ogura and Walsh (1991) and independently here during the course of this work (henceforth it will be referred to as HH 130). Ogura and Walsh (1991) show that it has a low shock velocity (85 km $\mathrm{s^{-1}}$) and that there is low interstellar extinction towards it. As there are no nearby IRAS PSC sources, the nearest being 7' away near HH 1 and HH 2, they suggest that HH 130 may be related to this system, in particular HH 2. Of the other optical outflows detected so far, Strom *et al.* (1985) has suggested that there maybe an outflow almost coincident with the HH 1/HH 2 system, the source of which is the Cohen-Schwartz star. As yet, this has not been verified in the literature. Reipurth *et al.* (1993) do however, report the discovery of a separate optical outflow to the west of the HH 1 jet (labelled HH 144 and 145). Many of these outflows, and some new ones will be considered in §2.4.

One of the newly discovered outflows (see §2.4.1) is associated with an infra-red source originally detected by Nakajima *et al.* (1986), the optical counterpart of which

was identified by Strom *et al.* (1989) and referred to as N^3K50. The pre-main sequence nature of this star has also been independently discovered here. Strom *et al.* (1989), identified N^3K50 as an IRAS-Class I object i.e., the SED has a steeply rising slope. Such an SED curve indicates that the star is only in the initial stages of its evolution and is still heavily embedded within dust. Strom *et al.* (1989) also examined the optical spectrum of N^3K50 and found that it exhibited strong Hα and [OI] emission. The authors classified the star as T-Tauri like with a spectral type G5-G7 and a derived bolometric luminosity of 30 $L_\odot$. This star is examined in detail in §2.4.1.

2.2 Observational Details and Data Reduction

2.2.1 Direct Imaging

Optical imaging of V380 Ori and its surrounding regions was made on two separate occasions in 1991, at La Silla in Chile. These observations were carried out using the 3.5m New Technology Telescope (NTT) in February, and with the 2.2m ESO/MPI telescope in December. V380 Ori was also imaged with an infra-red array in December of the same year, at the United Kingdom Infra-red Telescope facility (UKIRT).

The NTT observations were made using the direct imaging configuration of the ESO Multi-Mode Instrument (EMMI). They consisted of essentially two regions observed in both a narrow band [SII] filter (λ_c = 6730Å, $\Delta\lambda$ = 48Å) and a broad band I filter (λ_c = 8800Å, $\Delta\lambda$ = 2400Å). The first of these regions was centered on V380 Ori, and the second, containing the well known HH 1 / HH 2 system and the lesser known HH 130, was centered approximately 5.5' to the southeast. The detector employed was a 1024×1024 Thompson CCD with a pixel size of 19 μm^2 and an associated plate scale of 0.44" per pixel. This implies a field of view of 7.5' × 7.5' and consequently, it was just possible to observe most of the HH 1/HH 2 system and HH 130 at the same time. When imaging the region around V380 Ori, the central star was masked with a coronographic spot, thus allowing examination of possible nearby HH emission. The mounting of the spot plate caused vignetting and this reduced the field of view to 4' ×7.5'. Exposure times for the [SII] frames were 2400s for the image centered on V380 Ori and 1200s for the image located to the southeast; the seeing was measured at 1.2" and 1.4" respectively. In both cases the corresponding I band images had exposure times of 300s, with seeing of 1.3" and 1.7".

To compliment the NTT observations, imaging was conducted using the EFOSC 2 instrument on the ESO/MPI 2.2m telescope. Again the detector was a 1024×1024 Thomson CCD, but in this case the plate scale was smaller at 0.33" per pixel. This resulted in a field of view of 5.6' × 5.6' with V380 Ori located near its center. Two images were made, both through narrow band filters, one centered on Hα (λ_c = 6570Å,

$\Delta\lambda = 61$Å), the second centered on the nearby red continuum; the latter will henceforth be referred to as the r_{nc} filter ($\lambda_c = 6822$Å, $\Delta\lambda = 74$Å). Exposure times for these observations were 1800s and 600s respectively, while the corresponding seeing was 1.4" and 1.6".

Data reduction for the above observations was done in the usual manner using the Munich Imaging Data Analysis System (MIDAS). The purpose of the imaging was to examine the neighborhood of V380 Ori for the presence of HH emission. It is well known that HH objects can be found by comparing images through a narrow band filter centered on some suitable emission line (henceforth the emission line frame) and through a filter in which the bandpass is nearby but excludes this line (the continuum frame). See for example Ray et al. (1990) and Poetzel et al. (1992) and references therein.

Many young stars are surrounded by reflection nebulosity including V380 Ori. Due to the brightness of such nebulosity, it may be difficult to discern HH objects close to their source. In such cases it is best to produce a difference image (e.g. [SII]–r_{nc}), thereby revealing only emission line features. In this way confusion between HH objects and reflection nebulosity is automatically removed. To produce the difference image, the first step is to scale the continuum features in both emission line and continuum frames to match one another. In doing this, the background sky is first carefully removed from the images, and then, based on the stars in the field and any reflection nebulosity present, a scaling factor is estimated between their continua.

On subtraction of the scaled continuum frame from the emission line frame the resultant should contain pure emission line features. In practice, however, the initial scale factor is only a starting point; it is varied by small amounts and the difference frames compared visually until an optimum value is obtained. The process works best when both images are deconvolved to the same seeing profile. Deconvolution requires measurement of the average Full Width at Half Maximum (FWHM) of the stars in both images, then applying a Gaussian filter to increase the average FWHM to the largest value. Practically all starlight is removed in a correctly produced difference frame. In reality, it is accepted that some residual emission may remain due to colour terms and pixelation (see Poetzel et al. 1992).

In the case of V380 Ori, both [SII]–r_{nc} and [SII]–I band difference frames, are used to examine HH emission in its immediate vicinity, that is within NGC 1999. The choice of the [SII] filter for the emission line frame is because of NGC 1999. It is known that the nebula reflects the stellar spectrum of V380 Ori, and while this spectrum has a large Hα component it exhibits no [SII] emission (see Fig. 2.9). Thus, by using the [SII] image instead of the Hα image, any excess line emission detected in the difference frames should arise from some process other than reflection. Aside from HH emission the excess could be due to a HII region. It is unlikely, however, that V380 Ori ($L_{BOL} \leq 300\,L_{\odot}$) is the source of a HII region, and, although, this star and the entire area within the frame is known to be embedded in a weak HII region, its contribution to the background of the [SII] frame, can be removed to first order by subtracting the sky. In this case, although the background is not uniform and some residual emission may remain, its distribution is virtually uniform compared to the HH knots and structures that will be considered here.

As for the choice of difference frames, the question naturally arises as to why both the [SII]–I band and [SII]–r_{nc} images were selected. In general, the [SII]–r_{nc} image would be the better choice, the bandpass and central wavelength of the r_{nc} filter are closer to those of the [SII] filter. This in turn, would ensure that one minimizes colour effects in the subtraction process (but see §2.3.2 for further details). However, in the NTT [SII] and I band images, as previously mentioned, V380 Ori was masked by a coronographic spot, which is absent in the r_{nc} image taken at the ESO/MPI 2.2m telescope. The presence of the coronographic spot implies that close to the star (within about 10"), saturation effects due to V380 Ori itself are not present in the [SII]–I band difference frame (unfortunately, it was impossible to obtain a suitable narrow band continuum filter for the NTT). Outside this region, because of additional colour terms introduced by the I band image, the [SII]–r_{nc} difference frame makes a better choice for HH detection. The results of the difference subtraction can be seen in Figs. 2.2 and 2.3, and a detailed interpretation of the findings may be read in §2.3.

In studying the large scale HH emission around V380 Ori, primarily the Hα and the r_{nc} images are used. In this case, since the region outside NGC 1999 is being considered, there is little or no confusion with nebulosity and direct comparison between the emission

line and continuum frames is sufficient. This is also true of the region including the HH 1/ HH 2 system and HH 130, here direct comparison between the [SII] and the associated I band image is used to distinguish HH objects.

Finally, in an attempt to identify further candidate young stars in the vicinity of V380 Ori, the region was imaged using the infra-red camera (IRCAM) at UKIRT. The detector employed was a 62×58 InSb array with a plate scale of 0.62" per pixel. Observations were made in both the J and K bands and the exposure times were 120s (1 exposure) and 200s (5 co-additions of 40s) respectively. Data reduction was carried out using the IRAF package and the flatfielding was achieved by using the median average of several nearby sky frames. The observations were calibrated against the standard star HD 40335, the magnitudes of which are 6.55 mag and 6.45 mag in J and K respectively (Moore & Chandler 1989).

2.2.2 Spectroscopy

The majority of the long slit spectra for the region about V380 Ori, were produced with the 2.5m Isaac Newton Telescope (INT) on La Palma. These spectra were obtained over two observing runs; the first of these was a set of service observations, kindly performed by C. Benn in February 1990, and the second was conducted in September of 1991. An additional long slit spectrum was also provided by R. Hessman and was produced in February 1990 at the 3.5m MPI telescope on Calar Alto. Lastly, a long slit echelle spectrogram was made at the NTT in February 1991.

Spectra on the INT were obtained using the Intermediate Dispersion Spectrograph (IDS) and a record of the observations is presented in Table 2.2.1. In particular, one notes that in the earlier observations of Feb. 1990, a number of shorter exposures were made; this was to allow averaging and possible cosmic ray removal. Individual positional angles of the slits are quoted, and these are also illustrated in Fig. 2.3. In all cases the IDS was configured with a 500mm camera and a 1200 lines/mm (R1200Y) grating. Without substantial variation, this resulted in a spectral range of 6550–6750Å being covered. The detector used was a GEC P8603 chip, with $20\mu m^2$ pixels and a dispersion

Telescope	Object	Date	P.A.	Exposure Time(s)	Slitwidth"
INT	V380 Ori	8 Feb. 1990	149°	1000×3	0.8
	V380 Ori	8 Feb. 1990	62°	1000×5	0.6
	HH 130	8 Feb. 1990	110°	1000×3	1.0
	HH 130	8 Feb. 1990	50°	1000×3	1.0
	HH 35	3 Sept. 1991	119°	2700	1.1
	N^3K50	4 Sept. 1991	47°	2700	1.0
3.5m MPI	V380 Ori +4"	14 Feb. 1990	62°	1800	1.5

Table 2.1: Observing log for the spectra taken at the INT.

of 0.36Å per pixel, resulting in a spectral resolution of 32 km s^{-1}. The plate scale along the spatial direction was 0.3" per pixel, though the spatial resolution was set by the seeing of approximately 1" in all images.

For the spectrum obtained at the 3.5m MPI telescope, the red arm of the twin spectrograph was used. The instrument was configured with a GEC detector of 17μm^2 pixels and a TΦ5 grating, giving a dispersion of 0.88Å per pixel. The spectral range extended from 6290-6800Å and the associated spectral resolution was 81 km s^{-1}. It should be noted that this spectral resolution is almost a factor of three times poorer than for the spectra obtained at the INT. The plate scale along the spatial direction was 0.63" per pixel though the seeing limited resolution was approximately 2". Further details of this observation are given in Table 2.1.

In the results presented here, the [NII] doublet is often too weak to make proper measurements and is therefore neglected in the spectral analysis. Reflected Hα from V380 Ori also causes some difficulty, in that it often contaminates the Hα component of HH emission. Fortunately, only in the case of the lowest resolution spectrum is it impossible to distinguish between these Hα components. HH emission is normally extended over lengths greater than 2 or 3" i.e., it is spatially resolved. In principle, therefore, it should be possible to examine variations, in excitation temperature and electron density, over the entire length of the object. However, it is found for the long

slit spectra here, that with the exception of some of the brightest knots (located in the vicinity of V380 Ori, and HH 130), the signal to noise is generally weak, making very reliable measurements extremely difficult. In these cases, it was thought best to sum the individual two dimensional spectra over the extent of the object, to produce an "average" one dimensional spectrum. Measurements of spectra integrated in this manner, lead to an intensity weighted average for parameters such as excitation and electron density. The latter could be calculated from the computer program of J. Walsh (private communication) by using the ratio of [SII]λ6716/[SII]λ6731 line fluxes and assuming a postshock cooling temperature of 10^4K. Typical errors in the [SII] line ratio were of the order 10% and these corresponded to errors of $\leq$ 50% in the determination of electron densities between 200—2000cm^{-3} and $\geq$ 70% outside this range.

Finally, an echelle spectrum was obtained using EMMI (Moorwood 1990) on the NTT. The P.A. of the observation was 90°, with an exposure time of 2700s. The detector employed was the same as in the direct imaging mode of EMMI. The plate scale along the slit direction was 0.44" per pixel, the spectral range covered was 5800-7000Å, the slit width 0.9", and the spectral resolution was 56 km s^{-1}. A selected portion of this spectrum was reduced containing the [SII] doublet. For all spectral data reduction, namely bias removal, flatfielding, and spectral calibration, the IRAF package was used.

2.3 Results for V380 Ori and nearby outflows

2.3.1 Large scale HH emission about V380 Ori

In order to investigate the large scale HH emission about V380 Ori, an area of approximately 4' × 3.5' was examined. This region was extracted from both the Hα and the r_{nc} images and is displayed in Figs. 2.2 (a) and (b) respectively. The reflection nebula NGC 1999 is immediately apparent, and located near its center (marked by the largest cross) is the source of its illumination V380 Ori. Some 20" to the west of this position is the triangular shaped Bok globule. Of the other well known features in the region HH 35 is indicated and lies about 1' to the northwest of V380 Ori. Although, further HH emission is known to be contained within the Hα image, in particular several knots discovered by Strom *et al.* (1985) (see §2.1.3), these features are not apparent because of the contrast level. They are however, discussed later in the context of the [SII]–r_{nc} difference frame (see §2.3.2 and Fig. 2.3 (c)). Finally, both the Hα and r_{nc} images have been median filtered to remove cosmic ray contamination.

A direct comparison of the Hα and r_{nc} images reveals large amounts of extended Hα emission both to the north and to the west of NGC 1999. Perhaps the most striking feature, is however, the Hα loop structure, which is approximately 140"× 60" in size and can be seen to the west of the nebula. The loop is elliptical in shape and the major axis of this "ellipse" passes through V380 Ori at a P.A. of approximately 100°. The intensity is seen to vary about the structure, in particular it seems to contain a number of smaller condensations. One of these is in fact HH 35; it is the brightest HH object and can be seen at the beginning of the northern edge of the loop. Of the other condensations, the brighter ones have been labelled I, J and K, in order of descreasing brightness (the reason why this nomenclature is used will become clear later).

Condensation I is located in the southern part of the loop and interestingly, it is elongated roughly in the presumed direction of the local magnetic field i.e. 146° ± 10° (Strom *et al.* 1986). Condensation J, has a similar orientation to I, but is smaller in size being only some 30" long compared to the 50" length of I. Both these structures,

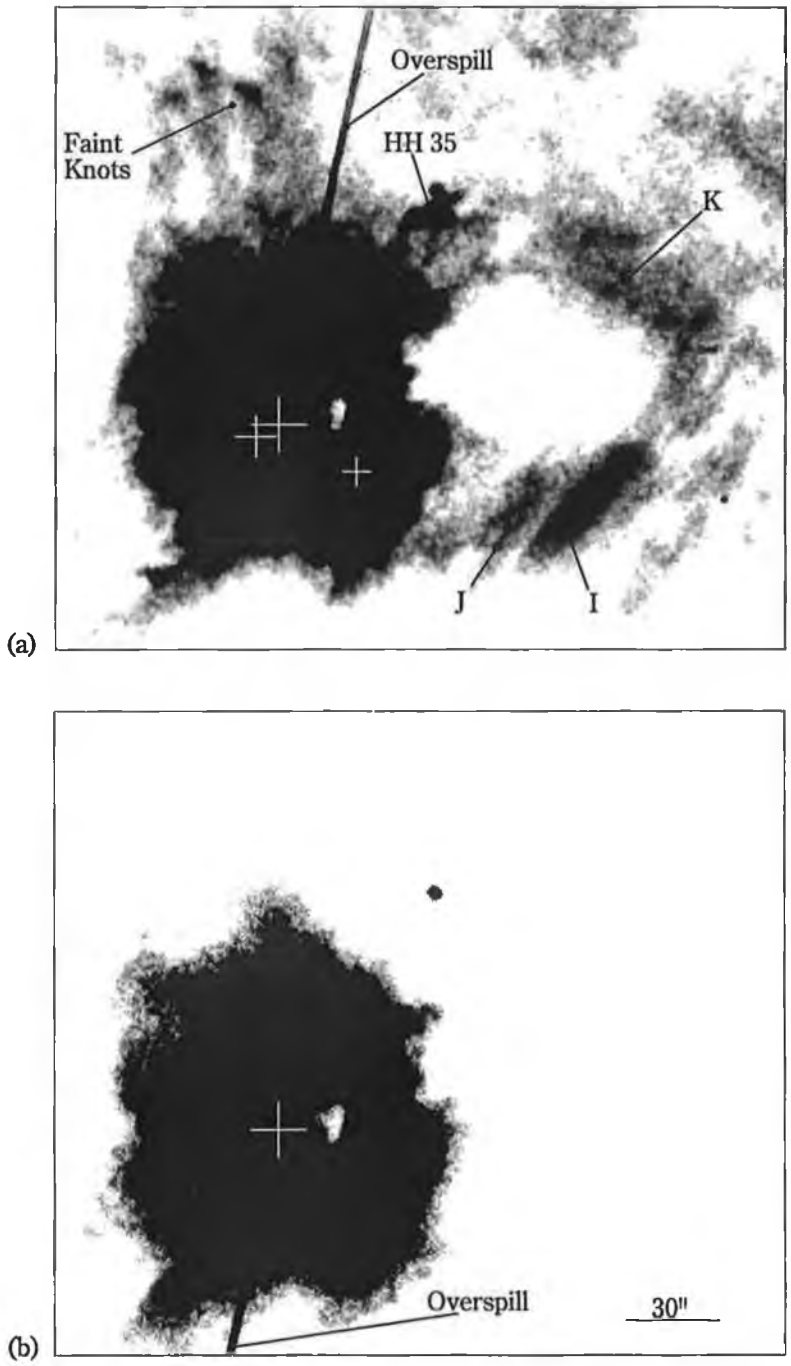

Figure 2.2: (a) A Hα image of NGC 1999 and the region to its west. The plus signs (+) in order of decreasing size mark the positions of V380 Ori, and the infra-red sources V380 Ori-B, and V380 Ori-C respectively. Prominent within the image is a "loop" feature which is composed of several sub-condensations; these include the well known HH 35, and a number of newly discovered objects, labelled I, J and K. To the north of NGC 1999, some faint knots are also seen at the ends of "finger-like" emission. (b) The same area as in (a) but through the narrow band r_{nc} continuum filter. Important here is the disappearance of both the "loop" feature and the emission knots to the north.

together with HH35, appear to be comprised of smaller knots. This is also true, in the case of the third condensation K, which lies in the northwest portion of the loop. K is about 50" in length and points roughly at right angles to the local magnetic field. Finally, of the remaining Hα emission, there is a peculiar set of structures to the north of NGC 1999. A series of four bright knots separated by about 110" from V380 Ori, are located at the end of "fingers" of weaker emission connected to NGC 1999. These features are somewhat reminiscent of the M42 "fingers" (Allen and Burton 1993).

2.3.2 HH emission close to V380 Ori

To search for possible HH emission within NGC 1999, primarily the [SII] and the r_{nc} images have been used (except for the region immediately surrounding the star, see §2.2.1); extracted portions of these images (4.5' × 6.5') are displayed in Figs. 2.3 (a) and (b) respectively. In a direct comparison of the frames, it is just possible to find the HH objects A and B which were marginally seen by Strom et al (1985), and because of the presence of NGC 1999, these objects are also difficult to see here. In stark contrast, however, A and B are immediately apparent in both the low and high contrast [SII]–r_{nc} difference frames, which are shown in Figs. 2.3 (c) and (d) respectively.

Unfortunately, there are some additional spurious [SII] excesses which are of concern, and these are a direct consequence of the colour dependent nature of NGC 1999, in the production of the difference image. A continuum frame made at a nearby wavelength can never exactly mimic variations of colour within such a nebula. Consequently, as is the case here if the continuum frame (r_{nc} or I band) is made redward of the emission line frame ([SII]), bluer parts of the nebula may not be fully subtracted and could appear as artificially enhanced. This behaviour is greatly reduced by using a continuum frame which has both a narrow bandpass and is close in wavelength to the emission line frame. As mentioned earlier, the r_{nc} image was chosen for just this purpose. In this case, only in those regions where the intensity of the nebula is either very blue (large amounts of scattering) or very intense is there likely to be confusion.

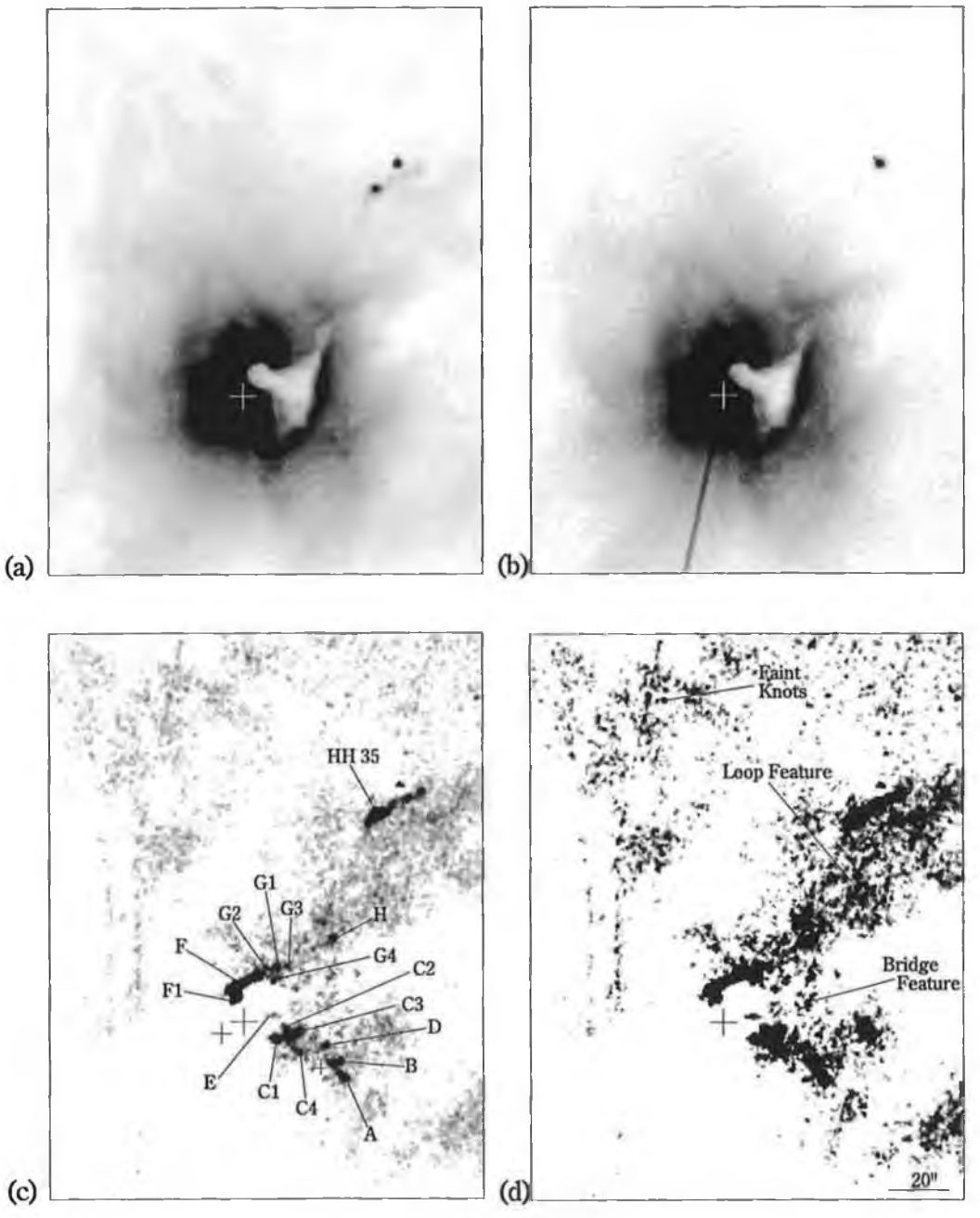

Figure 2.3: (a) A [SII] image of the region immediately about V380 Ori. (b) An r_{nc} image of the same area as in (a). (c) A low contrast difference frame of the [SII] and r_{nc} images (i.e. [SII]–r_{nc}) highlighting possible HH objects in the region. Plus signs indicate V380 Ori and the new infra-red sources (as in Fig. 2.1.). (d) As in (c) but at high contrast. One notes that in addition to the possible HH objects, the beginning of the Hα "loop" structure (seen in Fig. 2.1) together with the faint knots to the north of NGC 1999 are visible here. Also indicated is a possible spurious feature bridging the "loop". This most likely arises from colour effects in the difference procedure, as discussed in the text.

Inspecting the high contrast difference frame (Fig. 2.3 (d)), the most obvious feature is what appears to be the beginning of the "loop" structure, already seen in the Hα image (see Fig. 2.2 (a)). One must be careful though, given that most of this emission is of low intensity, it could in part derive from colour effects. In particular, it is well known that NGC 1999 becomes bluer towards its edges, and the western edge of the Bok globule is known to have an intensity comparable to the nebula's central regions (Brück 1974). Thus, it is possible that the faint emission seen to "bridge" the northern and southern parts of the "loop" (Fig. 2.3 (d)), is most likely a colour effect. Spectroscopy can help settle this matter.

One sees that in addition to the fainter [SII] emission, and coincident with it, there are a number of smaller condensations (see Fig. 2.3 (c)). These condensations are both knotty in structure and they are considerably more intense than the diffuse emission. As will be seen, many are confirmed spectroscopically to be HH objects (see §2.3.3). The coincidence in position between the knots and the faint emission also seems to suggest that they may either be just the brighter parts of the putative [SII] "loop" or at least, by themselves, trace the beginning of the Hα "loop". The northern boundary of the "loop", is marked by HH 35 and moving anticlockwise towards V380 Ori several knots are visible. The brightest of these are labelled H, G1 to G4, and finally the arc shaped object F. Object F is worthy of comment since it is coincident with the bright arc of emission, the intensity of which is similar to that of V380 Ori itself (see §2.1.1). It is thus, unclear how much of this feature is actually HH emission, though as will be shown later, some of it most certainly is, in particular knot F1 (see §2.3.3). Interestingly, if knot F1 marks the beginning of the "loop" structure then V380 Ori does not lie at this point but is displaced at least 4" to its southwest.

Along the southern boundary it is possible to identify objects A, B and C[1] with those first seen by Strom *et al.* (1985). For knot C, however, the difference frame reveals that it is more complex than previously thought; it is seen as a cross shaped object in

[1]With reference to the nomenclature used here, the first set of un-named knots discovered by Strom *et al.* (1985) are referred to as knots A, B and C. The nomenclature follows a clockwise direction around the "loop", with subsequent knots labelled accordingly. One exception is knot D which has been was discovered here ***within*** the area of knots B and C.

Fig. 2.3 (c) whereas in the images of Strom *et al.* (1985) it only appears as a diffuse patch. An additional bright knot D is also found some 7" northeast of B.

Finally, a faint knot, knot E, can just be seen in the [SII]–r_{nc} difference frames. It is however, better observed for the reasons mentioned earlier in the [SII]–I band difference frame and this is displayed in Fig. 2.4 (b). Indeed, most of the knots close to V380 Ori appear more distinct. This is not the case, however, for knots A, B and D, since these are only just detected in the [SII]–I band image while knots G and H are not visible at all. As to any additional [SII] excess in the region, there is marginal evidence in the [SII]–r_{nc} image (Fig. 2.3 (c) and (d)), for the presence of the knots seen to the north of V380 Ori in the Hα image.

2.3.3 Spectroscopy of HH objects near V380 Ori

Details of the long slit spectroscopy of the HH objects close to V380 Ori, were already summarised in Table 2.1, and the slit positions are indicated in Figs. 2.4 (a) and (b). Only, the brightest knot was detected in the spectrum of HH 35 (this is labelled HH 35a), and its average spectrum (see §2.2.2) is displayed in Fig. 2.5 (a). The spectrum is typical of HH emission; the brightest lines are those of Hα and the [SII]$\lambda\lambda$6716,6731 doublet, although [NII]$\lambda\lambda$6548,6584 doublet emission is also seen. Derived radial velocities, electron densities and excitations for this and other objects are summarised within Table 2.2. In the case of HH 35a, it is seen to be of moderate excitation (Hα/[SII]λ6716+6731 = 0.9), with an electron density n_e = 2200cm^{-3} and a very low radial velocity. The radial velocity is so low in fact that the motion of HH 35 must be close to the plane of the sky. Another feature in the north of the "loop" but closer to V380 Ori, is knot G1. Spectroscopically verified as HH emission (see Fig. 2.5 (b)), it is in contrast to HH 35, characterised by a lower electron density (n_e = 200cm^{-3}), a higher excitation (1.5) and is moderately blueshifted in radial velocity (V_{HEL} = -100 km s^{-1}).

Also along the northern boundary and nearest V380 Ori, is knot F1. Knot F1 is in fact part of a more extended structure, which is found to be at least 7" in extent from its long slit spectrum. The positions of the extremities for F1 are shown in the

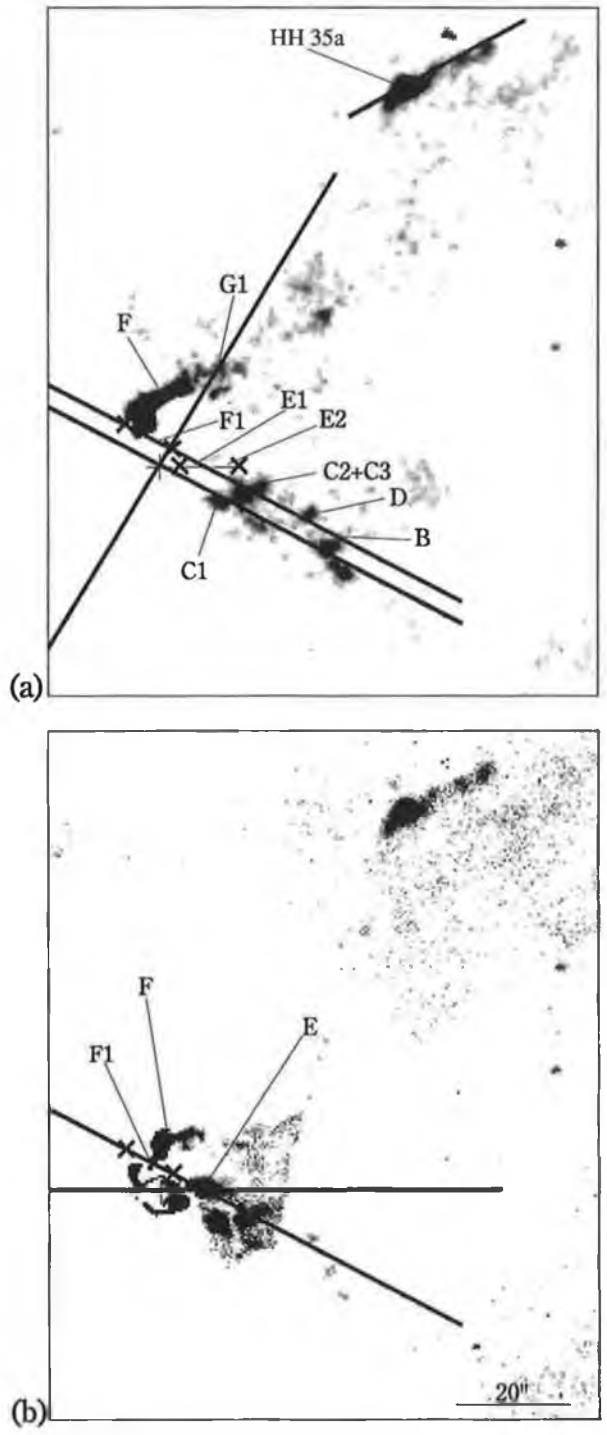

Figure 2.4: (a) An extracted portion of the [SII]–r_{nc} difference frame. The long slit positions are indicated, together with those objects which have been spectoscopically identified as HH emission. In the case of F1 and E, spectral analysis reveals they are actually greater in extent than observed in the difference frame, the positions of their extremities are marked here by crosses (x). V380 Ori is included for reference and is indicated by a plus sign (+). (b) A [SII]–I band frame of the same area as in (a). Note that the HH objects closest to V380 Ori appear brightest (see text for details). F1 and its extremeties, together with E are marked and the slit positions used for their spectral analysis are shown.

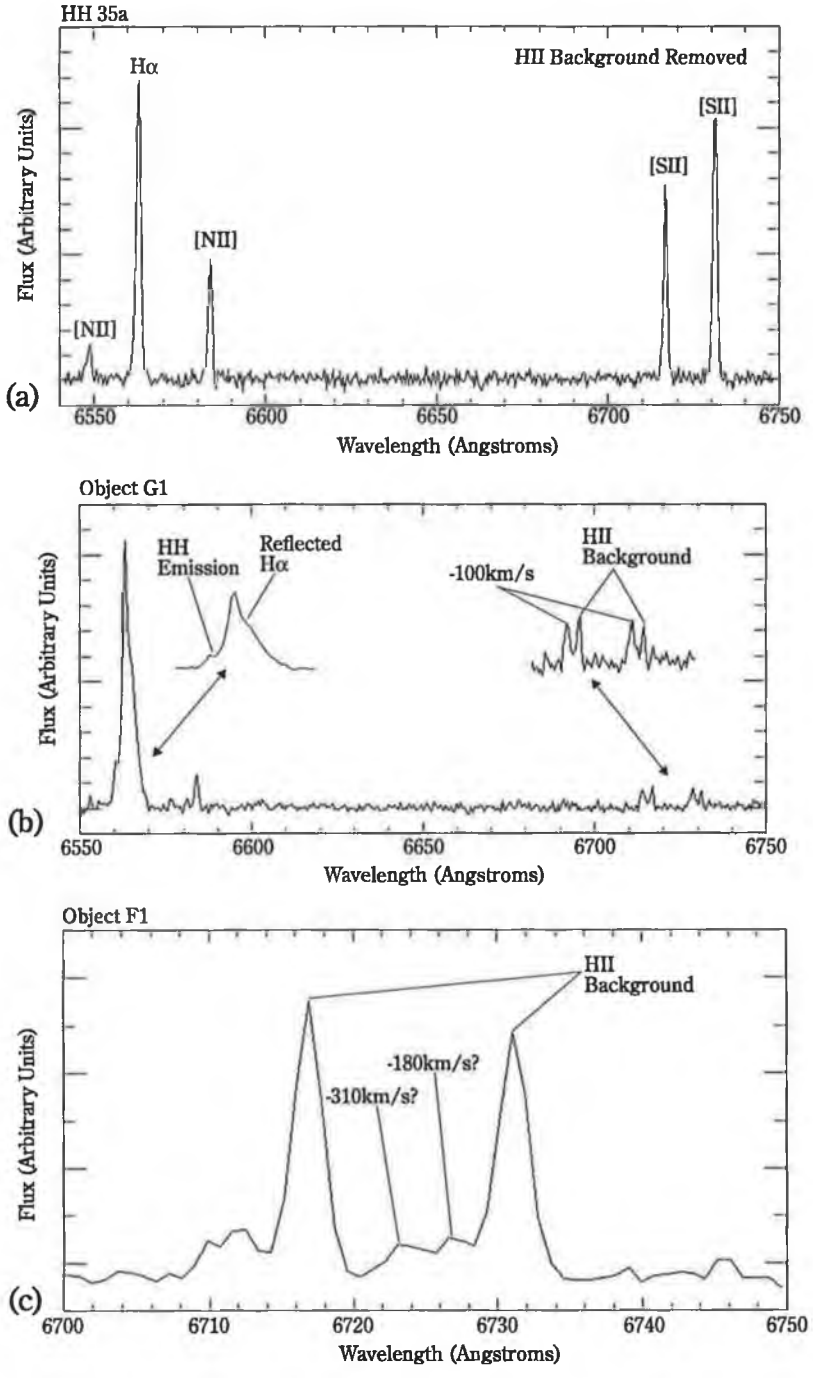

Figure 2.5: (a) The average spectrum of HH35a (see text for details on the averaging technique) in which the HII background emission has been removed. Note the characteristic HH spectrum with the [SII]$\lambda\lambda$6716,6731 forbidden line emission comparable in flux to Hα. Low radial velocities suggest HH 35a is moving almost in the plane of the sky. (b) The average spectrum of object G1. Blueshifed HH emission is clearly shown together with the background HII and reflected Hα emission. (c) As in (b) but for object F1 and only in the wavelength range covering the red [SII] doublet. Here, although HH emission with two blueshifted velocity components is clearly observed, the exact velocities are uncertain owing to the poor signal to noise.

difference frames (Figs. 2.4 (a) and (b)), and the absence of the complete object in these frames most probably arises from a combination of its weak intensity and the colour effects discussed earlier (see §2.3.2). In the averaged spectrum shown in Fig 2.5 (c), only the [SII]$\lambda\lambda$6716,6731 lines are shown (see §2.2.2). Clearly visible, are two velocity components ($V_{HEL} \approx$ -180 and -310 km s^{-1}) in addition to the background HII emission. Estimates of the average electron density and linewidths are not given owing to the very weak signal to noise of the spectrum.

Object Name	Rad. Vel. V_{HEL} (km s^{-1})	Elect. dens. n_e (cm^{-3})	Excitation Hα/[SII]	Linewidth (km s^{-1})
HH 35	+10	2200	0.9	50
V380 Ori-Knot G1	-100	200	1.5	50
V380 Ori-Knot F1	-180?			
	-310?			
V380 Ori-Knot C1	+350	100	0.7	80
V380 Ori-Knot C2+C3	+190?	800?		170?
V380 Ori-Knot D2	+230	300		70
V380 Ori-Knot D1	+200	400		100
V380 Ori-Knot B	+70	1800	1.1	150

Table 2.2: Measurements for HH objects near V380 Ori. A question mark signifies uncertainty in a measurement resulting from poor spectral signal to noise.

Possibly associated with F1, is the diffuse shaped object E. Although, in the [SII]-I band difference frame E appears only as a bright patch of emission, its long slit spectrum shows that it actually consists of two knots (henceforth labelled E1 and E2). Between the knots lies some weaker emission. As with F1 only some of object E can be seen in the difference frames, in particular E1 is partially observed, since most of the knot lies within the boundary of the coronographic mask (see §2.2.1). The position of the extremities for knots E1 and E2 are indicated in the difference frames (see Fig. 2.4) and a position-wavelength diagram for these knots is given in Fig. 2.6 (a). At least two velocity components are seen in E1, one at V_{HEL} = -50 km s^{-1} and the second, which is much lower in brightness, at -170 km s^{-1}. The post shock electron density can only

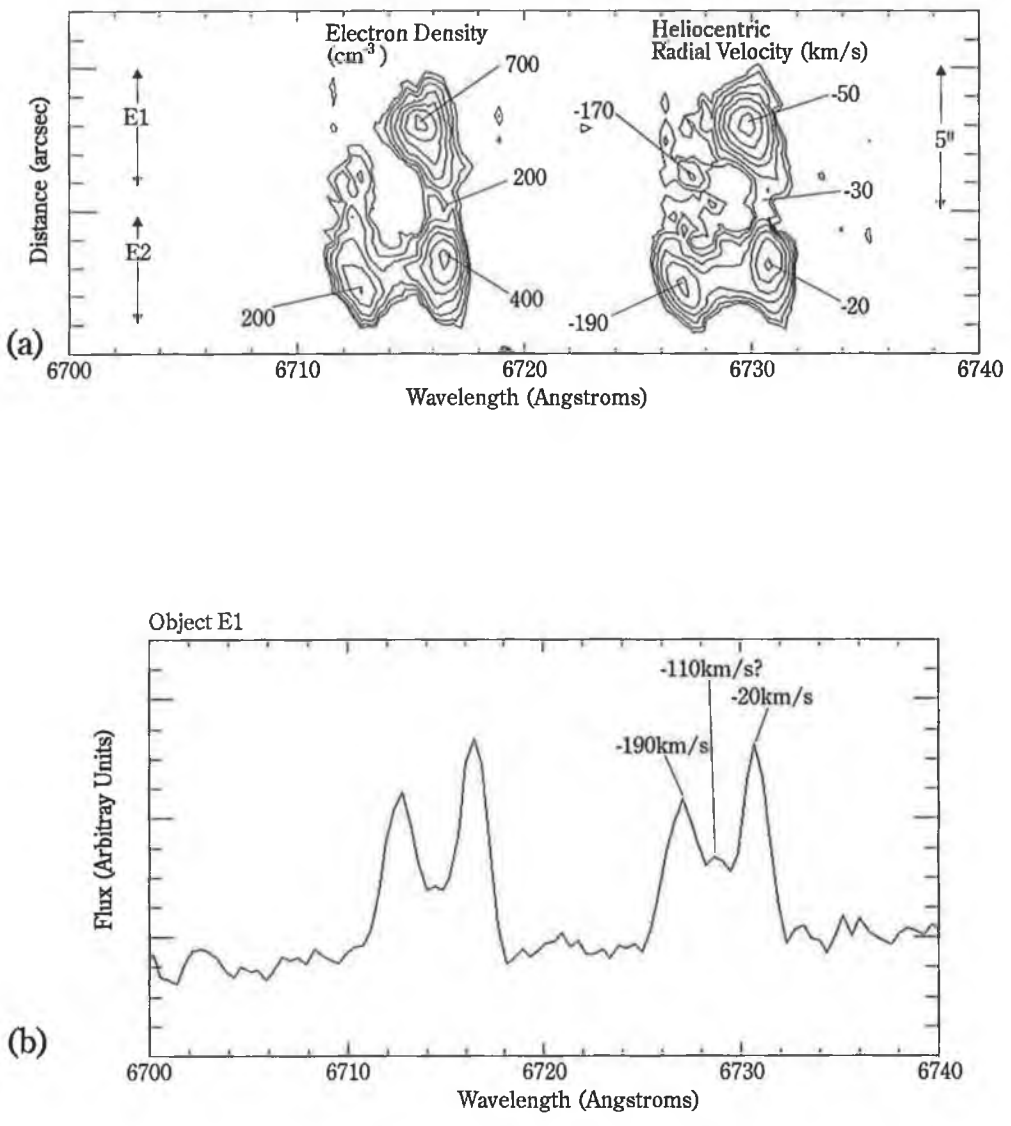

Figure 2.6: (a) A Position-Wavelength diagram for the HH object E in the [SII]$\lambda\lambda$6716,6731 lines, for which the background HII emission has been removed. It is apparent that E is comprised of two knots (E1 and E2), and that these have at least two main velocity components. Velocities and electron densities at various points are indicated. (b) A spectrum of the red [SII] doublet for knot E1. Note that in addition to the two main velocity components an intermediate component may be just visible.

be reliably determined for the low velocity component and a value of n_e = 700cm^{-3} is derived. For knot E2, two velocity components are also found (V_{HEL} = -20 km s^{-1} and -190 km s^{-1}), although in a spatially integrated spectrum of this knot (see Fig. 2.6 (b)), an additional intermediate component ($V_{HEL} \approx$ -110 km s^{-1}) may be just visible. As for the post shock electron densities of E2, they are similar in both the high and low velocity components (200 and 400cm^{-3}). It is also worth pointing out, that the higher velocity component of both knots E1 and E2, is similar to the lower radial velocity component of F1 discussed above.

As for the southern boundary of the "loop" the long slit spectrum taken at the 3.5m Calar Alto telescope, also encounters knots C2, C3 and D. For knots C2 and C3, their combined average spectrum is presented in Fig 2.7 (a), which includes the area of the red [SII] doublet. These objects are clearly redshifted ($V_{HEL} \approx$ +190 km s^{-1}), with an associated electron density of $n_e \approx$ 800cm^{-3}. Comparison with knot C1 (see Fig. 2.7 (b)), shows that C1 has a higher radial velocity (V_{HEL} = +350 km s^{-1}) and a lower electron density (n_e = 100cm^{-3}). Only in the case of C1 is it possible to estimate the Hα/[SII]λ6716+6731 ratio and this reveals an excitation (0.7) comparable in value to HH 35. For knot D, as is the case for objects F1 and E, its long slit spectrum reveals better spatial detail than the difference image. A position-wavelength diagram of this knot is displayed in Fig. 2.8, and also shown is the relevant portion of the [SII]–r_{nc} difference frame for comparison. In the difference frame the brightest knot is labelled D1 and the fainter emission preceding this (i.e. closer to V380 Ori), is labelled D2. In both cases their radial velocities are approximately V_{HEL} = +200 km s^{-1}. Lastly, in the southern part of the "loop", knot B is furthest from V380 Ori and in many respects is similar to HH 35a. Both the low excitation (1.1) and high electron density (1800cm^{-3}) are comparable to those derived for HH 35a. In fact the main difference between these objects is their radial velocities, B has a somewhat larger velocity (V_{HEL} = +70 km s^{-1}). Yet, even so, such a radial velocity is small and therefore like HH 35a, B maybe moving in the plane of the sky. The spectrum of knot B is presented in Fig. 2.7 (c).

Considering the emission knots collectively, in all cases their spectra are typical of HH emission. Interestingly, amongst these HH objects there seems a significant separation in their radial velocities with position. Predominantly blueshifted HH emission lies west

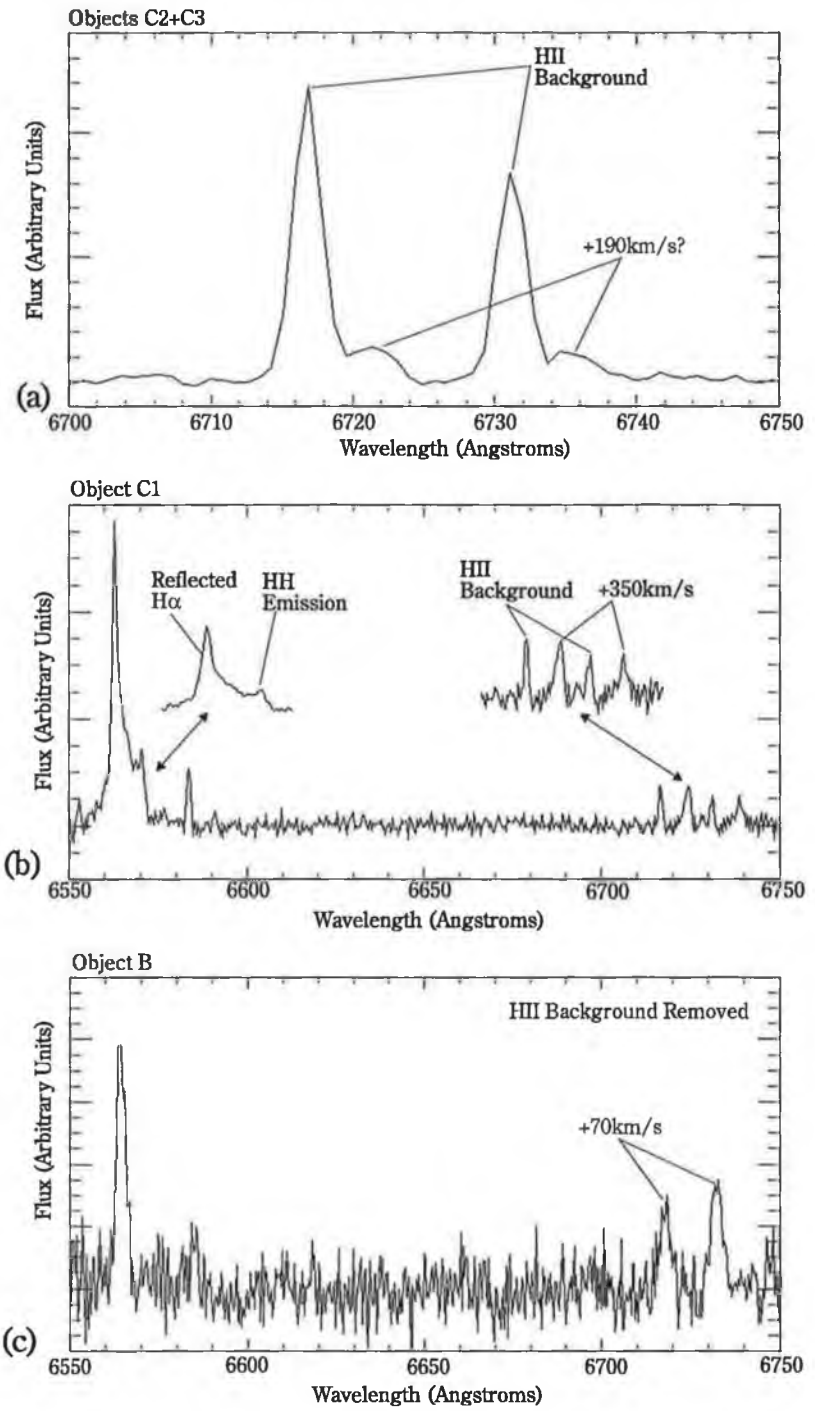

Figure 2.7: (a) An average spectrum for objects C2+C3, covering the wavelength range of the red [SII] doublet. The background HII emission and the presence of a redshifted HH velocity component are indicated. The exact velocity is uncertain owing to the poor signal to noise. (b) The average spectrum for object C1. Background HII emission together with reflected Hα from NGC 1999 are marked, and the presence of a redshifted HH component is clearly shown. (c) The average spectrum of object B, in which the background HII emission has been removed. The HH emission is seen to have low velocities suggesting its motion like HH35a is in the plane of the sky.

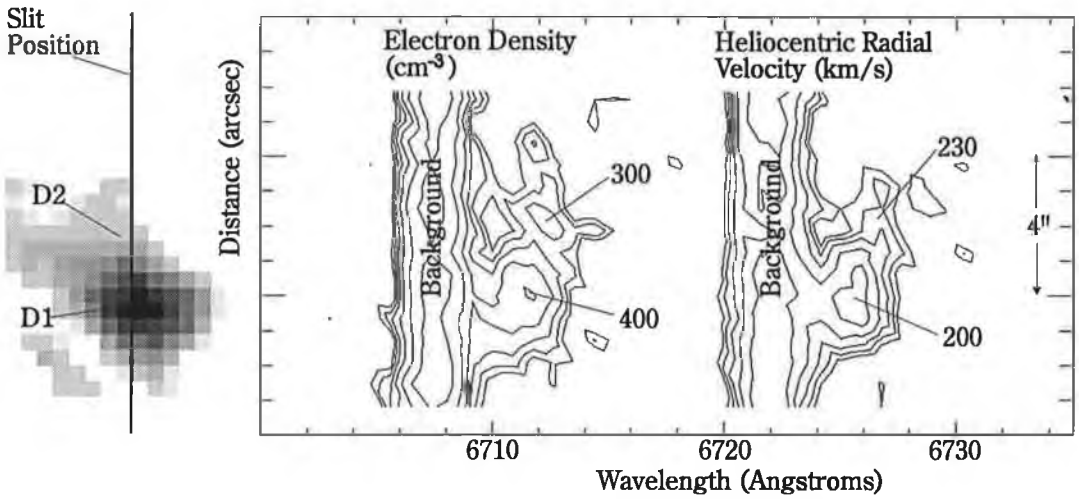

Figure 2.8: A position wavelength diagram for the HH object D in the red [SII] doublet. At least two knots are apparent (D1 and D2) and their velocities and densities are indicated. Also shown, is the same object from the [SII]–r_{nc} difference frame with the slit position marked for comparison.

of V380 Ori and to the north, while the redshifted HH emission lies south and southwest of this position. For both redshifted and blueshifted objects, radial velocities are highest near V380 Ori (greater than $\pm$ 300 km s^{-1}), then, with increasing distance from this point the radial velocities are seen to decrease. Indeed, radial velocities of the furthest knots i.e. HH35a and knot B, indicate motion more or less in the plane of the sky. As to trends in the Hα/[SII]λ6716+6731 ratio, values are available for only some of the HH knots, they range from 0.7 to 1.5 and are indicative of moderate shock excitation. Electron densities are interesting in that the highest densities appear to be associated with the HH objects furthest from V380 Ori i.e., those of lowest radial velocity. In the case of YSO jets for example, the opposite trend is found (Mundt *et al.* 1987). Lastly, one notes that a number of objects in Table 2.2 have large linewidths ($>$ 100 km s^{-1}). There are at least two possible interpretations; firstly, a number (or a range) of velocity components may exist within the object (as witnessed in object E and F1), but these cannot be resolved owing to the poor signal to noise of the data; secondly, the object may exhibit an acceleration or deceleration, which will cause a broadening of the line profile when spatially averaged. The first of these explanations is probably applicable to knots C2+C3, while the second might be relevant in the case of knot B (judging by the original data).

2.3.4 The Spectrum of V380 Ori and the Background HII Region

Turning now to V380 Ori, its spectrum (from 6550Å to 6750Å) is shown in Fig. 2.9, which for the purposes of presentation has had its continuum normalised to a constant value. The most prominent emission feature is the single peaked Hα profile, which unfortunately, is saturated at the stellar position. By examining the profile 1" from the star, it is possible to measure the equivalent width which is found to be -71Å. This value is well within the range of previous measurements (-58 to -105Å) given by Finkenzeller and Mundt (1984), and such variations in the equivalent width are typical of HAEBESs. The FWHM for Hα, when corrected for the instrumental response (FWHM$_c$ = 230 km s^{-1}) is also found to be slightly less than that measured by Finkenzeller and Mundt (1984) (FWHM$_c$ = 260 km s^{-1}).

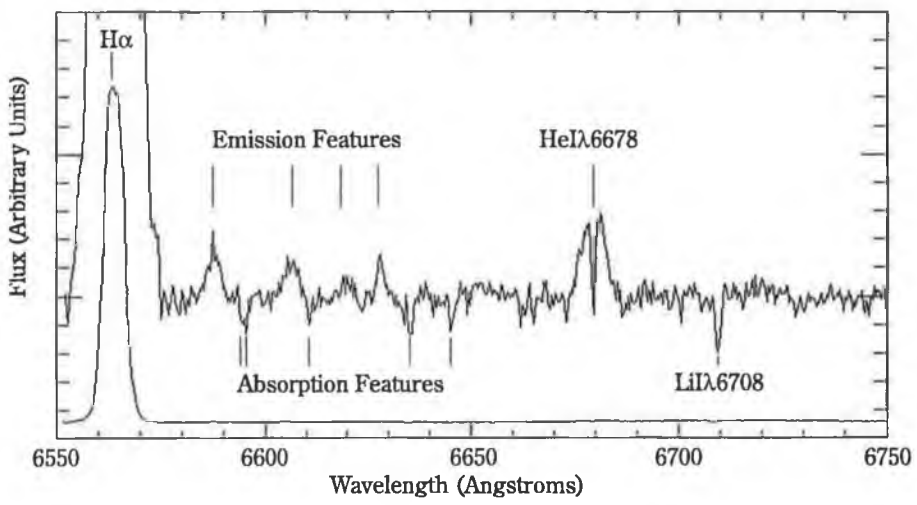

Figure 2.9: The spectrum of V380 Ori. The presence of various emission and absorption features are indicated. Note in particular the presence of the Liλ6708 absorption line, which suggests that V380 Ori's inclusion as a Herbig Ae/Be star may be incorrect (see text).

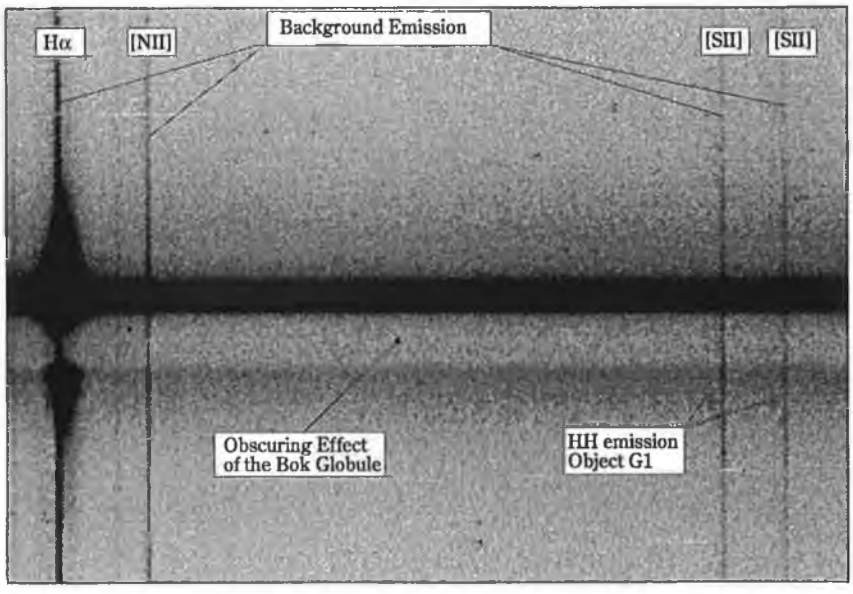

Figure 2.10: An INT long slit spectrum taken at a P.A. of 149° through V380 Ori. Note the obscuring effect of the Bok globule, while in emission one can see both the HH object G1 and the background HII region.

Excluding Hα, the most prominent emission line in this part of the spectrum is HeIλ6678, which may be indicative of a stellar wind (see e.g. Hartmann *et al.* 1993 and references therein). HeI lines originate from upper levels of considerably high excitation potential (20–50eV), although, it is still commonly found in the spectra of certain TTSs (Appenzeller *et al.* 1988). The observed profile for V380 Ori appears double peaked owing to a central absorption which is unresolved (FWHM = 40 km s^{-1}) and this feature could be interpreted as due to HeI at essentially the rest velocity of the star. The FWHM$_c$ of the entire HeI profile is 340 km s^{-1} and interestingly, this is larger than the value measured for Hα. Using both the Hα and HeI emission lines, it is possible to estimate their mean radial velocity, and the value found (V_{HEL} = 40 km s^{-1}) is close to the radial velocity of the molecular cloud (26 km s^{-1}) (see Finkenzeller and Jankovics 1984 and references therein).

A list of all emission lines detected in the spectrum is given in Table 2.3; for each line, measurements are given for the heliocentric wavelength, the equivalent width and the FWHM$_c$. Excluding the Hα and HeIλ6678 lines, the remaining metallic emission features are considerably weaker in intensity, and in general, their equivalent widths are at least a factor of two times smaller than the HeIλ6678 line. Characteristic of these weaker features is a broad triangular shaped profile, in fact most of the lines have a FWHM$_c$ > 160 km s^{-1}. The width of these profiles, together with the absence of night sky lines in the long slit spectrum, suggest that they are associated with the star. One possible exception is the feature at 6627Å which is within 10 km s^{-1} of an OH night sky line, indeed, it must be mentioned that when compared to the other emission lines, it is somewhat narrower (FWHM$_c$ = 90 km s^{-1}). Even so, since the line is not seen in the background away from the star, it too is most probably an FeI line of stellar origin. Identification of the lines, although rather difficult, owing to problems in determining their central positions, are given in Table 2.3.

Of the absorption features in the spectrum, the most interesting discovery is that of the LiIλ6708 blend. Li is seen as an indicator of youth in stars (Strom *et al.* 1989), thus verifying the pre-main sequence nature of V380 Ori. The LiIλ 6708 blend, however, is not seen in stars of spectral type earlier than F0 (R. Rebolo, private communication). If the absorption is photospheric, it seems unlikely therefore that V380 Ori is an A or B

Measured and Heliocentric Wavelength Å	FWHM$_c$ km s^{-1}	Equivalength Width Å	Identification and Laboratory Wavelength Å
6563.87	230	-71	Hα–6562.82
6587.28	150	-.15	NiI–6586.33(64) FeII blend 6586.69 (un)?
6605.85	180	-.10	ScII–6604.6(19)
6619.34	160	-.05	ScII–6617.9(un)
6627.51	90	-.15	FeI–6625.04(13) Airglow 6627.63?
6678.97	340	-.40	HeI–6678.15

Table 2.3: Emission line features in the spectrum of V380 Ori. Un is an unknown multiplet number and a question mark signifies uncertainty in the line identification.

type star in spite of its luminosity (see §2.1). Moreover, the other absorption features particularly those due to FeI (see Table 2.4) strengthen this idea as these lines are typical of T-Tauri stars (see Appenzeller *et al.* 1986 and Herbig 1990). One must be careful, however, since it is not certain exactly where these absorption lines form i.e. they may not be photospheric and could for example be produced in cooler gas outside the star. In the discussion (see §2.5.4) the cause of these absorption features and their implications for V380 Ori will be considered in more detail. For now, one notes that the mean radial velocity of the absorption lines, is $V_{HEL} = +50\,\mathrm{km\ s^{-1}}$, and this is reasonably close both to the molecular cloud velocity ($+26\,\mathrm{km\ s^{-1}}$), and the velocity determined for the emission lines above ($+40\,\mathrm{km\ s^{-1}}$).

As mentioned earlier (see §2.1) Hα emission (presumably from V380 Ori) is seen in reflection in NGC 1999. The reflected Hα component is clearly apparent in the long slit spectrum taken at PA 149° presented in Fig. 2.10. The slit position cuts across the Bok globule, and the obscuring effect that this produces can be seen in the sudden decrease of the reflected continuum. Of greater interest here, however, is the shape of the extended and reflected Hα emission, which is better examined in the contour plot shown in Fig. 2.11 (a). As already seen in the spectrum of V380 Ori, the Hα profile is single peaked and symmetric. Away from the star, however, in the extended and reflected Hα emission, one notes that the blueward side of the profile decreases in intensity at

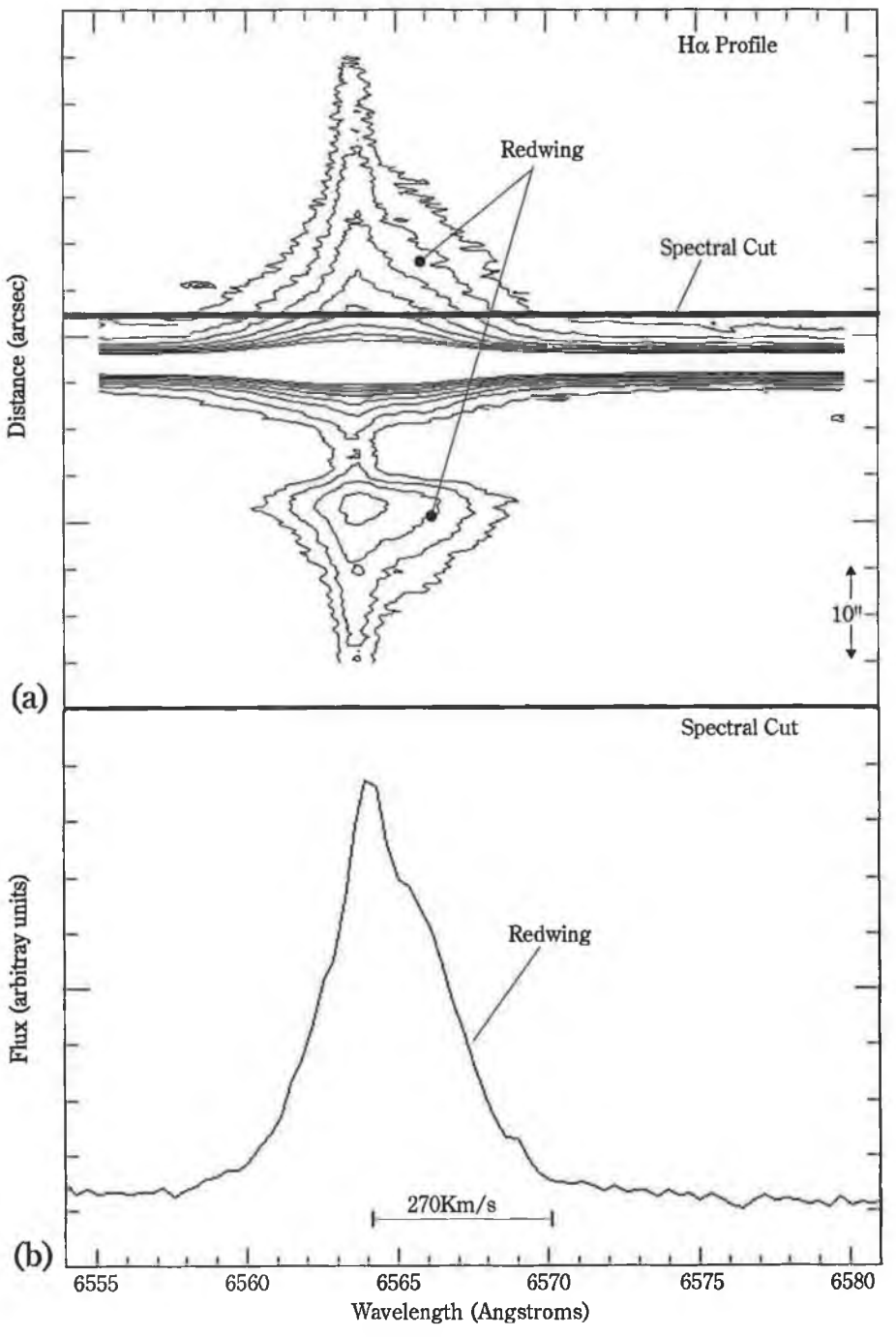

Figure 2.11: (a) A position-wavelength contour plot of the reflected Hα component from the INT spectrum in Fig. 2.9. Note the assymetry, which gives the appearance of a "redwing" to the emission. (b) A spectral cut through the reflected Hα component as marked in (a).

Measured and Heliocentric Wavelength Å	FWHM$_c$ km s^{-1}	Equivalength Width Å	Identification and Laboratory Wavelength Å
6594.15	40	.03	Blend:FeI–6592.92(268)
6594.95	unr.	.02	FeI–6593.88(168)
6610.26	30	.03	FeI–6609.12(206)
6635.04	40	.03	Blend: FeI–6633.44(Un)
			FeI–6634.10(1258)
6644.42	unr.	.03	NiI–6643.64(43)
6708.99	40	.06	Blend:LiI–6707.82

Table 2.4: Absorption line features in the spectrum of V380 Ori. Blend: signifies a blend of two lines and Un an unknown multiplet number.

a greater rate then the redward side thus giving rise to an asymmetric profile. The asymmetry of the reflected Hα emission can then be described by what seems to be a "redwing". To illustrate this apparent "redwing", a spectral cut is made at 6" from V380 Ori (indicated in the contour plot) and the result is displayed in Fig. 2.11 (b). Measurements reveal that the width of the "redwing", as determined from the central peak to where its intensity drops to the background value, is consistently 270 km s^{-1}. This velocity seems to be independent of the separation from V380 Ori. Furthermore the presence of the "redwing" has been confirmed, both by the long slit-spectra taken at PA 62°, and by the spectral observations made by Hessmann at Calar Alto.

As for background emission, one sees that in the long slit spectrum presented in Fig. 2.10, both Hα and the red [SII] doublet emission is extended over the entire length of the slit. Obviously, such a background is part of the environment of NGC 1999, and for this reason its densities and excitation (Hα/[SII]λ6716+6731) have been measured. To avoid confusion with the reflected Hα component measurements were made outside of the nebula. All the long slit spectra were used and since the signal to noise of the emission is in most cases very weak, the spectra were spatially averaged over the slit length.

Results indicate a low electron density medium ($n_e \approx 100$ cm^{-3}), but the excitation (Hα/[SII]λ6716+6731 $\approx$ 4.5) is higher by at least a factor of 3, than for any of the HH objects (see Table 2.4 for comparison). Differences are also found in the linewidths; whereas all the HH emission is resolved, this is not true of the extended Hα and [SII] features in the background. In the latter case the FWHM$_c$ is typically about 30 km s^{-1}, which is less than the instrumental profile even for the higher resolution INT spectra (FWHM = 37 km s^{-1}). Lastly, the background emission shows no spatial variations in its radial velocity; measurements reveal that it has a $V_{HEL} \approx 15$ km s^{-1} independent of direction and position. These results namely, the high excitation, narrow linewidths, and low radial velocities, show clearly that the background emission is due to a HII region.

2.3.5 Other stars in NGC 1999

The IRCAM images taken in J and K have revealed the presence of two new sources located within NGC 1999 (see Fig. 2.12(a) and (b)). Unfortunately, since V380 Ori is saturated in these images, it was not possible to provide new infrared photometry for this object. Photometry was however, carried out on the two new sources. One of these V380 Ori-B, is located at a P.A. of 150° with respect to V380 Ori and is separated by 9". Detected in both the J and K bands, measurements show V380 Ori-B to have m_J = 14.7 and m_K = 13.0 (i.e. a J–K colour of 1.7 mag). As for V380 Ori-C, this rather diffuse source is only detected in the K band. Its distance is 29" from V380 Ori at a P.A. of 238°, and its magnitude in K is found to be m_K = 13.7. For reference purposes the positions of these two new sources are marked in both the Hα and low contrast [SII]–r_{nc} images (see Figs. 2.2 (a) and 2.3 (c)). Lastly, it is worth stressing that the brightest near-infrared source in NGC 1999 is V380 Ori, with m_J = 8 and m_K = 6 (Strom *et al.* 1989). Even if both of the new sources were contained within a single aperture used to measure the K magnitude of V380 Ori, they would contribute less than 1% to the overall flux.

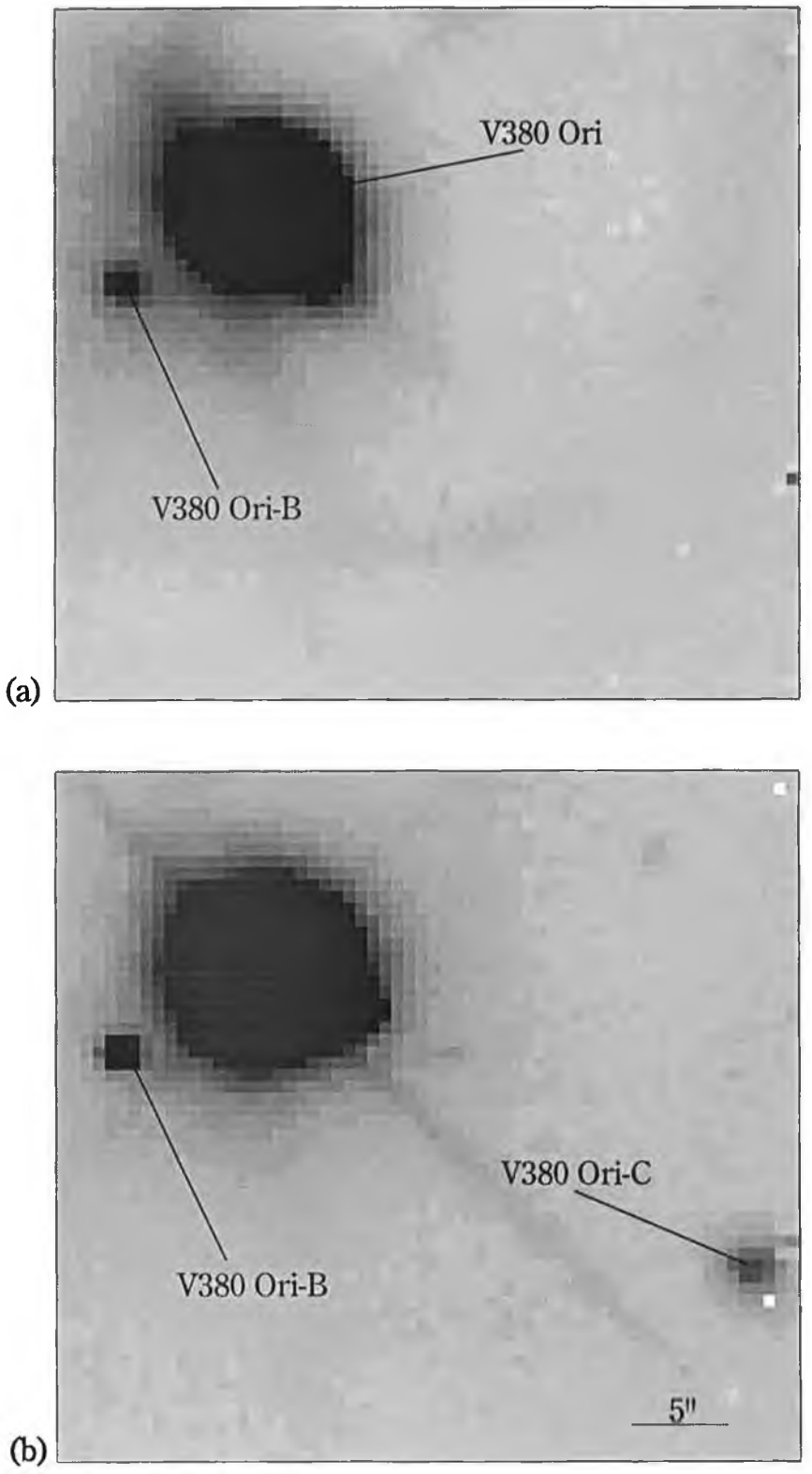

Figure 2.12: (a) A J band image of the region immediately about V380 Ori. The newly discovered infra-red source V380 Ori-B is indicated. (b) A K band image of the same area as in (a). In addition to V380 Ori-B, one notes the diffuse infrared source V380 Ori-C (see text).

2.4 Other Optical Outflows in the Vicinity of V380 Ori

The [SII] and I band images of the region located 5.5' to the southeast of V380 Ori are presented in Figs. 2.13(a) and (b) respectively. Comparing these images, the most striking feature is the amount of filamentary [SII] which is probably due to HH emission (as discussed below). There are in addition to this background at least four distinct optical outflows in the region; these are labelled in Fig. 2.13(a) and include the well known HH 1/HH 2 system, HH 36, HH 130 and a new outflow which will be referred to as HH 147[2]. Some faint knots are also detected south of V838 Ori (as indicated) and these too may be part of an optical outflow.

2.4.1 HH 147

The emission line [SII] and continuum r_{nc} images are displayed for HH 147 in Figs. 2.14(a) and (b) respectively. Clearly seen in the continuum frame are the limb brightened edges of a cone-shaped reflection nebula illuminated at its apex by N^3K50 (see §2.1.4). N^3K50 also appears to drive HH 147, which lies exactly within the conical structure of the reflection nebula. HH 147 appears in fact to be composed of at least three separate emission regions, one of these is bar shaped (labelled A) and lies nearest to N^3K50, while two bright knots (labelled B and C) are also found near the base of the nebula. The [SII]–r_{nc} difference image (see Fig. 2.14(c)) reveals that all components of HH 147 are emission line objects, perhaps best seen in the contour plot of this frame, presented in Fig. 2.14(d). In particular, HH 147 A is somewhat reminiscent of HH 83 (Reipurth 1989b). The outflow component is actually T-shaped (see Fig. 2.14(c)), with its axis (approximate length 9") directed towards N^3K50; further evidence that this star is the source of the optical outflow. HH 147 B is by far the brightest of the knot structures and is connected by an arc of weaker HH emission to HH 147 C.

Marked in the contour plot, is the the slit position passing through N^3K50 and the edges of HH147 A and B. In each case, the spectrum was summed spatially owing to

[2]This number has been assigned

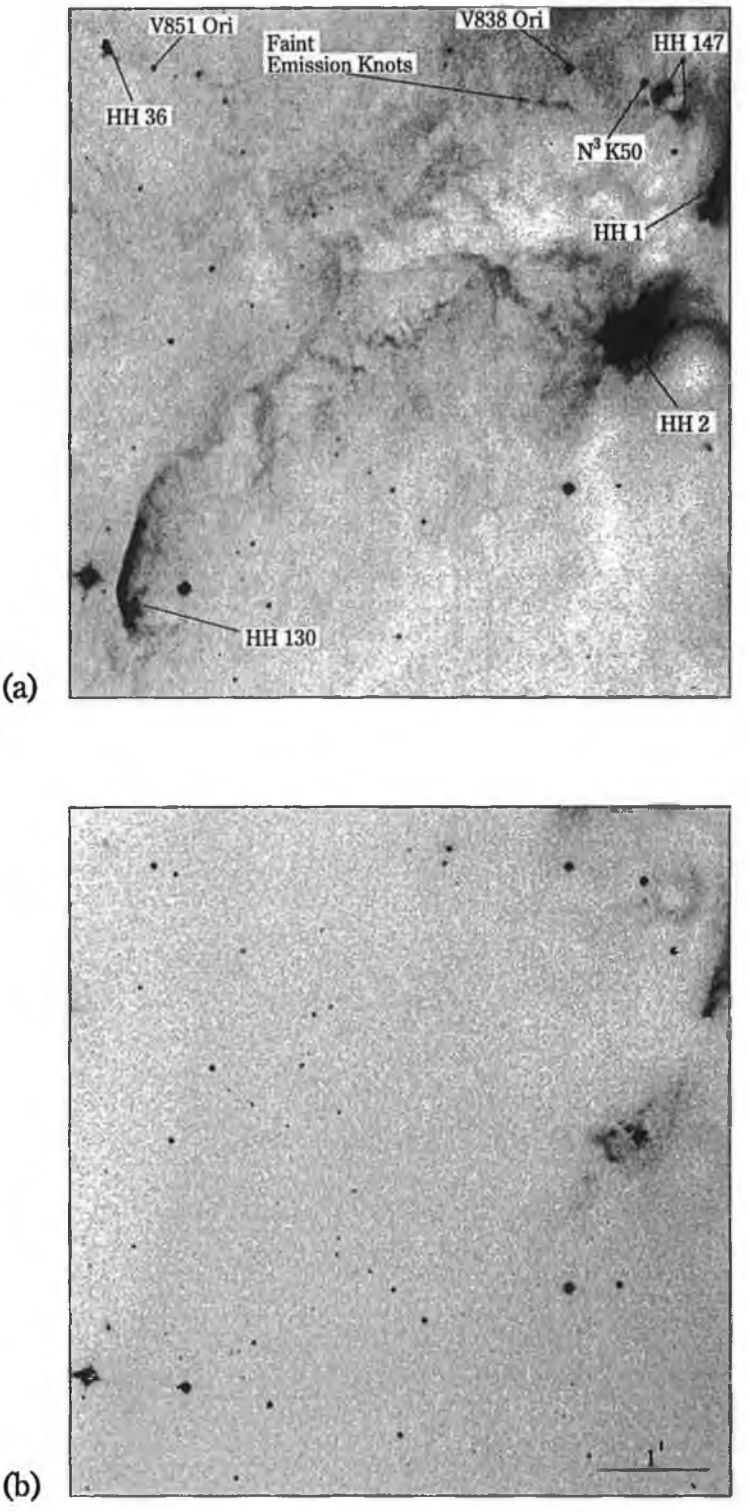

Figure 2.13: (a) A [SII] image of the region 5.5' to the southeast of V380 Ori. Within the image are at least 5 distinct optical outflows including the well known HH 1/HH 2 system. Also marked are the stars V851 Ori, and N^3K50, which are considered to be candidate sources for the HH 36 and HH 147 outflows. (b) An I band image of the same area as in (a). Comparison of (a) and (b) clearly reveals the optical outflows as [SII] emission.

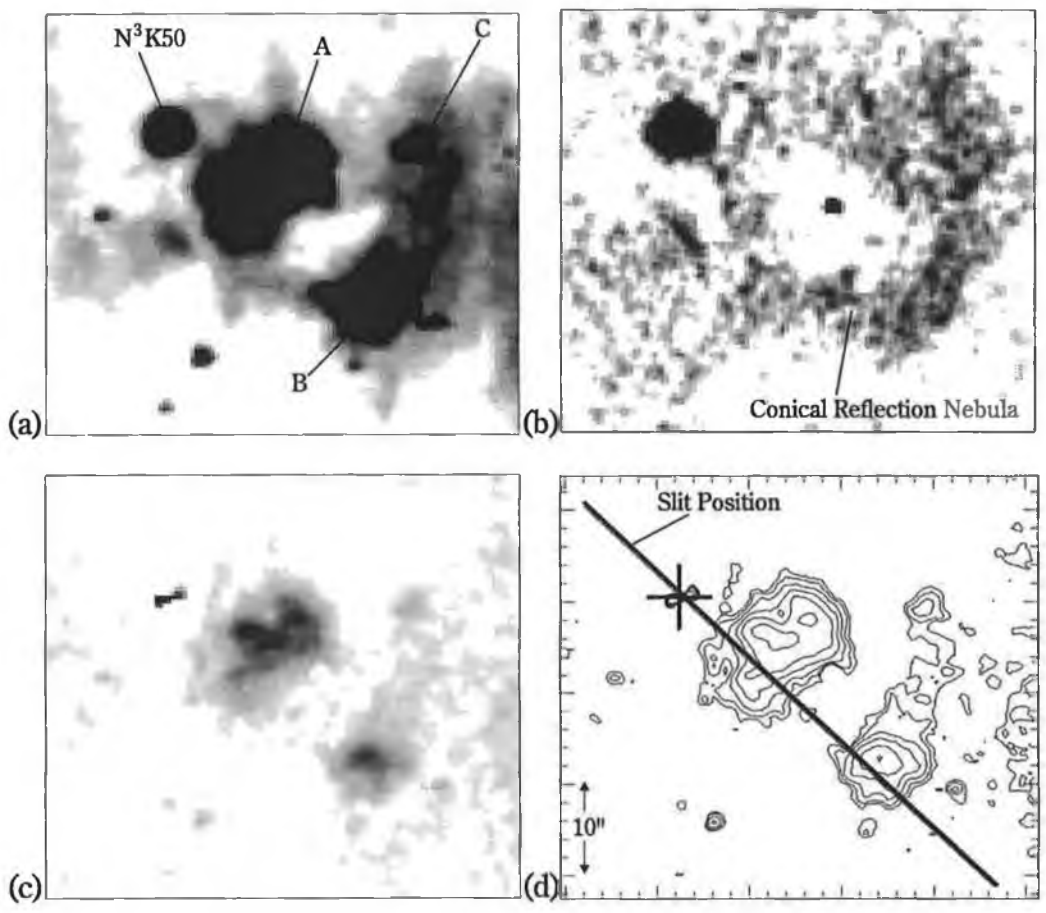

Figure 2.14: (a) A [SII] image of the newly discovered optical outflow HH 147, in which its brightest knots (A, B and C) and presumed source (N^3K50) are labelled. (b) The same area in (a) but through the r_{nc} filter where one sees a conical reflection nebula. (c) A difference frame of the [SII] and r_{nc} images (i.e. [SII]–r_{nc}), showing the morphology of HH 147 and its components. (d) A contour plot of the [SII]–r_{nc} difference frame, in which the slit position used for spectroscopy is indicated. N^3K50 is also marked by a plus sign (+) for reference purposes.

the weak signal to noise of the observation and both HH 147 A and B were found to be HH objects as expected. HH 147 A has a low electron density (300 cm^{-3}), and in its average spectrum the Hα profile is unresolved. An estimate can be made of its excitation ratio (Hα/[SII]λ6716+6731 $\leq$ 0.4) the value found being characteristically low (see §2.3.3 for comparison). In contrast, HH 147 B, although of similar electron density (n_e = 200 cm^{-3}) has a higher excitation ratio (approximately 1). For both objects the radial velocity is low, so low in fact that their motion must be close to the plane of the sky. There does seem to be however, a marginal increase in radial velocity from HH 147 A to HH 147 B (v_{HEL} = -10 to -60 km s^{-1}). Proper motions have also been measured for these objects (Eislöffel, private communication), both are directed away from N^3K50, unequivocal evidence that this is indeed their source. For HH 147 B the tangential velocity is 200 km s^{-1}, while in the case of HH 147 A a velocity is measured for the entire object of 315 km s^{-1}. A calculation of the spatial velocity of these objects then clearly reveals a deceleration from HH 147 A to HH 147 B (315 km s^{-1} to 210 km s^{-1}) i.e. with increasing distance from the source.

The spectrum of N^3K50 between (6530–6745Å) is shown in Fig. 2.15. The most distinctive feature (seen for the first time) is the presence of a classic Beals Type I P-Cygni profile in the Hα emission line. As mentioned earlier, N^3K50 has been classified as a T-Tauri star (§2.1.4) and occurrences of such P-Cygni profiles are known to be rare amongst the T-Tauri class (see Appenzeller and Mundt 1989). Using the full extent of the absorption dip to the Hα emission peak, it is possible to estimate the stellar wind velocity and this is found to be 430 km s^{-1}. It is noteworthy that the stellar wind is greater than the highest tangential velocities of the associated HH objects. Also detected within the spectrum is the presence of the [SII] doublet, and the radial velocity of these lines is v_{HEL} = -40 km s^{-1}. Since the molecular cloud in the region is known to have a heliocentric radial velocity of +26 km s^{-1}, the [SII] lines are blueshifted as expected (the presence of only blueshifted forbidden line emission is usually regarded as evidence for disks, see for example Edwards *et al.* 1993). It is interesting that the electron density as determined from the [SII] doublet is found to be 34000cm^{-3}, much higher than in the HH objects, and this is probably due to the convergence of the optical outflow close to the star.

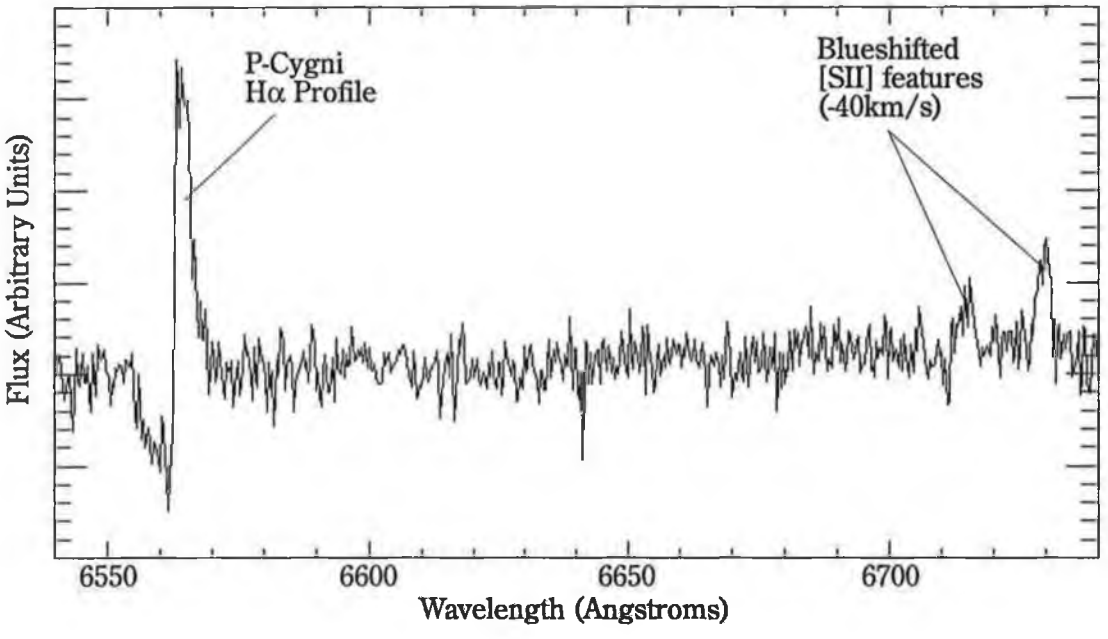

Figure 2.15: The spectrum of N^3K50. Note the characteristic Beals Type I P-Cygni profile in the Hα line, clear evidence for a stellar wind. The blueshifted red [SII] doublet is also marked and suggests the presence of a circumstellar disk (see text).

Finally there is no direct association of the HH 147 outflow with the nearby HH 1/HH 2 system. Eislöffel (private communication) has indicated that there maybe a second outflow overlapping the HH 1/HH 2 system but again the proper motion data implies that it is independent of HH 147.

2.4.2 HH 130 and HH 36

The most striking feature of the [SII] image presented in Fig. 2.13(a) is HH 130 shown at higher contrast in Fig. 2.16. On examination, HH 130 is seen to be extended over a length of some 5'. If one then assumes a distance to the region of 460pc, its projected size of 0.7pc makes it one of the largest optical outflows known (see Mundt *et al.* 1987). The brightest part of HH 130 is the arc of emission located in the southeast corner of the frame, the appearance of which resembles a partial bow shock. The majority of the optical outflow is however, comprised of fainter emission, which extends both from the western wing of the bow-shaped object, and also along its presumed central axis. One notes that along the central axis several emission knots can be seen. These knots are spaced over the entire extent of HH 130 and are identified by the sequence of letters a-g in Fig. 2.16. Of particular interest, however, is that with the exception of (f) the remaining knots have a filamentary structure and are reminiscent of similar features observed in the optical outflow of ZCMa (Poetzel *et al.* 1989). The best examples of these filaments are associated with knots (b) and (d) which can be clearly seen to bridge the region between the central axis and the extended wing. The same is also true for knot (a) which for reasons of contrast is best seen in Fig. 2.13. Indeed most knots appears to extend west of the central axis, and this gives the appearance that only one half of HH 130 is visible. Knot (g) in contrast, or more correctly its component labelled (g1), is arc shaped and unlike other filaments, it is positioned almost symmetrically about the central axis.

In Fig. 2.17, a contour plot of the brightest part of the bow-shaped object HH 130 is presented together with the slit positions used for the spectroscopy. These spectra verified the HH nature of this object independently from the work of Ogura and Walsh (1991). Of the two slit positions used, the first (at P.A. 50°) encountered the head of the object and one of the filaments (a), while the second, positioned some 20" to the

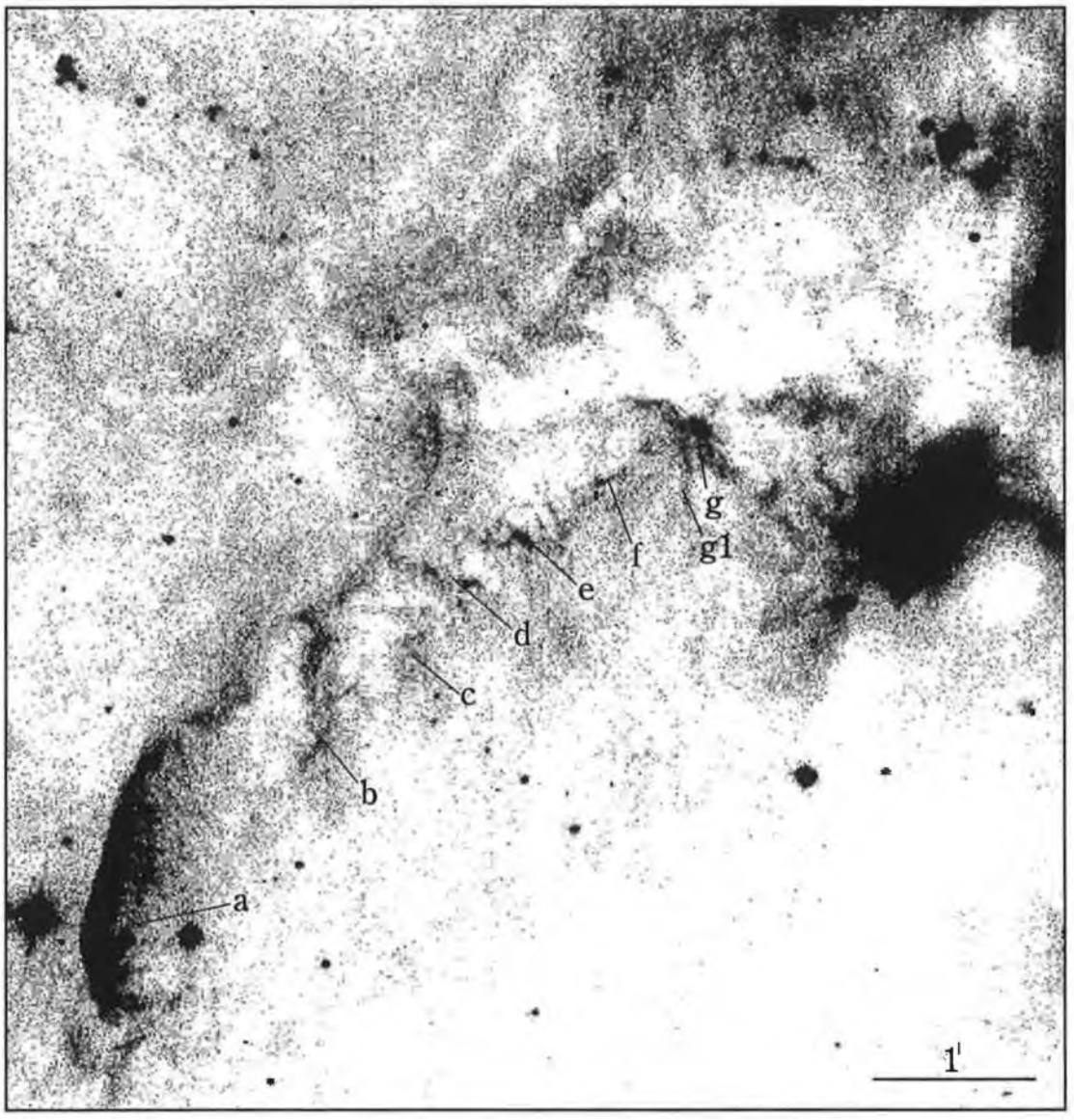

Figure 2.16: A [SII] image of the region 5.5' to the southeast of V380 Ori, as in Fig. 2.12(a) but at higher contrast. One notes that HH 130 in addition to its known bright arc of emission, is seen here to have a highly extended and previously undetected filamentary structure. Several bright knots are seen along the presumed axis of HH 130 and are labelled a-g. Of particular interest is the faint knot g1, which appears bow shaped.

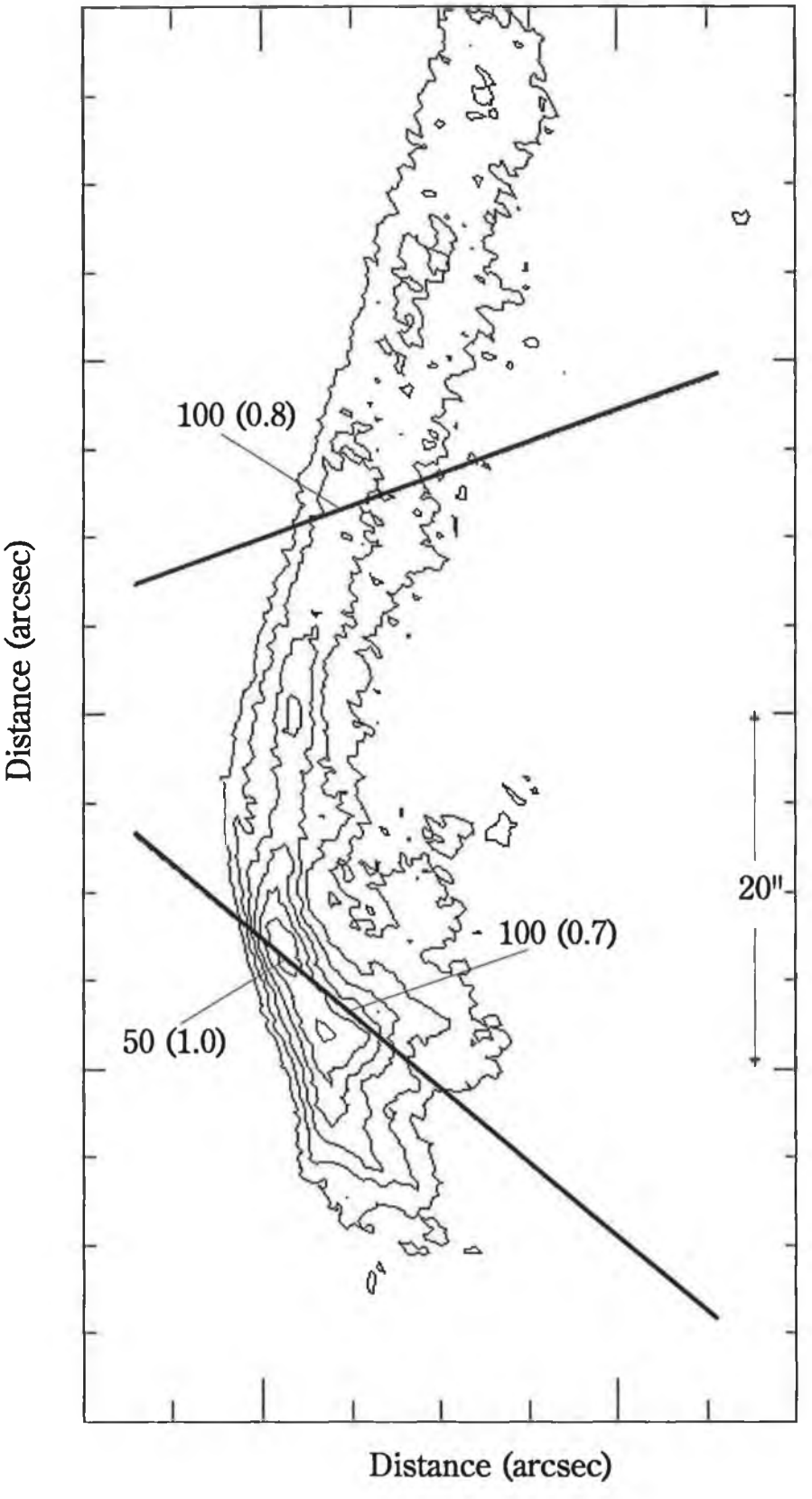

Figure 2.17: A contour plot of the bright arc of HH 130 with the slit positions marked. Electron densities are shown for a number of features and excitation values (Hα/[SII]λ6716+6731) are quoted in brackets.

north (at P.A. 110°), provided a cross-section of the bow-shaped object's wing. For both spectra, the position-wavelength diagrams revealed a knotty structure and an example of this is given (for P.A. 50°) in Fig. 2.18. Only in the case of large scale features, namely the head and wing of the bow shaped object and filament (a), were measurements made of the average electron density and excitation ratio (Hα/[SII]λ6716+6731). Comparison of the results reveal that the electron density, irrespective of the slit position has consistently the same low value ($\leq$ 100cm^{-3}). A similar electron density (100cm^{-3}) was also determined for the head of the bow-shaped object by Ogura and Walsh (1991). Although only marginal changes are found for the excitation ratio, nevertheless, one notes that the highest value occurs at the head of the object (1.0) and this is seen to decrease both further along the wing (0.8) and towards the east in filament (a) (0.7). The V_{HEL} for all line emission is close to +20 km s^{-1}.

Finally, in Fig. 2.19 we show the [SII] image of HH36. Very little is known about this outflow since its original discovery by Herbig (1974). In the image presented here, additional HH knots are observed and the optical outflow appears to be centered on V851 Ori.

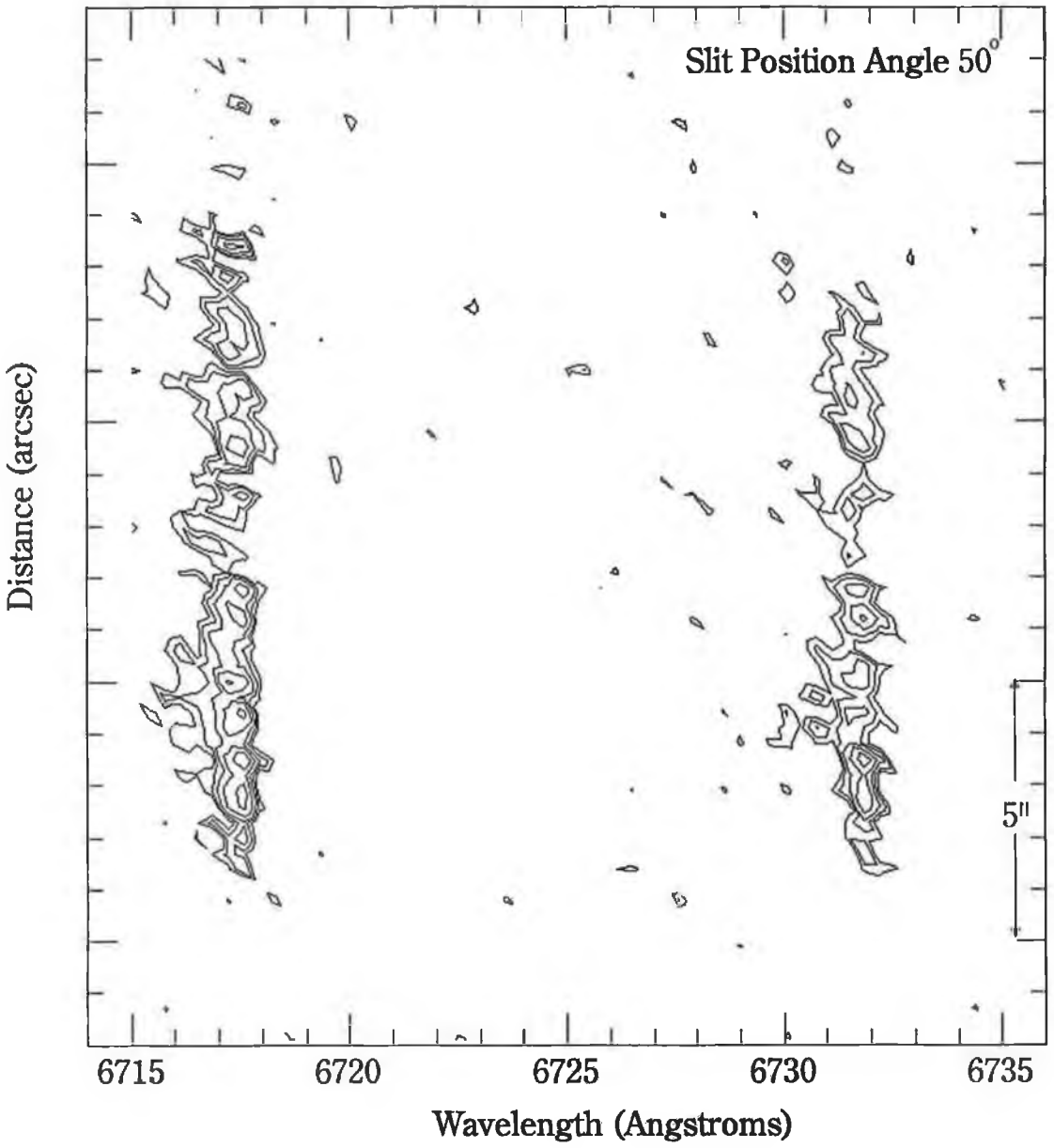

Figure 2.18: A position-wavelength diagram for HH 130 from the INT observation at P.A. 50°. Note its extremely knotty structure.

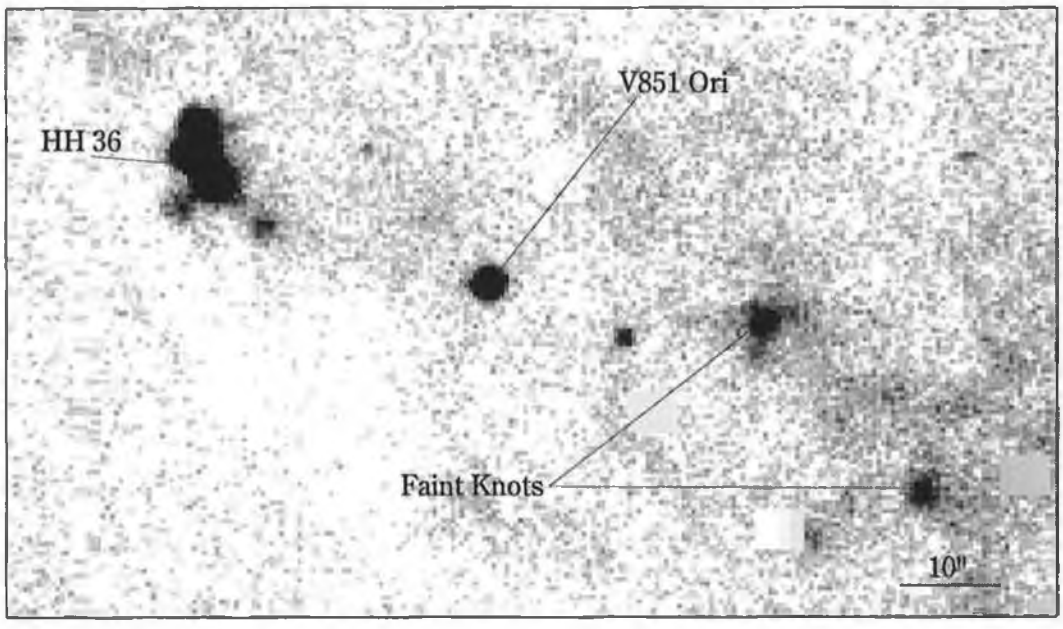

Figure 2.19: A [SII] image of the region about HH 36. Several faint knots are seen, and the entire outflow appears centered on V851 Ori.

2.5 Discussion

2.5.1 The Possible Outflow Sources in NGC 1999

As mentioned previously, by far the most striking emission line feature in the region near V380 Ori is the "loop" structure, traced in Hα to the west of NGC 1999 and seen closer to V380 Ori in [SII] line emission. From its structure alone, one is tempted to argue that it originates from a poorly collimated wind. Implicit in this explanation, however, is the assumption that a single YSO is responsible, but, as pointed out earlier, in addition to V380 Ori there are a number of K band sources in its vicinity (see §2.3.5). These could be optically obscured young stars, and if such are potential sources of any outflow. This possibility is examined briefly here.

V380 Ori-B is fainter in both the J and K bands than V380 Ori itself by some 7 mag. If this companion was a YSO of comparable luminosity to V380 Ori, one might explain its lower magnitudes as a result of extinction, i.e, if it was more deeply embedded within its parent molecular cloud. In this case, however, one would expect the object to have been detected by IRAS. In fact, V380 Ori-B lies just outside the positional uncertainty of the IRAS point source (05339-0644), while V380 Ori is located within 2" from the centre of the uncertainty ellipse (see Fig. 2.20). It is most likely therefore, that the IRAS point source is associated with V380 Ori alone, and that its companion source is of considerably lower luminosity.

As for the other near infrared object, V380 Ori-C, it is clearly outside the uncertainty ellipse of 05339-0644 and is in fact most likely not a YSO. It was noted earlier that this object is only detected in the K band. If V380 Ori-C was stellar in origin, its absence in J would then have to be explained by a very high degree of extinction but another possibility is that it simply has no emission in the J band. Instead, one notes that the 2.12μm emission line of shocked molecular H_2, lies within the bandpass of the K filter i.e. this object could be a shocked H_2 knot within the outflow. Certainly, its diffuse morphology (see Fig. 2.12) is consistent with such an interpretation. Moreover the object's location, situated close to the known HH objects in the southern component

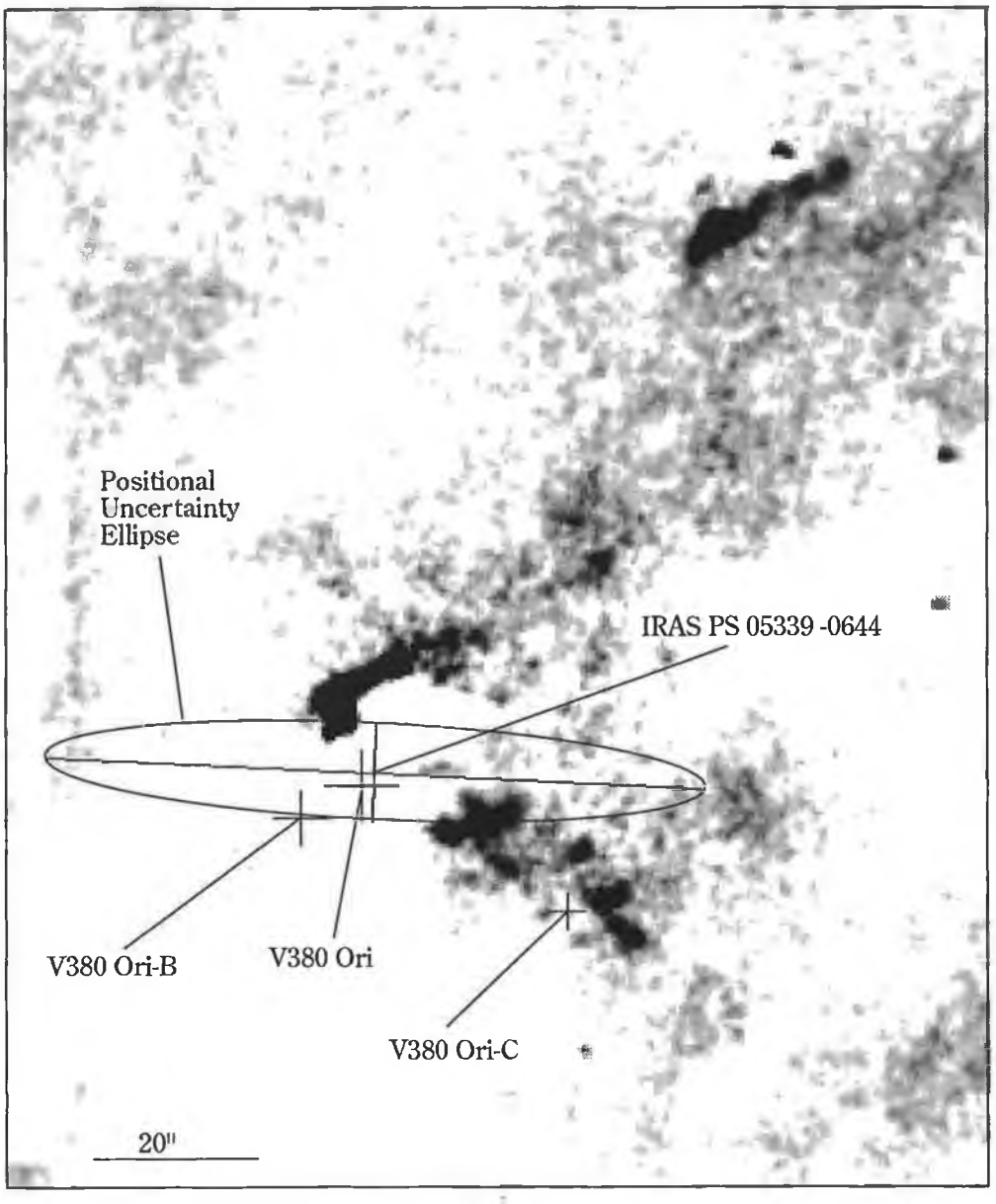

Figure 2.20: An extract from the [SII] image of V380 Ori. The IRAS point source 05339 -0644 is marked together with its positional uncertainty ellipse. Also indicated is V380 Ori and the two near infrared objects V380 Ori-B and V380 Ori-C. Note that both of the infrared objects lie outside the positional uncertainty of the IRAS point source, but that V380 Ori lies close to its center (see text).

of the "loop" (see Fig. 2.3 (c)), would further substantiate such a claim; optical HH emission is known to be spatially associated with molecular H_2 emission in many cases (see for example Lane 1989).

The emission line "loop" appears therefore to originate from V380 Ori. Moreover, this YSO seems, from the [SII]–r_{nc} difference image (see Fig. 2.3 (c)), better positioned to drive such an optical outflow. There also appears to be, on the basis of 2D imaging polarimetry and the nebula's spectrum, no question that V380 Ori illuminates NGC 1999 (see Warren-Smith *et al.* 1980 and Herbig 1960 respectively). In most cases where HH emission is found in the vicinity of a reflection nebula, the driving source of that HH emission is also the illuminating source of the nebula e.g. R Mon (Strom *et al.* 1986 and references therein), PV Cep (Neckel *et al.* 1987). For all these reasons, it will be henceforth assumed that V380 Ori is most likely the source of the "loop".

2.5.2 The Geometry and Orientation of the Outflow from V380 Ori

In addition to the optical outflow of V380 Ori, there is, of course, its well known molecular outflow, the most recent maps of which have been published by Levreault (1988), and at a better sampling rate by Morgan *et al.* (1991). One of the most interesting features about this outflow is that only its red lobe is apparent. Such a characteristic can be easily understood if the outflow source lies at the edge of its parent molecular cloud; in this case only the swept up CO within the cloud itself would have sufficient density to be detected. The absence of the blue CO lobe could then be explained by the blue shifted outflow moving into the lower density medium outside the cloud. Even so, the blueshifted wind might still be detectable by using another tracer such as shocked optical emission. In Fig. 2.21, the ^{12}CO map of Morgan *et al.* (1991), is reproduced together with the optical emission features discovered here. What is immediately obvious is the way the optical outflow compliments its molecular counterpart; to the west of V380 Ori lies the red CO lobe, while to the east lies the optical emission "loop".

The geometry of the outflow, (see Fig. 2.21), shows a simple east–west orientation, with V380 Ori and NGC 1999 located at its center. In addition, it is considered here that

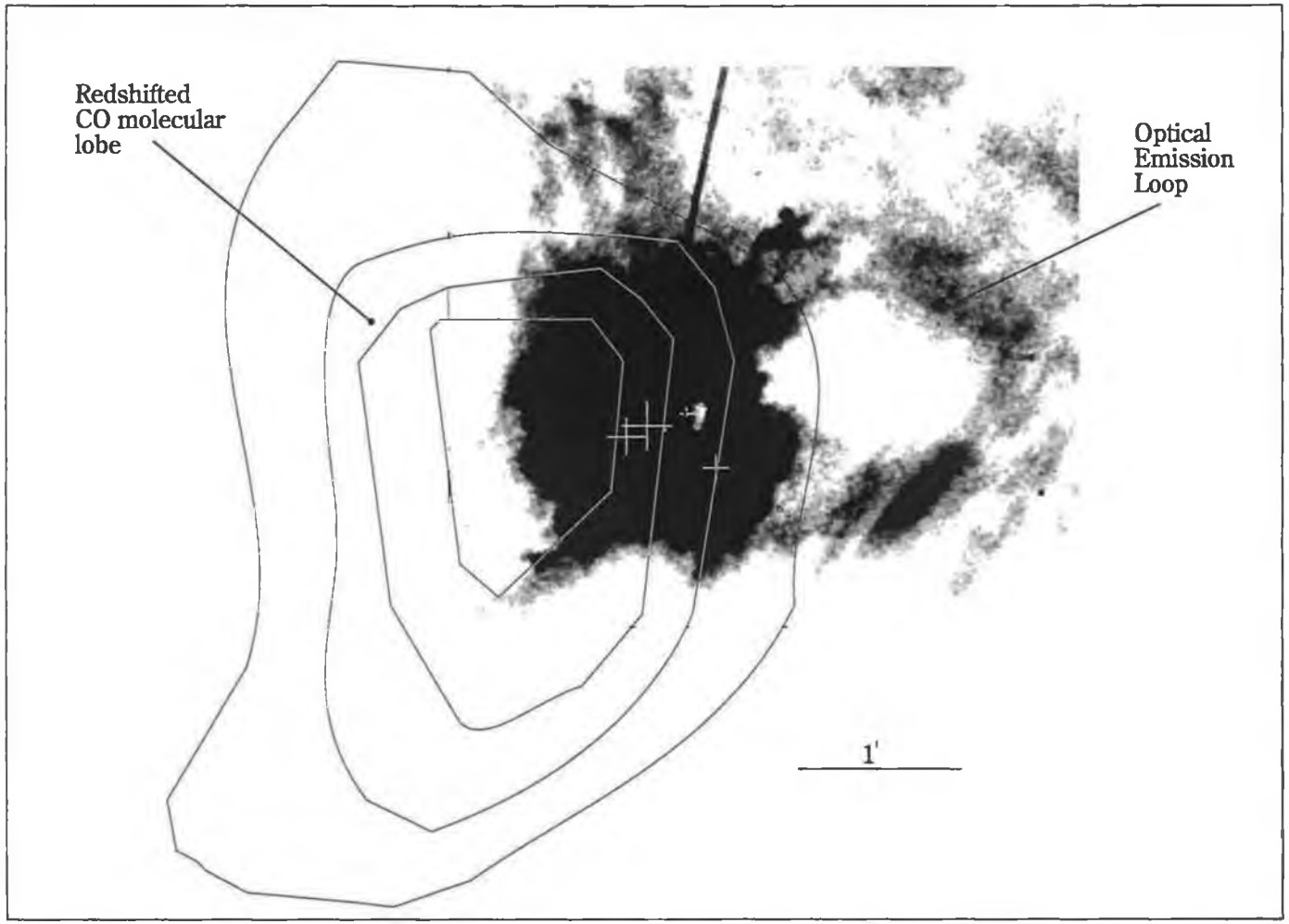

Figure 2.21: A schematic showing the redshifted CO molecular lobe (taken from Morgan *et al.* 1991), together with the optical emission "loop" discovered here. The distribution of redshifted CO to the east of V380 Ori and the optical emission loop to its west reveals the bipolar nature of the outflow (see text).

the principal flow direction is not only east–west, but lies close to the plane of the sky as for example is the case for HH 147 (see §2.4.1). Indeed, for at least HH 35 and Knot B, part of V380 Ori's optical outflow, radial velocities are found to be so low (see §2.3.3) that their motion must be virtually perpendicular to the line of sight. Examination of the radial velocity for the molecular outflow suggests a similar scenario, for example, in the red lobe of V380 Ori Levreault (1988) measured a maximum radial velocity of 10 km s^{-1}. Such a value is small when compared to typical radial velocities of molecular outflows (see Bachiller and Gómez–González 1992).

With the outflow axis lying close to the plane of the sky, it is also possible to understand the reflected Hα component in the nebula NGC 1999 (see §2.3.4). As mentioned previously, while at the star the Hα profile is broad and symmetric; within the nebula it has an apparent "redwing", the extent of which from the central peak to the background level is about 270 km s^{-1}. The key to understanding this, is that the presence of a "redwing" here is equally well described by the absence of a blue counterpart, which of course suggests P-Cygni absorption in a wind. With this in mind, it is proposed that when looking at V380 Ori and the nebula, one views two different lines of sight towards the star. The wind from V380 Ori is expected to be non-isotropic and is presumably collimated in the direction of the outflow. If indeed, the outflow/wind axis lies in the plane of the sky, the broad Hα profile will be unaffected when looking directly at the star. However, surrounding gas and dust in NGC 1999, could mirror the view seen within the lobes of the outflow, and so here the cooler gas of the wind would be seen through P-Cygni absorption.

2.5.3 A Model for the Outflow of V380 Ori

It has been shown that V380 Ori is most likely the source of a bipolar outflow, the principal axis of which lies close to the plane of the sky. The "loop" is naturally interpreted as tracing the edges of an oval-shaped cavity and the formation of such cavities have been examined by a number of authors including Cantó (1980), Barral and Cantó (1981), Eichler (1982) and Königl (1982).

According to the model of Cantó (1980), the wind from a young star can, in the presence of a pressure gradient, produce an oval shaped "cavity" elongated in the direction of the gradient. Cantó (1980) suggested the wind both drives shocks into and is shocked by the ambient medium. Wind impacting on the edges of the cavity does so mostly at oblique angles, so that the normal component of the wind to the shock interface is greatly reduced while the tangential component is unaffected. In this manner, a supersonic flow occurs in the postshock region along the cavity walls, and the centrifugal pressure of this flow combined with the ram pressure of the wind serves to balance the external ambient pressure. As the ram pressure decreases with distance from the source the ambient medium eventually causes the flow to bend back on itself forming the characteristic oval shape. Cantó (1980) assumed a single pressure gradient caused by the presence of the star at the edge of a molecular cloud, with the result that only a single cavity was formed. In the case of V380 Ori, the outflow is clearly bipolar (see Fig. 2.21) so this is an unlikely scenario. However, in a subsequent paper, Barral and Cantó (1981) examined the formation of bipolar cavities by supposing the star was embedded in a self gravitating interstellar disk, surrounded by a medium of constant pressure.

There are many difficulties with the momentum driven models of Cantó (1980) and Barral and Cantó (1981). The largest of these is however, that they predict that the flow along the cavity edges will terminate at the apex of the cavity with an enormous shock e.g. Cantó (1980) suggests that 40% of the wind mechanical luminosity could be deposited there. Clearly, in the emission "loop" east of V380 Ori (see Fig. 2.2) such a bright shock is not seen. Smith (1986) has extended these models by considering a more realistic circumstellar disk surrounding the young star. The suggestion is that the oblique shock at the beginning of the cavity, arises at the surface of this disk and possible outflow configurations are considered for a number of external pressure gradients ($P \propto r^{-n}$). For constant pressure, Smith (1986) finds essentially the same result as in the earlier models. However, for $1 < n < 2$, a weaker termination shock is expected, as the cavity appears more candle-shaped. Even so, such a model is still not applicable here since the predicted cavity shape is inconsistent with the observations (the emission "loop" is elliptical rather than candle-shaped).

Cantó (1980) and Smith (1986) have explored an alternative scenario, in which the cavity is formed by the wind pressure alone. Close to the source, one will still obtain oblique shocks, and a flow along the cavity walls, but further away the wind will be brought into pressure balance with the ambient medium through a spherical shock front i.e. a shape more consistent with the observations. From Smith (1986) one finds that such a model is most applicable where $n < 1$, and although it appears that the expected pressure gradient is shallow, one notes that Harvey *et al.* (1979) calculated a density gradient for the immediate region about V380 Ori of $n \propto r^{-1}$ ($r = .01$ to $11''$). Indeed, recently, Natta *et al.* (1993) have pointed out that both low and high density gradients are found in the surrounding environments of HAEBESs, e.g. R Mon ($n \propto r^{-0.7}$).

Based on the presence of a supersonic flow along the cavity edges it is now possible to explain the observed HH objects close to V380 Ori, in particular their radial velocity trends as seen in the results (§2.3.3). There are in fact two main trends; both blueward and redward radial velocity HH objects appear spatially separated, blue radial velocities are located north and west of V380 Ori, while red velocities are found in the southern part of the "loop". In both cases, the radial velocity is seen to decrease dramatically with increasing distance from the star. This decrease could be explained by a line of sight effect: the suggestion is that as one moves closer to the star, the north of the "loop" moves more towards the observer, while the southern portion recedes; this is illustrated in Fig. 2.22. The large radial velocities closest to the source i.e., C1 ($+350\,\mathrm{km\ s^{-1}}$) and F1 ($> -210\,\mathrm{km\ s^{-1}}$) could then be a consequence of simply a large opening angle in the cavity. As to the presence of the HH object F1 lying 4" east of V380 Ori, this might result from a projection effect, for example if the axis of the outflow was not exactly in the plane of the sky. Alternatively, it may be part of the counterflow, the remainder of which is optically hidden by the molecular cloud.

There is a problem in applying the spherical shock model discussed above. The highest electron densities are found in the HH objects furthest from V380 Ori, namely HH 35a and object B. This implies either a proportionately higher shock velocity and/or higher wind density further from the star. As the cavity expands the wind density should fall off, so one should not expect higher densities further out. The alternative explanation, in that the higher electron densities are due to larger shock velocities, seems

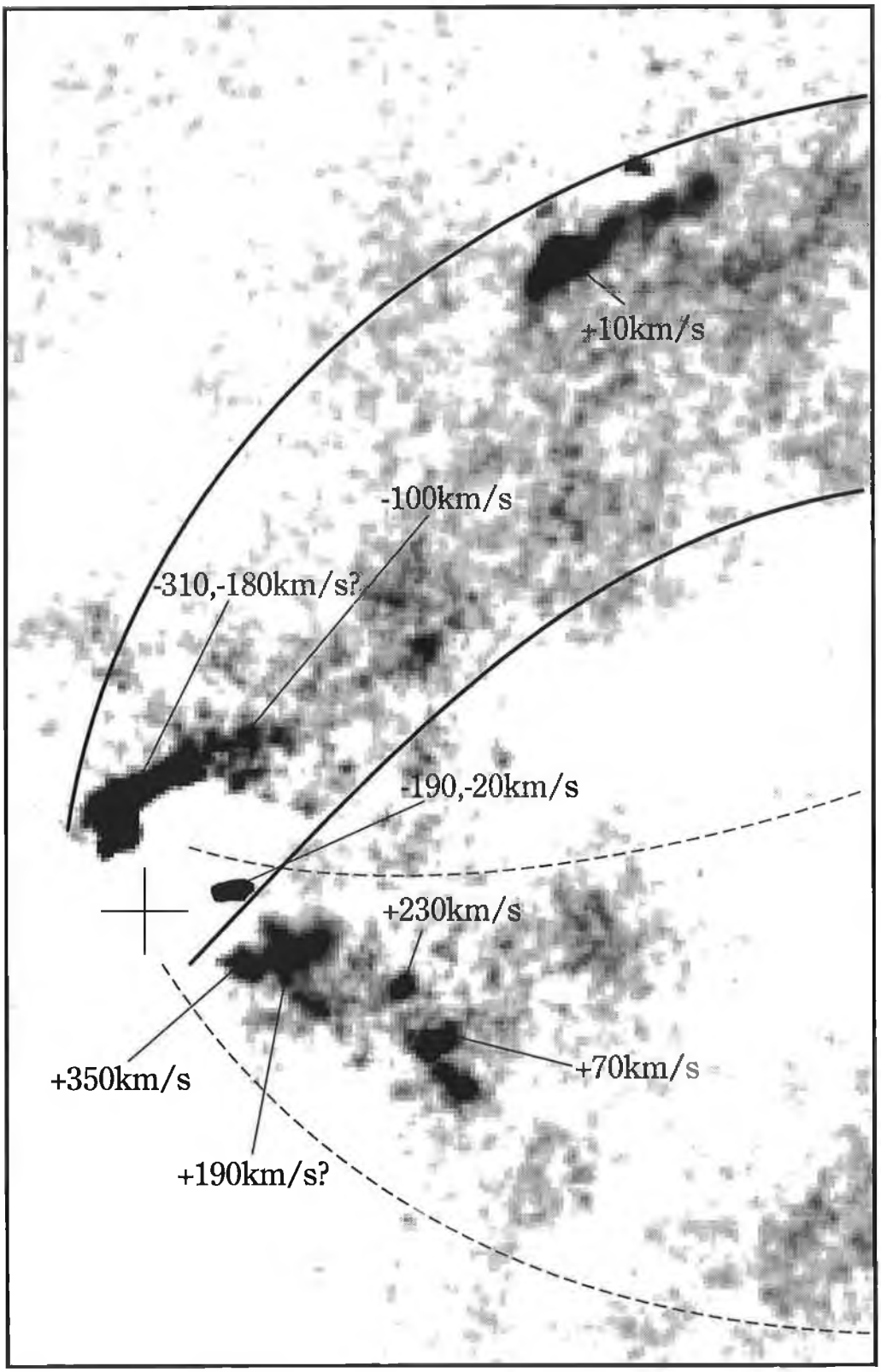

Figure 2.22: A schematic of the HH emission in the near vicinity of V380 Ori (+), which illustrates how the objects in the north of the loop move towards the observer and those in the south recede. A question mark indicates uncertainty in a velocity owing to poor spectral signal to noise.

also unrealistic, since there is no evidence for this in either the linewidths or excitation of either HH 35a or Object B.

For the outer objects I, J and K their exact nature seems also unclear. It is uncertain for example whether they are indeed HH objects, although, almost certainly the features outline the edge of the wind blown cavity. In the model discussed above it seems possible at least, that they are part of the outer spherical shock front. This however is by no means a unique explanation, they could for example arise from gas which is collected along the edges of the cavity, and might be weakly ionised, i.e they might form part of the weak HII region which is known to extend over the entire area (see §2.3.4). If partially ionised, it might explain why I and J are apparently aligned parallel to the large scale magnetic field (see §2.3.1), being due to magnetic pressure.

In light of the difficulties found with the present cavity model, it is worth considering an alternative explanation. At some time in the past V380 Ori, might have gone through an extremely active outburst (perhaps akin to the FU Orionis phenomenon). A bipolar outflow was produced which moved ballistically into the surrounding medium. Given the high contrast in densities expected inside and outside the molecular cloud, this would explain the apparent similarities in the size of the molecular outflow and the optical emission "loop" (see Fig. 2.21). Such wind blown cavities would have formed in a dynamical time scale τ_D of order L/V where L is a characteristic length for the cavity and V is the wind velocity. Since the outflow is time variable, at some point the wind would have essentially been switched off. The cloud would then collapse at a rate of L/C, where C is the sound speed of the medium.

The present wind velocity from V380 Ori can be estimated from the P-Cygni profile in the nebular Hα component, together with the stellar Hα profile. It is found to be 360 km s^{-1} which is close to the highest radial velocity measured for a HH object (+350 km s^{-1} for Object C1). Using this as indicative of V, a value of 5 km s^{-1} for C (of the order of the CO molecular linewidth in the region), and with a cavity length of 0.3pc, one finds that the dynamical lifetime is approximately 10^3 years. It would take however some 10^5 years before the cavity would be completely collapsed, which is comparable to the age of a HAEBES (Palla and Stahler 1993). It is possible therefore

that the observed optical emission "loop" and molecular outflow could be the remnants of a previous outburst from V380 Ori. In this sense it would be easier to understand the emission line nature of I, J and K in terms of residual gas that has collected along the cavity walls, and which is weakly ionised as proposed above. The low radial velocities found for the molecular outflow would also be accounted for, as it is no longer being supplied by a high mass, high velocity wind and because its motion is in the plane of the sky. As to the HH emission seen close to the star, this may simply be the result of the present wind impacting off the existing cavity. Indeed this wind may perhaps be due to a new outburst from the star (but see §5.1). The above interpretation of the directional change for the radial velocities, might still be correct, however, as a further advantage it would not require high excitations for the furthest HH objects. Moreover, variability could also explain the higher densities at the largest distance from V380 Ori.

One difficulty not addressed so far, is that of the faint extended features seen to the north of NGC 1999. These features were briefly mentioned in §2.3.1 and are observed in both the Hα and the [SII]–r_{nc} difference frames (see Figs. 2.2 (a) and 2.3 (b) & (c) respectively). If, as appears to be the case, they are brighter in Hα than [SII], then they are presumably of relatively high excitation. The morphology of these objects, namely four bright knots, situated at the ends of weak trails of emission connected to NGC 1999, argues for their association with this nebula. Indeed, the bright knots at the end of the trails might suggest the termination point or working surface of ejecta, the source of which would presumably lie within the nebula. As pointed out earlier, V380 Ori is likely to be the most luminous source in NGC 1999 and thus it is the most likely candidate for the source of these outflows. One notes in this respect that these objects are coincident with the north–eastern edge of the molecular outflow and are perhaps related. Moreover, the bright knots if they are indeed ejecta, would mark the highest density regions of the optical outflow in this direction, indicating that like the outflow west of V380 Ori, the highest densities are associated with the HH objects furthest from this star.

2.5.4 The Spectrum of V380 Ori

It is interesting to note that, Herbig (1960) when examining the spectra of V380 Ori remarked *"The bright line spectrum of V380 Ori is much like those of advanced T-Tauri stars, except in certain details...."*. The details which were referred to, were the weaker emission lines of FeI and other neutral metals in comparison to "advanced" T-Tauri stars i.e. T-Tauri stars with a spectral type of G. Herbig (1960) thus seemed to suggest some uncertainty with regard to V380 Ori's classification. Indeed, contrary to what one might expect in a Herbig Ae/Be star, he noted the marginal presence of the FeIλ4063 emission line in V380 Ori's spectrum: this satisfies at least one of the spectral criteria for its inclusion in the T-Tauri class (Appenzeller and Mundt 1989). Indeed, HPa also suggest the spectra of V380 Ori is very similar to that of the CTTSs.

The presence of the Liλ6708 and FeI absorption lines from the spectra presented here show that, a spectral type of later than F0 would be more appropriate, i.e. V380 Ori is in fact a T-Tauri star, assuming of course that these features are photospheric. In this respect, it has already been mentioned that the absorption features could arise in a different manner, perhaps in a cooler region outside the star. It is stressed however, that the absorption lines were found to be extremely weak (their measured equivalent widths being less than 60mÅ) exactly, what one would expect in the photospheric spectrum of a T-Tauri star which is heavily veiled (see Appenzeller and Mundt 1989 and references therein). Moreover many of the absorption features are resolved and have similar values for the $FWHM_c$ (see table 2.4): this is in stark contrast to the central absorption of the HeI line which being unresolved is best interpreted as arising from a cooler stationary region outside the star.

As regards the derived bolometric luminosity of the star of 80–300 $L_\odot$(see §2.1), although this appears rather high for a T-Tauri star, one notes that luminosity estimates require amongst other things an accurate knowledge of the spectral type, and the local extinction, the latter of which is also poorly known (but see also Strom *et al.* 1989). Moreover, it is possible that much of the luminosity could simply derive from an active disk. Lastly, it is worth pointing out that V380 Ori could still be a HAEBES in spite of its apparently cooler photosphere. In the recent models of Palla and Stahler (1993),

it was predicted that deuterium shell burning could last in such stars, for a substantial part of their lifetime, but most importantly during this phase, the photosphere would have the appearance of a cooler F or G type star.

2.5.5 Other Optical Outflows: HH 147

The newly discovered optical outflow, HH 147, is particularly interesting in that its source N^3K 50 is one of the few T-Tauri stars known to exhibit a classical Type I, P-Cygni profile. As mentioned earlier occurrences of such a profile in T-Tauri stars are rare. In fact, only six such stars are known amongst the T-Tauri class and of these, only one is previously known to be associated with an optical outflow, AS 353A (Appenzeller and Mundt 1989).

The most likely explanation of the N^3K50 conical nebula, is that it results from a wind blown cavity seen almost edge on. Certainly, the cavity axis would be expected to lie in the plane of the sky as indicated by the proper motion and radial velocity measurements of HH 147. A poorly collimated wind is also required to explain HH 147 B and C seen near the base of the nebula, but located at its edges. There is also however, some evidence for a more highly collimated outflow i.e. a jet linking HH 147 A to N^3K50. Moreover, one notes that this jet lies close to the axis of the nebula as in R Mon, I548C27, HH 34-IRS, and Haro 6-5B (see Mundt *et al.* 1987 and references therein). Lastly, as mentioned earlier, HH 147 A has a shape reminiscent of HH 83 (Reipurth 1989b). However, there is one particularly striking difference, whereas HH 147 A is entirely HH emission, HH 83 actually refers to a jet and reflection nebulosity (see also Rolph *et al.* 1990).

2.5.6 Other Optical Outflows: HH 130

It is clear from the observations presented here (see Fig. 2.16) that the earlier images of HH 130 (Reipurth 1985, Ogura and Walsh 1991) revealed only the brightest part of a much more extended (some 0.7pc) optical outflow. Ogura and Walsh (1991) have stated that HH 130 may be related to HH 1/HH 2, but the new observations suggest it is instead

a separate outflow. HH 130 is almost certainly a bow shock, and a jet (or the remnants of one) can be seen running along the principal outflow axis. This outflow however, at the closest separation to HH 2 is still at least 1' distant.

That the apparent bow-shock is only partially observed is not unusual since in general such features are non-axisymmetric, e.g. HH 34S (Bührke *et al.* 1988). Moreover, the spectra shown earlier (see §2.4.2) indicated a marginally higher excitation at the head of HH 130 and such a characteristic is in keeping with the model predictions for a bow shock (Bührke *et al.* 1988 and references therein). One would also expect a drop in the electron density with increasing distance from the bow shock apex. It would be unlikely, however, that such a variation could be found here, since at the low values detected ($\leq 100\mathrm{cm}^{-3}$), the measurements are likely to be very unreliable. According to Hartigan *et al.* (1987), the FWZI_c should be a good approximation to the bow shock velocity (v_{bs}). From the long slit spectrum (P.A. 50°), the [SII]$\lambda\lambda$6716,6731 lines imply V_{bs} = 60 km s^{-1}. Ogura and Walsh (1991) have estimated the shock velocity on the basis of excitation ratios measured from a low excitation spectrum and they suggest a value of about 85 km s^{-1} i.e. in good agreement with the estimate here.

For HH 130, although a bow shock is clearly observed, there is absolutely no evidence for a Mach disk. Both this result and the low value measured for the bow shock velocity have important consequences for the nature of the driving outflow. Balancing the ram pressures of the jet shock (Mach disk) and the bow shock (Norman *et al.* 1984), one has,

$$\frac{n_j}{n_a} = \frac{v_{bs}^2}{\beta(v_j - v_{bs})^2}$$

where n_j, n_a, v_j represent the jet density, the ambient density and jet velocity respectively. The term β is a constant, which is included to account for momentum transfer efficiency from the jet to the working surface, and following Hartigan (1989) a value of 0.7 is adopted. Although the jet velocity is unknown, it is well established that the typical flow speeds range between 200 and 400 km s^{-1}. Therefore, using v_{bs} = 60 km s^{-1}, one calculates that the ratio of the jet density to the ambient density is likely to be between 0.04 and 0.26. Importantly, this shows that for typical jet speeds the density in the jet is substantially smaller than in the surrounding medium i.e. the driving outflow is a "light" jet.

To test whether the presence of a "light jet" is in keeping with the observation that only the bow shock is apparent, one first determines a value for the preshock density n_o. Using the formula of Dopita (1978),

$$n_0(cm^{-3}) = \left(\frac{n_e(SII)}{43 \pm 15}\right) \times \left(\frac{v_s}{100\,\mathrm{km\ s^{-1}}}\right)^{-2}$$

where v_s is the shock velocity and n_e is the postshock electron density. and adopting the characteristic electron density as approximately n_e = 100 cm^{-3} (see §2.4.2), v_s = v_{bs} (60 km s^{-1}), and $n_0 = n_a$, one calculates for the ambient density a value of $\approx$ 10 (hydrogen atoms cm^{-3}). With the assumed flow speed between 200 and 400 km/s, one then finds from the models of Hartigan (1989), that for this range of flow velocities and the derived ambient density, the bow shock will be visible but that the Mach disk will not. A value of n_j of only 0.6 (hydrogen atoms cm^{-3}) is also derived, which is low by jet standards (see Mundt *et al.* 1987). A possible explanation for this, is that the mass loss rate from the source of the outflow has decreased. Certainly optical outflows are expected to be time variable (see Ray and Mundt 1993).

The reason why only a bow shock is visible can be found by examining the ratio of the cooling lengths of this and the Mach disk. Following Blondin *et al.* (1990),

$$\frac{d_{bs}}{d_{md}} \approx \left(\frac{n_j}{n_a}\right)^3$$

From the values determined above for the jet and ambient density ratio (v_j = 200-400 km s^{-1}), one finds that the cooling length of the bow shock (d_{bs}) will be between approximately 10^{-2} and 10^{-5} times smaller than that of the Mach disk (d_{md}). An exact value of d_{bs} can be calculated, using the general formula of Blondin *et al.* (1990),

$$d_{bs} \approx 4.5 \times 10^{16} n_a^{-1} \left(\frac{v_{bs}}{100\,\mathrm{km\ s^{-1}}}\right)^4 cm$$

Upon substitution of v_{bs} = 60 km s^{-1} and n_a = 10 (hydrogen atoms cm^{-3}), one finds d_{bs} = 5×10^{14} cm. For the Mach disk however, the value of d_{md} will be some 10^2–10^5 times bigger for the range of jet velocities 200–400 km s^{-1}. The length scale calculated for the bow shock is of the order of 10^{17} cm and it is thus clearly radiative, but the Mach disk will be non-radiatively cooled and henceforth will not be observable.

A "light" or diffuse jet, when it collides with the ambient medium will produce a cocoon of backflowing hot tenuos material (Norman *et al.* 1982 and Blondin *et al.* 1990). It may well be the case, that one is observing this cocoon by weak shocks in the backflow of HH 130. As to the filaments of emission, which appear to connect the extended wing with the central axis of the outflow, similar features are seen in some of the jet models of Lind *et al.* (1989) and Blondin *et al.* (1990) and may be associated with a process known as vortex shedding. Finally, it is unclear where the source of the HH 130 outflow is positioned. If object g1 is in fact the bow shock of a counterflow, than obviously it lies along the central axis between the two bow shocks. Alternatively, the source might be to the northwest of knot g. Here, as seen in the [SII] frame in Fig. 2.16 background emission decreases, presumably as a result of higher extinction.

Chapter 3

Cepheus A

3.1 Introduction

Cepheus A (henceforth abbreviated to Cep A) is a molecular cloud discovered by Sargent (1977) and is part of the larger Cep OB3 association. Located at a distance of 725pc (Garmany 1973) it is a very active star formation region. In particular, it is probably the site of what is considered the archetypal high luminosity outflow source, having a far infra-red luminosity of $2.5\times10^4\,L_\odot$ (Evans *et al.* 1981) and associated H_2O and OH masers (Norris 1980 and Lada *et al.* 1981). The cloud core itself cannot be observed optically due to high extinction (Lenzen *et al.* 1984) but has been investigated at radio wavelengths.

Early radio continuum observations at 20cm (Hughes and Wouterloot 1982) showed two separate regions of emission; one of these was coincident with a red nebulosity originally discovered by Gyulbudaghian *et al.* (1978) and is usually referred to as GGD 37, the second was some 200" to the east and is located near the far infra-red source (an area that will be referred to as the central region). Hughes and Wouterloot (1984) found that at higher resolution there are in fact at least 14 radio continuum sources in the central region and it is not clear exactly how many young stellar objects are present (Hughes 1988). However, it is generally accepted that the object or objects responsible for most

of the stellar activity, are located near two of the compact radio sources HW-2 and 3 (Cohen *et al.* 1984, Weliachew *et al.* 1985 and Lenzen 1988).

3.1.1 Optical and Near-Infrared observations

To the west of Cep A lies GGD 37, which was originally considered to be a possible HH complex (Gyulbudaghian *et al.* 1978) and this was later verified by Lenzen *et al.* (1984). GGD 37 appeared to be blueshifted, but of particular interest was the large velocity dispersions observed in its spectrum ranging up to 300 km s^{-1}. Later studies by Hartigan and Lada (1985) showed that GGD 37 is in fact a complex mixture of HH objects and reflection nebulosities. Indeed, in a subsequent paper (Hartigan *et al.* 1987) the HH objects were modeled successfully as bow shocks, the large linewidths originally detected by Lenzen *et al.* (1984) being explained by high shock velocities. Proper motion measurements of these bow shocks (Lenzen 1988) revealed high tangential velocities (near 200 km s^{-1}), but most importantly they located the possible origin for the GGD 37 optical outflow as the radio source HW-2 or its immediate vicinity. The only other HH emission detected in the region was discovered by Lenzen (1988) who found a bow shaped object to the north-east of the central region. Interestingly, the linewidths of this object were smaller than those of GGD 37, typically less than 60 km s^{-1}. Moreover, both the HH object in the east and those in the west were blueshifted in radial velocity. Once again, the source of the new HH object as determined by its proper motion measurements also seemed to be close to HW-2.

The earliest observations of Cep A in the near-infrared (Bally and Lane 1982) detected the presence of both continuum and molecular hydrogen emission. The continuum emission was later found by Lenzen *et al.* (1984) to originate from a bright infra-red reflection nebulosity, extending east from the radio objects at the center of Cep A. Using both K and L band imaging Lenzen *et al.* (1984), suggested that only the eastern component of the reflection nebula was apparent because its western counterpart was obscured by extinction. The source of the reflection nebulosity was not directly observed and they estimated that at least 75 magnitudes of visual extinction was present. Doyon and Nadeau (1988) mapped the molecular hydrogen emission and found it to be in three

principle locations, the first to the west coinciding with GGD 37, the second to the north of GGD 37 near an optical reflection nebula, and finally northeast of the central region where it is extended beyond the 6cm continuum radio sources. The origin of most of the molecular hydrogen emission they suggested was shock excitation. The recent images of Lane (1989) show that Cep A has extensive shocked H_2 emission, some of which coincides with the known optical shocks in GGD 37 and the new HH object to the north-east of Cep A.

3.1.2 Molecular Observations

It has been known for over a decade that Cep A is the source of a bipolar molecular outflow (see, for example, Rodríguez *et al.* 1980). However, the question as to whether there is more than one outflow has been raised. Rodríguez *et al.* (1980) originally suggested the presence of a single molecular outflow with an east-west orientation, the red lobe incorporating GGD 37. Richardson *et al.* (1987) later mapped the same region in the J = 3–2 transition of CO and found what appeared to be two separate outflows; a bipolar flow centered on both the radio objects and maser positions, with its orientation east-west, and the second flow although not bipolar, coincident with GGD 37. In stark contrast, Levreault (1988) using the J = 1–0 transition of CO interpreted his results in terms of a compact bipolar outflow centered on Cep A. In this case however, the orientation was in an northeast-southwest direction. Levreault (1988) suggested that the differences in the molecular outflow orientations and number, are due to different sampling and resolution effects. Most recently, Hayashi *et al.* (1988) suggest the presence of two bipolar outflows, a low velocity flow orientated northeast to southwest, and a higher velocity flow in the east-west direction.

Finally, there have been various observations of the Cep A region in such high density tracers as for example NH_3 (Torelles *et al.* 1985), HCN (Weliachew *et al.* 1985) and CS (Moriarty-Schieven *et al.* 1991). In all cases it is uncertain what role if any these condensations play in collinating or redirecting the outflow. As pointed out by Hughes (1988) the detection of such high density material only indicates the location of the denser parts of the cloud core.

3.2 Observational Details and Data Reduction

3.2.1 Direct Imaging

Direct imaging was made on the 4.2m William Herschel Telescope (WHT) on La Palma, and the 3.5m telescope at Calar Alto, in September 1988 and October 1987 respectively.

WHT observations were made using Taurus-2 in direct imaging mode with the f/2 option. The detector, a 400×590 GEC P8603 CCD, had a projected pixel size on the sky of 0.51" resulting in a field of view of 3.4'×5.0'. Imaging was carried out with both a narrow band [SII] filter (λ_c=6730Å, $\Delta\lambda$=48Å, exposure time = 1800s) and a nearby continuum filter, r_n (λ_c = 6890Å, $\Delta\lambda$ = 195Å, exposure time = 1800s). Observations at the 3.5m Calar Alto Telescope were made at the prime focus and a 656×1024 RCA CCD was employed as the detector. The scale of the detector was 0.26"/pixel and therefore the overall field of view was 2.7'×4.3'. The filters used for imaging were [SII] (λ_c=6740Å, $\Delta\lambda$=70Å, exposure time = 2000s) and Hα (λ_c=6580Å, $\Delta\lambda$=100Å, exposure time = 2000s). Seeing conditions for the Calar Alto and WHT images were 1.6" and 1.4" respectively.

The usual technique for imaging HH objects and HH-like jets, was employed by taking two frames: one through a suitable narrowband emission line filter (the [SII] filter) and another through a nearby narrowband "continuum" filter (the r_n filter). For details of the technique see §2.2.1. Since both WHT images were taken under the same seeing conditions, it was unnecessary to use a gaussian filter to match their profiles, a smoothing filter was however, applied to reduce background noise. Subsequently, after suitable scaling of the continuum frame, the "continuum" frame was subtracted from the emission-line frame.

As mentioned in the Introduction (§3.1), radio continuum observations have revealed a group of sources close to the core of Cep A and it has been suggested that these are either a cluster of HII regions (Hughes and Wouterloot 1984) or thermal shocks (Lenzen *et al.* 1984; Joyce and Simon 1986 and Hughes 1993). These sources, however, are deeply embedded and they are not coincident with the features which will be described later in

Telescope	Object	Date	P.A.	Exposure Time(s)	Slitwidth"
INT	HH-NE + HH-NE2	7 Aug. 1987	101°	3000	0.8
	HH-NE	30 Aug. 1991	71°	2700	1.1

Table 3.1: Observing log for the spectra taken at the INT.

the text. Thus irrespective of whether they are HII regions, they need not concern us from the point of view of image analysis. Finally, one notes that for the high contrast WHT images, namely the [SII] and difference frames, a median filter was employed to reduce image noise.

3.2.2 Spectroscopy

The long slit spectra were obtained on two observing runs in August 1987 and September 1991, and both of these were conducted at the 2.5m Isaac Newton Telescope (INT) on La Palma. Details of these observations are presented in Table 3.1. The instrument used in both cases was the IDS, and this was configured in an identical manner to that already described for the spectroscopy of V380 Ori (see §2.2.2). Spatial resolution along the slit was 0.3"/pixel although the actual resolution was determined by the seeing (between 1 and 1.1" for both observations). Spectral analysis was in general carried out using the [SII]$\lambda\lambda$6716,6731 lines, except when measuring excitation.

3.3 Results

3.3.1 Imaging

[SII] and continuum images east of Cep A are presented in Figs. 3.1(a) and (b) respectively. The brightest HH object in Fig. 3.1(a), has already been studied by Lenzen (1988) who referred to it as Cep A HH-NE (henceforth abbreviated to HH-NE). Further east, another prominent HH object can be seen which will be referred to here as HH-NE2. Although HH-NE and HH-NE2 have complex structures, both contain bow-shaped components. The most striking feature of Fig. 3.1(a) is, however, the broken ring-like structure of HH emission of which HH-NE and HH-NE2 appear to be just the brightest parts. This can be clearly seen both in the high contrast [SII] (Fig. 3.2(a)) as well as the "pure" emission line (Fig. 3.2(b)) frames.

The "ring" has an approximately elliptical shape, the major axis of which runs east-west. In certain locations, there appears to be some continuum emission mixed with, or close to, the "ring". In particular, there is a faint reflection nebula on the western side of the ellipse (see Fig. 3.2(a)) and the continuum nature of this emission is verified by its disappearance in the high contrast [SII]-continuum difference frame (Fig. 3.2(b)). This is the reflection nebulosity previously seen by Lenzen (1988) in his I band images. Moreover, the western part of the HH emission-line loop discussed here is also shown in the Hα image of Lenzen (1988), however, he did not interpret this as HH emission, rather as the same reflection nebulosity that occurs in his I band image. On closer examination of these images, this interpretation seems unlikely, both the reflection and Hα nebulosities have substantially different structure and brightness.

A [SII] image extending further east and taken at the Calar Alto 3.5m Telescope is shown in Fig. 3.3. Aside from displaying additional faint knots, a diffuse nebular feature is seen above HH-NE. Comparison with a nearby continuum frame (not published here) has revealed that these are emission line features. In particular the faint knots are almost certainly HH emission owing to their structure and their location. Using a Hα image also taken at the Calar Alto 3.5m telescope, the relative excitations within the emission

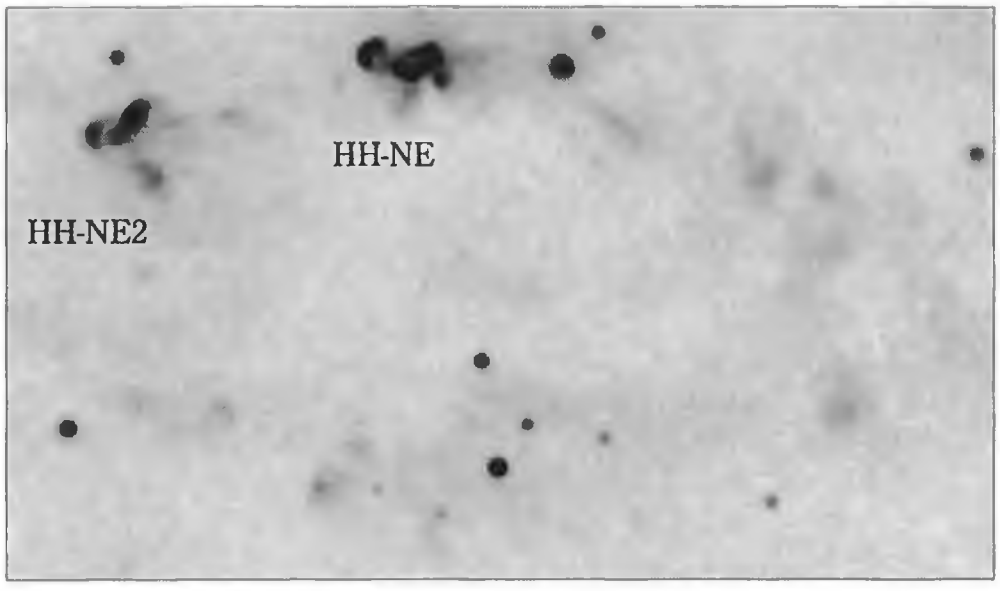

(a)

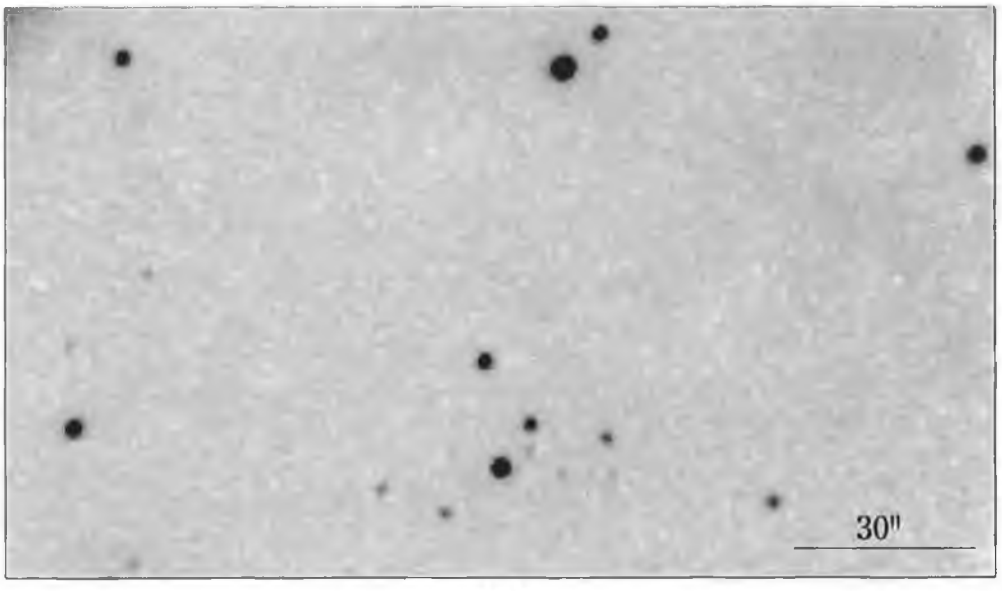

(b)

Figure 3.1: (a) A [SII] image to the east of Cep A taken with the William Herschel Telescope (WHT). Two prominent HH objects are clearly seen, HH-NE and HH-NE1 both of which are indicated. A faint diffuse ring-like structure can also be made out; this is much more easily seen in the high contrast images. (b) The same area as in (a) but this time through a narrowband continuum filter close to the red [SII] doublet. Note that the HH objects and diffuse "ring" disappear.

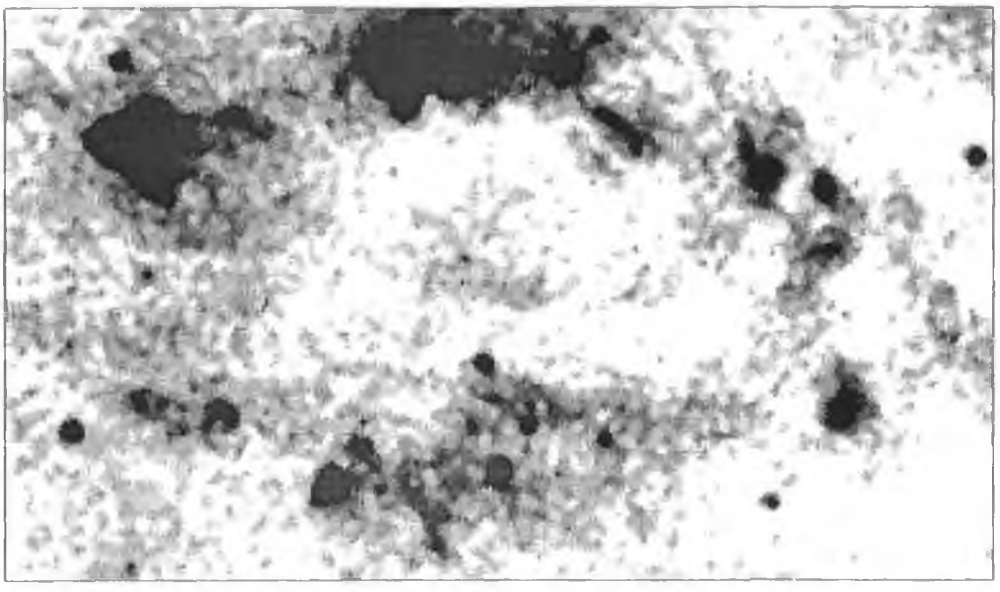

(a)

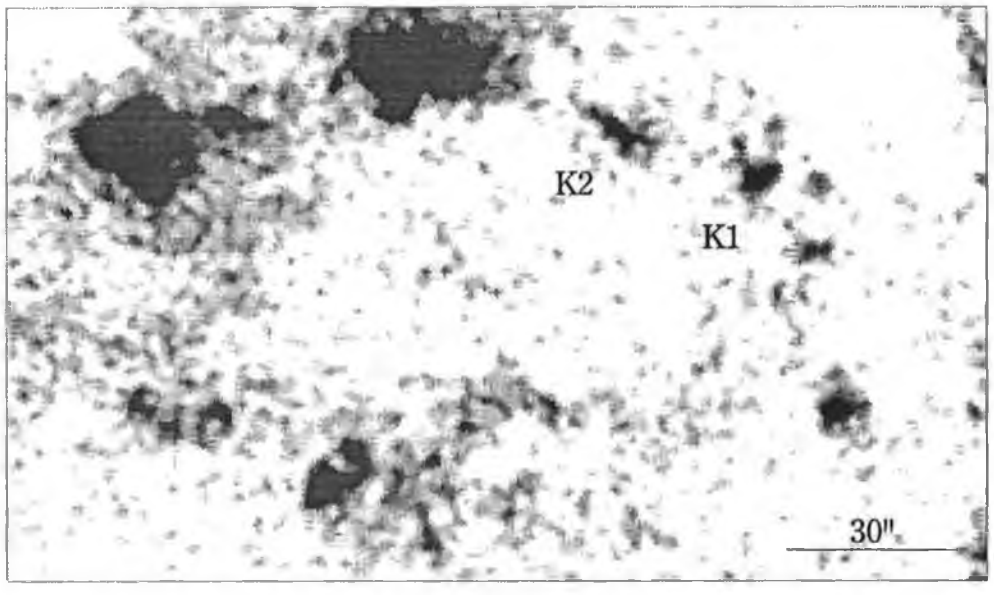

(b)

Figure 3.2: (a) As in Fig. 3.1(a) but at high contrast. Some of the emission on the western side of the "ring" is due to a reflection nebulosity as can be seen by comparing this image with the lower one. (b) A [SII]-r_n "pure" emission line frame of the same region as in (a). Stars and reflection nebulosities essentially disappear in this frame although there is some residual "ghost" emission (see text). Two condensations in the "ring" K1 and K2 roughly coincide with some of the known H_2 knots.

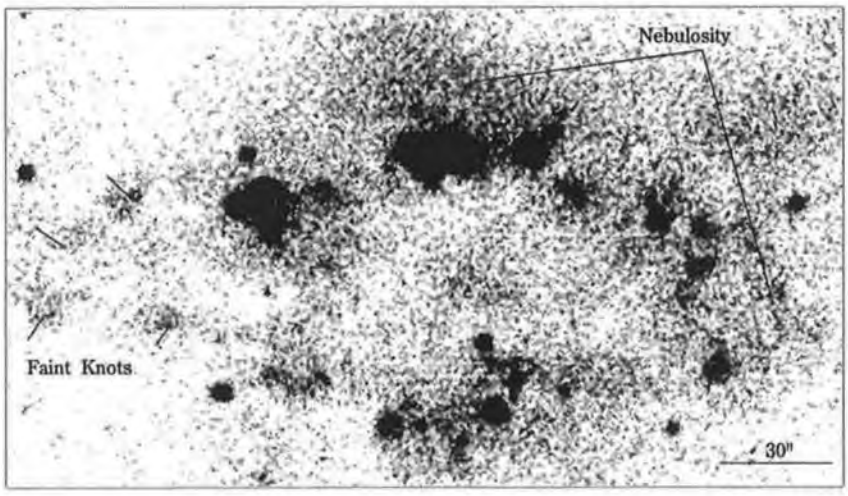

Figure 3.3: (a) A [SII] image, of the Cep A HH "loop" extending further east than those of Figs. 3.1 and 3.2. Note the additional very faint knots which are almost certainly HH emission and the nebulous feature situated above HH-NE.

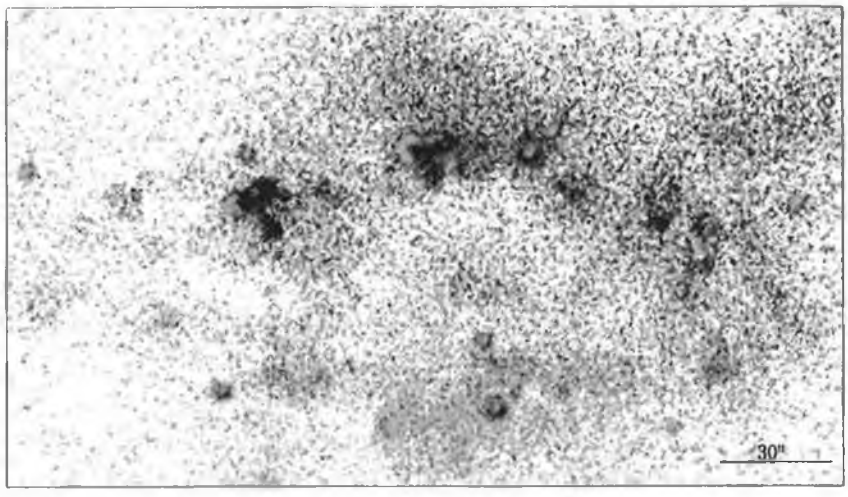

Figure 3.4: A Hα/[SII] image illustrating the relative excitations in the "loop". The colour variations from grey to black represent the transition from high to low excitation. With the exception of the two brightest objects the separation of high and low excitation between the north and south of the "loop" is clearly seen. Note also that the apexes of HH-NE and HH-NE2 are of relatively high excitation as would be expected of bow shocks.

loop are shown by the Hα/[SII] images in Figs. 3.4. In particular, one notes that even excluding HH-NE and HH-NE2, there is a marked contrast between the north and south excitations, the south is predominantly higher. As to HH-NE and HH-NE2, excitation varies considerably across these objects. In both cases the general features are the same with a concentration of higher excitation towards the apexes of their bows.

Finally one notes that the symmetry axes of the bow shock structures of both HH-NE and HH-NE2 point back at Cep A, and that the major axis of the incomplete "ring" delineated by the optical emission also goes through this source.

3.3.2 Spectral Analysis

The results of the long slit spectroscopy for HH-NE and HH-NE2 are shown in Figs. 3.5(a) and (b) respectively. Contour plots of the [SII]–r_n images for both objects are displayed with the slit orientations illustrated. At various points of interest within these HH objects, the measured electron density (n_e), and excitation calculated using the ratio Hα/[SII]$\lambda\lambda$6716+6731 are shown. Measurements were also made of the heliocentric radial velocities (v_{rad}), and linewidths which are corrected for instrumental effects.

Lenzen (1988) found the mean heliocentric radial velocity of HH-NE to be around -80km/s and the average deconvolved width of its lines to be $\leq$ 60km/s. Our measurements for this object are comparable with a mean value for v_{rad} of -70km/s and an average deconvolved linewidth of $\leq$ 80km/s. The structure of HH-NE can be clearly seen in Fig. 3.5(a), it consists of an arc-shaped head and an extended knotty structure towards its tail. Derived excitations verify that the highest value (1.1) is located near the apex of the object, this was expected from the Hα/[SII] image of Fig. 3.4(b). Immediately behind the apex, the excitation falls off rapidly (1.1 to 0.4) and there is a corresponding decrease in density (9300cm^{-3} to 1900cm^{-3}). Towards the tail of HH-NE the excitation is low (typically less than 0.6), but there is one notable exception to this: the bright knot encountered by the most northern slit has a higher excitation (1.1) but its density is typical of the tail (less than 1900cm^{-3}).

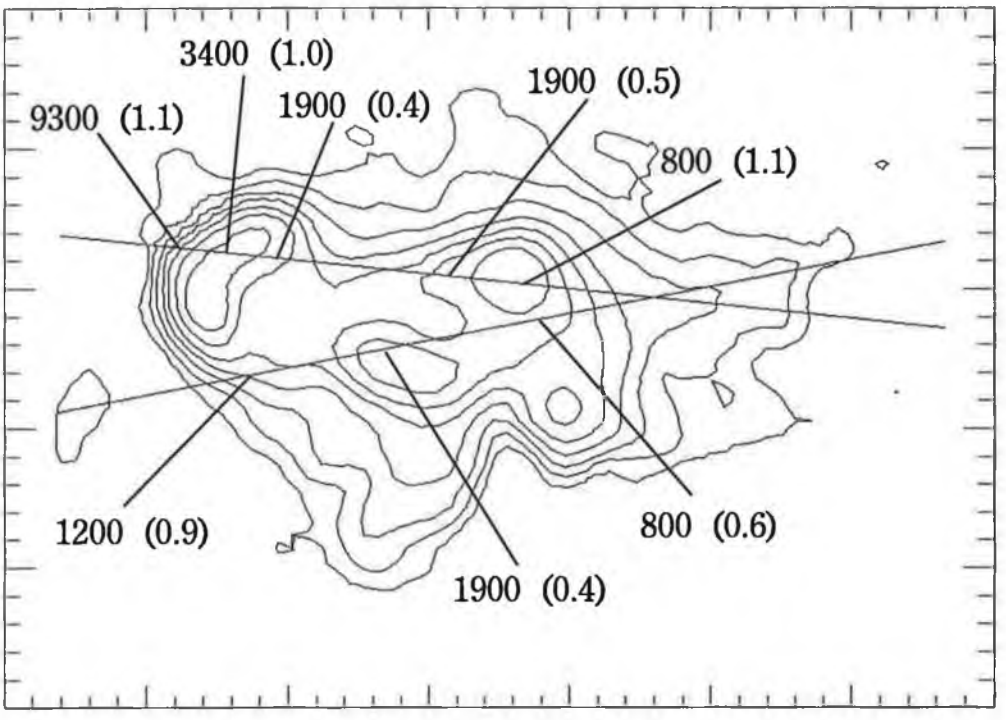

(a)

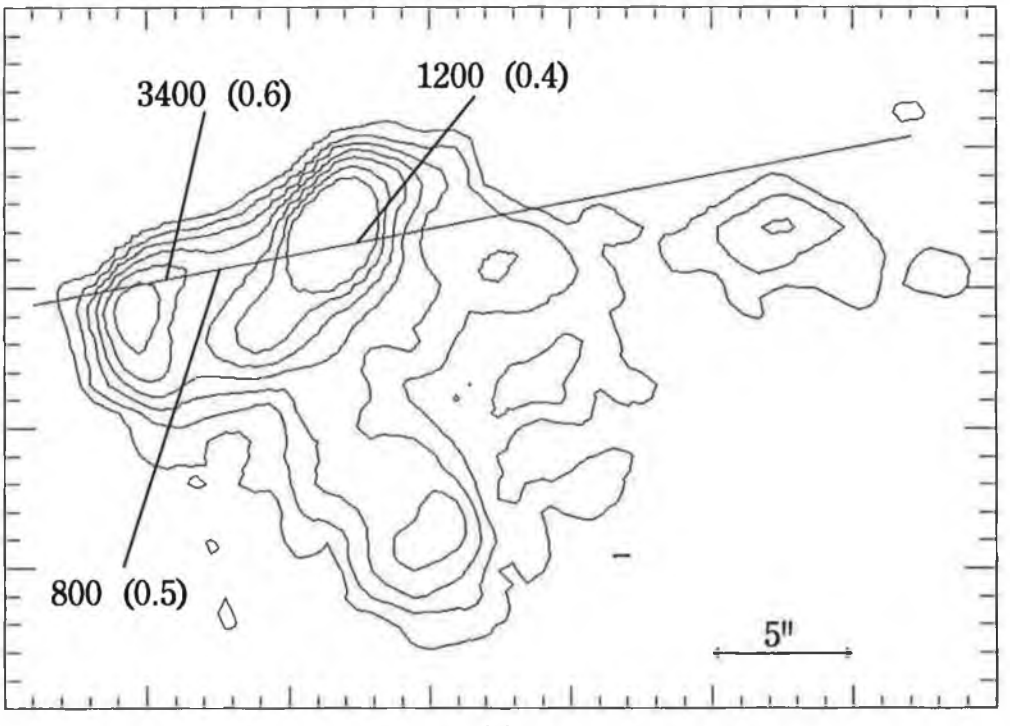

(b)

Figure 3.5: (a) A contour plot of the [SII]-r_n image of HH-NE with the slit positions marked. The ratio between the contour levels is 1.5. At various points within the object, the densities are indicated together with the excitation as measured by the ratio Hα/[SII]$\lambda\lambda$6716+6731 quoted in brackets. (b) As in (a) but for HH-NE2.

For HH-NE2, a similar structure to that of HH-NE can be seen in the contour plot of Fig. 3.5(b). In this case, however, the density (3400cm^{-3}) and excitation (0.6) near the apex of HH-NE2 is substantially smaller than HH-NE. Moreover, although the tail of HH-NE2 is lower in density and excitation than its head (see Fig. 3.5(b)), these differences are marginal. Another difference is that while most of the emission in HH-NE had a similar radial velocity, it is found for HH-NE2 that the radial velocity increases from its apex to the tail. Derived values for v_{rad} are -30km/s at the apex and -50km/s at the position of the bright knot covered by the slit. The average deconvolved linewidth for HH-NE2 is 60km/s and this is comparable to HH-NE.

3.4 Discussion

Studying the images of this region, the most striking feature is the virtual "loop" of HH emission east of Cep A (see Figs. 3.1–3.3). What then is the origin of this "loop"? As will be seen, its geometrical relationship with the other outflow tracers, and the fact that it axis points east-west through the core of Cep A (like the molecular outflow), clearly implies that the partial ring of emission is the eastern optical outflow from Cep A. The extent of the ring is therefore obvious evidence of a poorly-collimated wind. Loop-like structures are not unknown near YSOs, e.g. LkHα 198 (see Chapter 4) and AFGL 2591 (see Poetzel *et al.* 1992) but these features are either optical or near-infrared reflection nebula.

3.4.1 The Bipolar Optical Outflow of Cep A

To put the shocked optical emission east of Cep A in context, Fig. 3.6 is a schematic of this feature together with the, 2.12 μm data (Lane and Bally 1993), a radio continuum map (Hughes and Wouterloot 1984) and the NH_3 detections (Torelles *et al.* 1985). Given the center of Cep A is located close to HW-2 and 3, it can be seen that one is witnessing various manifestations of the impact of a poorly-collimated wind from Cep A on its surroundings. First of all consider the H_2 shock-excited emission (Doyon and Nadeau 1988; Lane 1989; Lane and Bally 1993). In particular one must concentrate on the H_2 "finger" stretching approximately 1' to the northeast of Cep A and the additional faint H_2 knots in the same direction (see Fig. 3.6). If one assumes that this shocked emission delineates the northern interface of the impacting wind with its surroundings then the northern section of the optical emission can be seen as a continuation of this boundary. If this is the case, then the question naturally arises as to why a southern H_2 "finger" is not seen? The obvious explanation is extinction. Certainly the visual extinction increases (to $\approx$ 75 mag in V) as one approaches Cep A from the east (Lenzen *et al.* 1984) but there is additional extinction in the region where one expects to see the southern "wall", as confirmed by the L/K maps of Lenzen *et al.* (1984). Extra extinction to the south would also explain other anomalous observations in this region: for example, why the

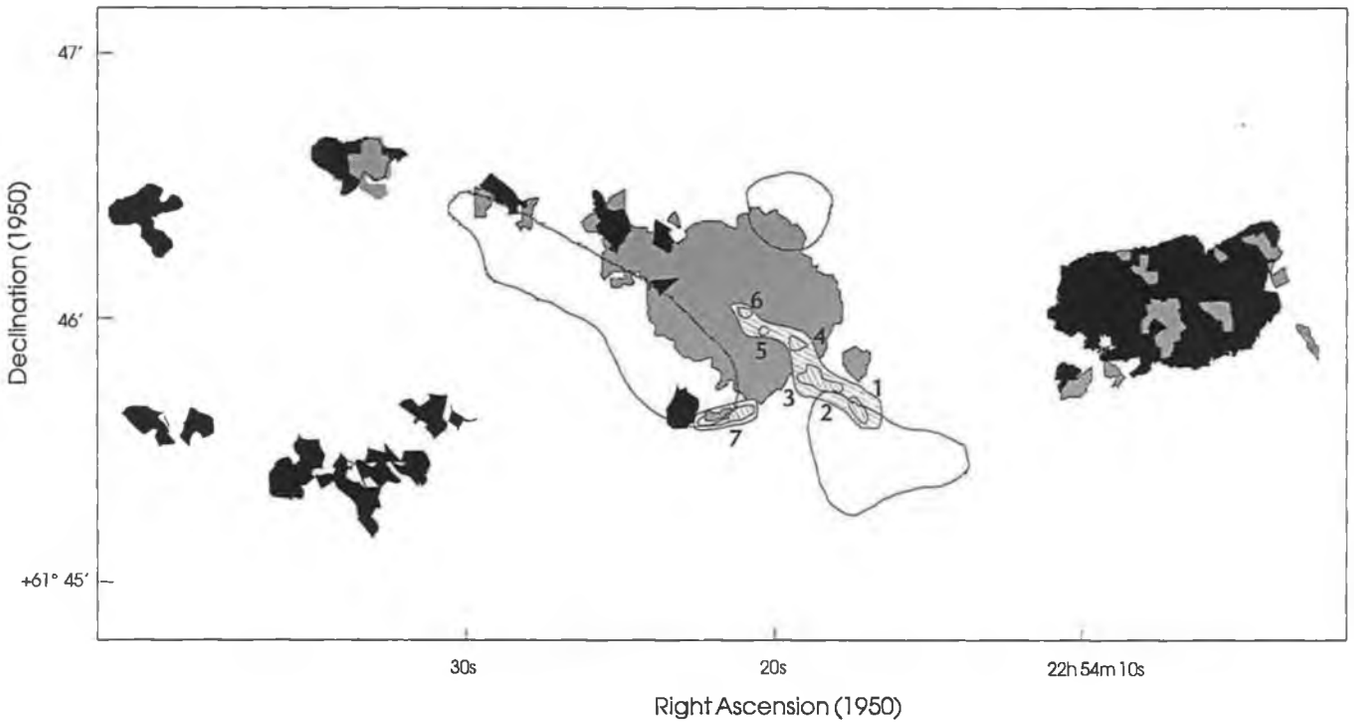

Figure 3.6: A schematic of the outflow tracers to the east of Cep A showing the optical emission (black features), 2.12μm data including the shocked emission H_2 and the near-infrared reflection nebula (gray features), radio continuum emission (hatched features) and the NH_3 detected (contour lines). References to this data are contained within the text.

axis of the conical infrared nebula appears to point to the northeast (see, for example, Lane 1989) but the general outflow direction is east-west. It would further resolve the question as to why the near-infrared polarisation vector of Cep A is not north-south (see Sato *et al.* 1985), as would be expected for an east-west outflow (Bastien 1987), but is instead to the northwest[1]. Returning now to the shocked H_2 emission northeast of Cep A, it is found that some of the faint knots seen by Lane (1989) roughly coincide with the optical ([SII]) knots K1 and K2 (see Fig. 3.2) observed by us. This is not surprising given that both the H_2 and the low excitation [SII] emission arises from low velocity shocks.

Turning to the radio continuum data its interpretation has proved to be quite controversial. In the past, it was assumed that the 14 radio continuum sources close to the core of Cep A were ultra-compact HII regions, each region was believed to be excited by an individual star (see Hughes and Wouterloot 1984). This interpretation has been certainly questioned by a number of authors. For example Torrelles *et al.* (1985), detected NH_3 condensations in the immediate vicinity of Cep A (see Fig. 3.6), the edges of two of which appear to coincide with the outer radio continuum objects. Torrelles *et al.* (1985) suggested that UV excitation from the central region (HW-2 and HW-3) could be ionizing the edge of these condensations. In contrast, Weliachew *et al.* (1985) suggested the source of these radio structures was shock excitation; they suggested high density gas in the eastern region (detected in the HCN lines), was most likely to form an obstruction to the stellar outflow and this would produce a shocked ridge along the edge of the obstruction.

The most recent observations now make it clear that the cause of the outer radio objects is most likely shock excitation (Joyce and Simon 1986, Lenzen 1988 and Hughes 1993). What is not clear is how this shock excitation takes place. A proposal which fits in with the model suggested here, is that the shocks occur at the boundary of a wind-swept "cavity" (Lenzen 1988). The simplest scenario then is that the northern boundary

[1]To understand the latter point note that Cep A itself, is not seen in the near-infrared but instead only by its associated reflection nebula. As the polarisation vectors in the latter follow the usual circumferential pattern (see Lenzen *et al.* 1984), and essentially, only the northern portion of the infrared nebula is observed, the *integrated* polarisation vector is biased to the northwest.

of the "cavity" is marked first by the radio continuum emission, then the shocked H_2 and finally the optical shocked emission. The southern boundary is not so clearly seen near the source except at radio wavelengths, this is because of extinction, there are however faint traces seen optically and in the near-infrared (i.e. in shocked H_2). As to the high density gas observed to the east of Cep A (Torrelles *et al.* 1985 and Weliachew *et al.* 1985), this is most likely on the outside of the outflow. If not then an east-west outflow interacting with any obstruction, would produce a bright shock probably perpendicular to the outflow direction and directly opposite the source. As seen in Fig. 3.6 there is no evidence of any such shock.

While the images to the east of Cep A, clearly support the idea of a poorly-collimated wind in that direction, little has been said about the region west of Cep A (i.e. GGD 37). GGD 37, as mentioned, consists mainly of several bow shocks (Hartigan *et al.* 1986; see also the shocked H_2 bows to the west of Cep A in Lane and Bally 1993) along with more diffuse emission. This HH emission can be explained as arising from a poorly-collimated inhomogeneous wind, the inhomogeneities of which give rise to the bow shocks. Clearly, such a wind model might be applicable to the region east of Cep A as well. Although the "loop" of emission to the east of Cep A and the GGD 37 complex are on similar scales, there are clear morphological differences between these two structures. However, whether the morphological differences can be partly attributed to an intrinsic asymmetry in the east-west outflow from Cep A or wholly due to the different environments in the east and west is still an open question. Certainly strong asymmetries are seen in bipolar optical outflows from lower mass stars (Mundt *et al.* 1991). Ho *et al.* (1982) has even suggested that the environments east and west of Cep A shape at least its CO molecular outflow. Indeed, as mentioned above, high density gas NH_3 (Torrelles *et al.* 1985), HCN (Weliachew *et al.* 1985) and CS (Moriarty-Schieven *et al.* 1991) have been detected in the region. The distribution of this high density gas is assymetric, most of it being found centered on and just east of Cep A.

3.4.2 The Question of Molecular Outflows in Cep A ?

There seems to be some question as to whether there is more than one bipolar outflow in the Cep A region and even, if there is only one, where its axis lies (Richardson *et al.* 1987; Levreault 1988; Hayashi *et al.* 1988; Moriarty-Shrieven *et al.* 1991 and references therein). Clearly the axis of the optical emission to the east of Cep A is orientated east-west. Given the position of GGD 37, an east-west outflow would seem obvious, and this would be consistent with the early CO data (Rodríguez *et al.* 1980). Recently, however, Hayashi *et al.* (1988) have suggested on the basis of their data that, in addition to the higher velocity east-west CO outflow, there is a lower velocity molecular outflow in the northeast-southwest direction, i.e. along the line defined by HW-2 and HW-4 to HW-6. Moreover, they cite as additional evidence for such an outflow the polarisation angle for Cep A determined by Sato *et al.* (1985), along with the presence of an NH_3 clump and an optical reflection nebulosity (detected on the POSS R plate); both of which are elongated in the direction of the proposed outflow. As already pointed out, however, the result of Sato *et al.* (1985) is almost certainly biased because of extinction. Furthermore, the faint red nebula seen on the POSS plates just delineates the northern boundary of the reflection nebula seen partly in the infra-red. Rather interestingly this nebula may have faded considerably over the past thirty years. The nebula is just seen here, on the deep narrowband continuum CCD images (see Figs. 3.3 and 3.4), and in an unpublished R band INT image obtained by us. On the basis of the circumstantial evidence alone, it is not clear that there is an outflow in the NE-SW direction.

With reference to the molecular line data of Hayashi *et al.* (1988), there are at least two further possible explanations for what they observed aside from their interpretation of two separate outflows. Either the assumption is made that the east-west outflow is viewed almost edge on and that the molecular outflow is probably formed in an expanding shell about a windblown cavity, or that the molecular outflow fills the cavity (Cabrit 1989). In the first case, it is expected that the highest CO velocities will be observed along the central axis of the cavity but lower velocities will be seen towards its edges. For this situation the motion of gas at the edge of the cavity could mimic a separate outflow, particularly if the gas is clumpy. In the second case, the highest radial

velocities would determine the stellar outflow axis and the lower velocities towards its edges could be explained by a latitude dependent wind from the source. In either case a number of velocities will be observed over a range of directions, but the highest velocity will determine the true outflow direction, namely east-west. Thus for example although Hayashi *et al.* (1988) suggested only 2 outflow components, an examination of their Fig. 3 reveals that within the velocity intervals -17 to -15 km/s and -8 to -7 km/s there are additional structures to the SE and the NW. These velocities and those seen in the NE and the SW are, however, much smaller than those of the east-west molecular outflow.

Of the two possible scenarios suggested here for the molecular outflow, either the "latitude wind dependent" model or the "edge on-model", the latter is favoured. It is known for example that both GGD 37 and HH-NE have high proper motions and low radial velocities (Lenzen 1988 and Hartigan *et al.* 1986), implying motion more or less in the plane of the sky (see below §3.4.3). Consequently, since the optical outflow seems to be moving close to the plane of the sky, it is tempting to suggest the molecular outflow does likewise. Indeed, the molecular outflow data of Richardson *et al.* (1987) seems to substantiate this. As mentioned earlier (see §3.1), Richardson *et al.* (1987) detected the presence of two apparent molecular outflows in the J = 3–2 transition of CO; one of these was located near GGD 37 , the second was located 2' to its east i.e., coincident with the center of Cep A and the HH emission "loop" discovered here. This behaviour is exactly what one would expect if a single molecular outflow was seen edge on, the seemingly separate outflows would then simply represent the east and west lobes of the single outflow.

3.4.3 HH-NE and HH-NE2

Both HH-NE and HH-NE2, as can be seen from the contour plots of Figs. 3.5, are bow-shaped. As such, they resemble similar structures seen to the west of Cep A in GGD37, which have been successfully modeled by Hartigan *et al.* (1986) in terms of bow shocks. If one assumes that the radial velocities of HH-NE and HH-NE2 are representative, then their observed low values, typically less than about -70 km/s, might suggest motion more or less in the plane of the sky. Indeed Lenzen (1988) has measured the proper motion of

HH-NE and found it to lie between 180 and 250 km/s i.e. its direction of motion makes an angle of greater than 70° to the observer's line of sight. Aside from their morphology there is additional evidence that both HH-NE and HH-NE2 are bow shocks. It was shown, using the Hα/[SII] image (Fig. 3.4), and from the spectroscopic study (Fig. 3.5) that the apexes of both objects are of relatively high excitation as predicted by bow shock models (see, for example, Morse *et al.* 1992). Another result, expected on the basis of bow-shock models, is the "skirt" of shocked H_2 emission that is found to lie close to HH-NE (Lane 1989). Here the emission is thought to occur in the oblique tail of a bow shock (Smith 1991). Although, the images of Lane (1989) do not extend as far east as HH-NE2, it is however known that this object is also associated with similar H_2 emission (Bally, private communication).

Given they are bow shocks, both HH-NE and HH-NE2 must derive from inhomogeneities (essentially "bullets") within the wind from Cep A if the poorly-collimated wind hypothesis is correct. If one now assumes that the ambient medium which HH-NE is moving into is stationary; then the bow shock velocity can be roughly estimated by combining HH-NE's tangential velocity as given by Lenzen (1988) i.e. 230 km/s with the characteristic radial velocity measured here (70 km/s). The derived shock velocity is approximately 240 km/s, a value consistent with the observed degree of excitation at the apex. Such a shock velocity should also be close to the velocity of the "bullet" giving rise to HH-NE providing the density of the ambient medium is not considerably larger than that of the bullet. Furthermore, using the models of Hartigan *et al.* (1987), the full width zero intensity (FWZI) of the emission lines in a bow shock should be approximately v_b, the velocity of the bow shock. The FWZI was measured by fitting a Gaussian to the [SII] lines of HH-NE integrated over its entire spatial extent. The value calculated for the FWZI when corrected for instrumental broadening ($FWZI_c$), is approximately 200 km/s which compares well with the derived value for V_b of 240 km/s above. Clearly the bow shock interpretation seems correct for HH-NE.

Finally it is noteworthy, that the two brightest HH objects to the east of Cep A appear as part of the "loop" structure rather than at random positions superimposed on the wind-blown "cavity". It is interesting that in the wind-blown cavity of the outflow source L1551 IRS 5, the brightest objects HH 28 and HH 29 also occur near the edge

of the cavity and are in fact bow shocks (Stocke *et al.* 1988). A similar property has been found for the "loop"structures detected in the case of V 380 Ori (see Chapter 2) and HH 7-11 (see Chapter 5). The implications of these results will be considered later (in Chapter 5).

Chapter 4

LkHα 198 and V376 Cas

4.1 Introduction

LkHα 198 (V633 Cas) is located in a small dark cloud (Lynds 1265) in Cassiopeia and was considered by Herbig (1960) as a candidate intermediate mass young star. In his analysis, another star (V376 Cas) located some 35" to the north of LkHα 198 was also investigated owing to its association with a bright and highly variable nebulosity. Herbig (1960) did not however, determine a spectral type for V376 Cas, and interestingly, he detected no emission line features in its spectrum; its inclusion as an intermediate mass young star was therefore somewhat uncertain. Cohen and Kuhi (1979) detected emission line features in both these stars, including Hα and the [OI]λ6300 line and assigned spectral types of B3 and B5 to LkHα 198 and V376 Cas, respectively. Thus, as stated by Chavarría (1985), V376 Cas also fulfills the requirements for inclusion as an intermediate mass young star (Herbig 1960, Catala 1989). Both stars are highly variable, for instance Herbig (1960) has reported changes of m_{pg} = 16 to 18 mag for V376 Cas. In the case of LkHα 198, which has been observed in much greater detail, Chavarría (1985) has witnessed flare activity on timescales of a minute, together with changes in its SED within a period of several years. Variability in the Hα equivalent width of this star was also reported by Nakano *et al.* (1990) from 118Å to 65Å over a timescale of one year.

Shevchenko and Yakubov (1989) have shown that both LkHα 198 and V376 Cas are located within the same compact star formation region. Its distance was originally estimated by Herbig (1960) at 1000pc, however, more recent photometry places it at about 600pc (Racine 1968, Chavarría 1985, Shevchenko and Yakubov 1989), and the latter value is adopted here. Shevchenko and Yakubov (1989) have found at least 12 further stars which are associated with the cloud, with spectral type between F0 to B9. The authors estimate the cloud size at 2pc and its mass at $800\,M_{\odot}$. Other sources located within the cloud have also been detected at a number of wavelengths. In the near–infrared, Loren (1977) has detected three sources (excluding LkHα 198 and at least 2' distant from this star). The infrared colours of these sources suggest that although they are located within the cloud they are not deeply embedded. Rodríguez and Cantó (1980) have detected three radio sources (the nearest of these being 40" to the west of LkHα 198) and they interpret these objects as HII regions possibly arising from B-type stars. LkHα 198 is not found however, to be associated with any radio emission (Rodríguez and Cantó 1980, Evans *et al.* 1987).

4.1.1 Outflows in the LkHα 198 and V376 Cas Region

The first CO molecular studies in the region about LkHα 198, were conducted by Loren (1977), in which, two temperature maxima were found on either side of the star (separated by about 5' along a NE–SW direction). The most important result, however, was the detection of a slight shift in radial velocity between the cloud components to the north and south of LkHα 198 and a broadening of the molecular linewidths towards this star. Bally and Lada (1983) and Cantó *et al.* (1984) later found that the broadening and radial velocity shifts were in fact the result of a bipolar outflow. Cantó *et al.* (1984) mapped the region in the ^{12}CO molecular line and found an assymetric bipolar outflow aligned roughly in the NE–SW direction (the separation of the red and blueshifted lobe maxima being $\approx$ 1'). In this map the redshifted lobe is centered about LkHα 198, extending NE–SW, while the blueshifted lobe is only detected in the northeast. Cantó *et al.* (1984) also detected the large scale temperature maxima seen by Loren (1977) and concluded that they were unconnected to the outflow and resulted either from local temperature enhancements or were indicative of two separate clouds. Levreault (1988)

has recently remapped this region and found essentially the same result as Cantó *et al.* (1984). In addition, Levreault (1988) suggests that the observed assymetry in the bi-polar outflow might result from the presence of density gradients within the surrounding cloud.

There has been some question as to whether LkHα 198 or V376 Cas is in fact the driving source of the molecular outflow. It has been proposed for example by Chavarría (1985) that V376 Cas ($500\,L_\odot$) is actually more luminous and better positioned to drive the outflow than LkHα 198 ($\geq 160\,L_\odot$). That V376 Cas is optically fainter (Herbig 1960) is then attributed to it being more heavily obscured. The quoted luminosity for V376 Cas has, however, been disputed by Levreault (1988) who points out that Chavarría's proposal is based on the extrapolation of the near–infrared photometry of Cohen and Kuhi (1979) and that this is an uncertain procedure. Moreover, Levreault (1988) also notes that the IRAS Point Source Catalogue lists only one source in this area (IRAS 00087 +5833), the position of which is just 4" from LkHα 198. Recently, Natta *et al.* (1992) have made far infra-red observations of LkHα 198 which appear resolved at 100μm, and the measured flux of LkHα 198 agrees well with the IRAS point source data (but see §4.4.7). Moreover, it appears that in the far–infrared, less than 30% of the IRAS flux originates from V376 Cas. Natta *et al.* (1992) estimate the total luminosity of V376 Cas at $\approx 150\,L_\odot$, and that of LkHα 198 at $\approx 260\,L_\odot$. As LkHα 198 is more luminous they consider it a more likely source of the molecular outflow. As to the suggestion that V376 Cas is better positioned for driving the outflow (Chavarría 1985); Nakano *et al.* (1990) has observed the LkHα 198 region in many different molecular lines including those of ^{12}CO, ^{13}CO, HCO^+, HCN, and CS. They found dense molecular features around LkHα 198 but no traces of such structures near V376 Cas, thus supporting the notion that the source of the molecular outflow in this region must be in the vicinity of LkHα 198. The NH_3 observations of Fuente *et al.* (1990) and CS observations of Fuente *et al.* (1992) also reveal high density material towards this source.

LkHα 198 is particularly interesting, in that as a HAEBES, like V380 Ori (see Chapter 2), it is also apparently associated with an optical outflow. Strom *et al.* (1986) observed the region about LkHα 198 through a [SII] filter and observed a bright knot at

P.A. 100° with respect to this star. By tilting the [SII] filter, it was possible to observe changes in the morphology of the knot with radial velocity. The object appeared brightest when the peak transmission of the filter corresponded to a $V_{LSR} = 0\,\mathrm{km\ s^{-1}}$, thereby suggesting that the knot might be a HH object with a low radial velocity. This feature has also been recently observed by Goodrich (1993). Goodrich (1993) also detected the presence of a fainter knot, which lies at P.A. 160° and at a distance of 81" with respect to LkHα 198. As to the other HAEBES, V376 Cas, the only report of HH emission from this object is thus far, an undetailed private communication by Neckel, in Leinert, Haas and Lenzen (1991) (hereafter LHL).

4.1.2 The Local Environment of LkHα 198 and V376 Cas: Polarisation Studies

The local environment of LkHα 198 and V376 Cas was investigated by Bastien *et al.* (1988). The authors find an extremely high degree of polarisation for V376 Cas and describe the appearance of faint plumes of nebulosity extending west from this object. For LkHα 198, what is described as a "bubble" shaped nebulosity is seen to its southeast. Most importantly, however, Bastien *et al.* (1988) suggests that in their linear polarisation map (which is not shown), the alignment of vectors near LkHα 198 provides evidence for a surrounding c.s. disk.

LHL have also examined the environments of both stars, and this was done in great detail using a variety of imaging, polarimetry and speckle techniques. For V376 Cas, LHL noted an elongation of the surrounding nebulosity (P.A. 120°) which persists to the smallest scales of their speckle observations. This elongation they suggest is best interpreted as a bipolar nebula. A polarisation map shows that V376 Cas clearly illuminates this nebula, but they also note that the alignment of polarisation vectors at the star indicates the presence of a c.s. disk. For LkHα 198, LHL find a much more complicated situation, with a variety of polarisation directions on different size scales. Firstly, the star is decomposed by their speckle interferometry into a central unresolved region (100 A.U.) and a more diffuse halo (1000 A.U), where the polarisation directions are 154° and 96° respectively. On larger scales, in their I band image, elongations of the so

called "bubble" nebula are noted by the authors towards P.A. 135° and P.A. 90°. The situation is then further complicated by the multicolour polarimetry of the star and the surrounding nebula. Within apertures of $\approx 10^4$ A.U., the measured polarisation directions vary between 169° and 163° (corrected for interstellar polarisation, B to I bands). LHL has further pointed out that it is very difficult to resolve any of these directions with the axes of the molecular and optical outflows (see above). Lastly, in their polarisation map, the "bubble" nebula is clearly seen to be illuminated by LkHα 198 (or possibly by another source in its near vicinity as will be seen), yet there seems to be no direct evidence for a disk structure as suggested by Bastien *et al.* (1988).

In the most recent polarisation observations, Piirola *et al.* (1992) substantiate the interpretation that the elongated nebula near V376 Cas, is in fact a bipolar reflection nebulosity. Moreover, they also confirm the presence of a disk based on the alignment of polarisation vectors close to the star, and the fall off in polarisation percentage towards null points. The latter, they interpret as resulting from the transition, from the optically thick inner parts to the optically thin outer parts of the disk. On this basis, Piirola *et al.* (1992) estimate the disk size as $\approx$ 500 A.U.. For LkHα 198, Piirola *et al.* (1992) found under excellent seeing conditions (0.4") an apparent alignment of polarisation vectors within a region of diameter 0.5" centered about this star. This alignment at P.A. 138°, they suggest, results from obscuration of the central source by a dense disk. However, they are uncertain of the disk orientation by 90°, which depends on the disk optical thickness.

4.1.3 The Local Environment of LkHα 198 and V376 Cas: Photometry

Harvey *et al.* (1979) were the first to observe LkHα 198 from 40–160μm. The authors suggested that the emission they detected although unresolved, might be thermal emission from spherically distributed c.s. material left over from the star formation process. Assuming spherical symmetry, they modeled the flat portion of the SED as arising from dust with a density gradient proportional to r^{-1}. With the adopted distance of 600pc (Harvey *et al.* 1979 used 1000pc) the density gradient would only apply within a range 1 to 10^4 A.U from the star. Hillenbrand *et al.* (1992) classified LkHα 198 and V376 Cas,

as Group II objects (see §1.3), which they argue are best explained as stars, (or possible star+disk systems) surrounded by c.s. dust. As pointed out by the authors, at least for these two stars, there is a large body of evidence which suggests that in the optical they are not seen directly but through scattered light (see also HPc and §1.3).

As mentioned previously (see §1.3) the most recent far–infrared observations (50 and 100μm) of LkHα 198 have been conducted by Natta *et al.* (1992). Natta *et al.* (1992) and Natta *et al.* (1993) have then used existing photometry in the optical and near–infrared together with their far–infrared observations, to determine the SED of LkHα 198. This SED they suggest is best explained by a two component model, in which the far-infrared flux arises from a spherical envelope, and the near–infrared emission arises from the presence of a disk. In particular, that portion of the envelope responsible for the far–infrared flux must be spherical, since the source is resolved at these wavelengths and appears centro-symmetric. To model the SED, Natta *et al.* (1992) and Natta *et al.* (1993) require a knowledge of the radiation field (including the stellar luminosity and effective temperature). In Natta *et al.* (1993), the models are constrained by the extent of the 50 and 100μm emission regions, the 50/100μm colour temperature and the flux at 100μm. It will be shown later that there is an inherent flaw in their model for the particular case of LkHα 198. A second source detected in the near vicinity of this star, LkHα 198B is of comparable luminosity in the mid-infrared.

4.2 Observation Details and Data Reduction

4.2.1 Direct Imaging

Optical direct imaging was obtained on the 4.2m William Herschel Telescope (WHT) on La Palma in September 1988. The observations were made using Taurus-2 in direct imaging mode with the f/4 camera option. Using a 400×590, GEC P8603 CCD as the detector, the projected pixel size on the sky was $0.27''^2$ resulting in a field of view of $1.7' \times 2.6'$. Direct imaging was carried out with both a narrow band [SII] filter (λ_c=6730Å, $\Delta\lambda$=48Å) and a nearby continuum filter, r_n (λ_c = 6890Å, $\Delta\lambda$ = 195Å). Seeing conditions were 1.4" and 1.2" for the [SII] and r_n images respectively and exposure times were 1800s.

Data reduction of the optical imaging was done using MIDAS, and the usual technique was employed to look for possible HH objects and HH jets (see §2.2.1 and §3.2.1). As mentioned previously, subtraction of a suitably scaled continuum frame (r_n) from the emission line frame ([SII]) reveals only emission-line regions which can either be HH emission or, in certain circumstances, HII emission. The latter need not be of concern here since LkHα 198 and V376 Cas are not associated with HII regions. Finally, to further highlight HH objects in the difference frame a median filter was applied to this image to reduce background noise.

To compliment the optical images, infrared imaging of the regions about LkHα 198 and V376 Cas was also carried out using the infrared camera facility (IRCAM) at UKIRT. Although the observations were principally made in the K band, an additional exposure of LkHα 198 was taken in J. The detector, exposure times and method of reduction are as previously described (see §2.2.1), however, the standard star used here was HD 30029 (m_J=7.26 and m_K=7.09).

Object	Date	P.A.	Exp. Time(s)	Slitwidth"	Grating	λ_c
LkHα 198	7 Aug. 1987	100°	2500	0.8	R1200Y	6650
V376 Cas	29 Aug. 1991	281°	2700	1.5	R1200Y	6631
LkHα 198	2 Sep. 1991	27°	2700	1.1	H1800V	6299
V376 Cas						
LkHα 198	3 Sep. 1991	27°	2700	1.0	H1800V	5889
V376 Cas						

Table 4.1: Observing log for the spectra taken at the INT.

4.2.2 Spectroscopy

Long-slit spectral observations were made at the 2.5m Isaac Newton Telescope (INT) in August 1987 and September 1991 using the intermediate dispersion spectrograph (IDS). In all cases the instrument was configured with a 500mm camera, and a GEC P8603 CCD with 22μm^2 pixels, as the detector. For the wavelength regime $\approx$ 6550–6750Å the R1200Y grating was chosen, since this afforded a dispersion of 0.36Å per pixel with a resolution (2 pixels) of 32 km s^{-1}. To examine the wavelength regions containing the [OI]$\lambda\lambda$6300,6364 and the NaD lines, the H1800V grating was selected. The dispersion for the H1800V grating was 0.23Å per pixel and the corresponding resolution (2 pixels) was 22 km s^{-1}. Details of the individual observations are given in Table. 4.1. For all images the scale along the slit direction was 0.3" per pixel and seeing varied between 1.1" and 1.3". All data reduction was performed using the IRAF package. For the purpose of spectral analysis the [SII]$\lambda\lambda$6716,6731Å lines were chosen, and except for measuring excitation, the Hα and the nearby [NII] lines were ignored.

4.3 Results

4.3.1 Optical Imaging

Comparing the [SII] and the r_n image of the LkHα 198 area (see Figs. 4.1(a) and (b)), a prominent HH object is seen at a P.A. of approximately 100° and at a distance of 12" from this star. This is the object first found by Strom *et al.* (1986) using a tilting interference filter technique (see §4.1), and it was presumed to be associated with LkHα 198. Henceforth it shall be referred to as Knot A. Another notable feature in both these images is the elongated "loop" structure, which has already been discovered by Bastien *et al.* (1988). This structure occurs both in the [SII] and continuum images and so is continuum (i.e. reflected) rather than shocked emission. The major axis of this "loop" (Loop A) lies approximately at P.A. 135°. Examination of the higher contrast continuum frame (see Fig. 4.1(c)) reveals that Loop A is in fact the brightest of two such structures. The fainter Loop B is seen to be displaced to the east, and one also notes the "rim" of nebulosity which may be the north western edge of this structure. The orientation of Loop B's major axis is approximately 130°, and therefore although Loop A and B are not concentric, their major axes have roughly the same position angle.

Turning now to the [SII]–r_n difference image, i.e. Fig. 4.1(d), it is possible to see, in addition to the known HH object, several fainter features and knots scattered within the frame. One of the most interesting is a prominent "tail", stretching back at a position angle of 135° from Knot A. Although both the "tail" and Knot A lie along the major axis of the inner reflection loop (Loop A), one notes that the optical outflow *does not point towards* LkHα 198 but, in fact, it points towards a bright stellar-like knot some 5" northeast of LkHα 198 (visible in Figs. 4.1(a) and (b)). The position of this knot is marked in Fig. 4.1(d) by the smallest plus sign and although, it is embedded in the nebulosity surrounding LkHα 198, it appears to be a star (this will henceforth be referred to as LkHα 198B).

Closer examination of the nebulosity also reveals that LkHα 198B lies at the north eastern apex of Loop A with knot A orientated along its main axis. One also notes that

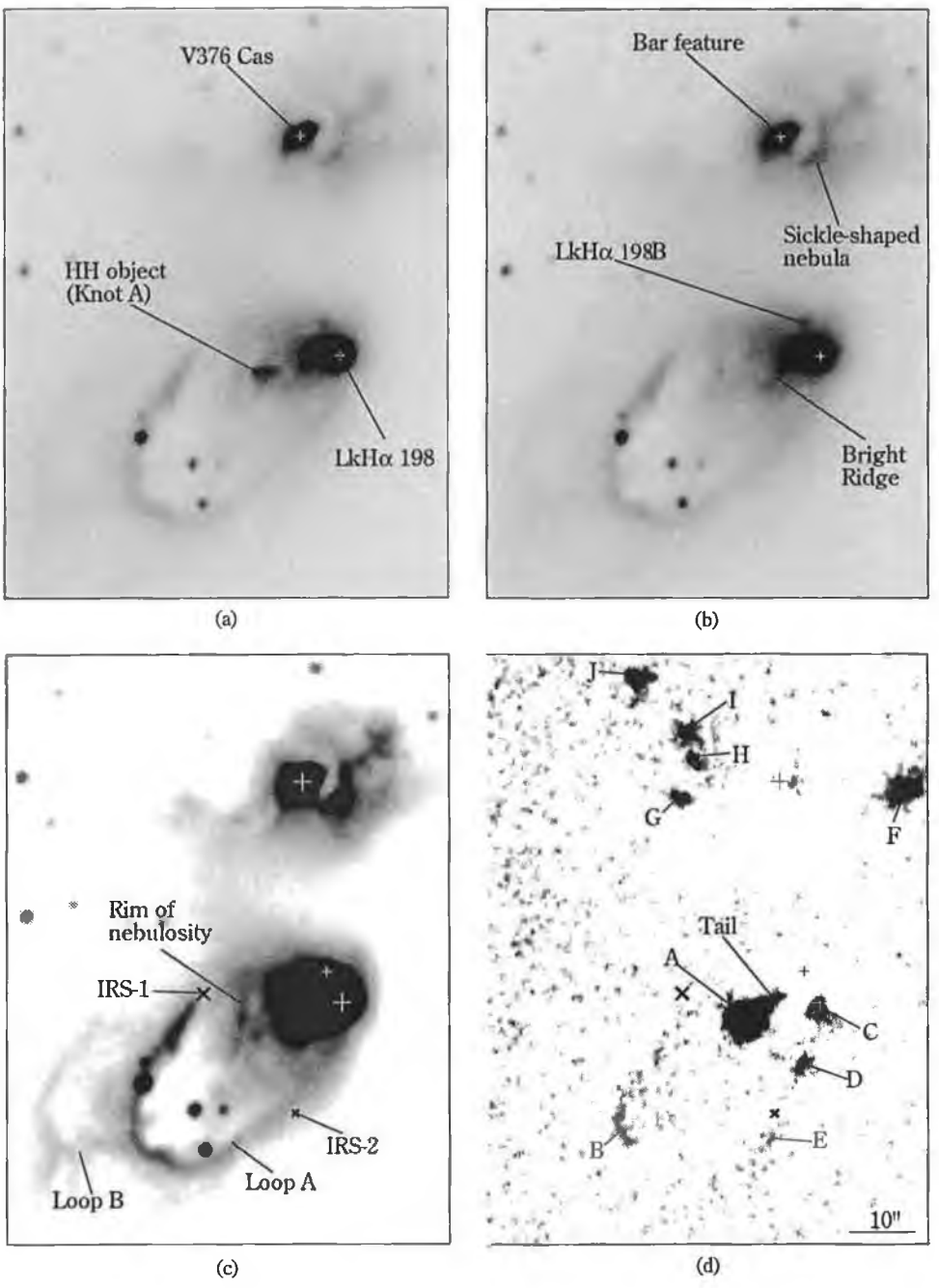

Figure 4.1: (a) A [SII] image of the region about LkHα 198 and V376 Cas. Note the presence of the known HH object (knot A) to the southwest of LkHα 198. (b) The same area as in a but through a nearby continuum filter (r_n). Note that the HH object disappears. Other features of interest include a diffuse knot (LkHα 198B) situated about 5" north of LkHα 198 and certain nebulosities. (c) As in (b) but at higher contrast which reveals the presence of additional faint "Loop" structures. Also marked are the positions of two infrared sources IRS–1 and IRS–2 (see text for details). (d) A [SII]–r_n difference image in which the distribution of the previously known and newly discovered HH knots is shown. One notes that for knot A, an extended "tail" is seen. In all frames north is to the top and east is to the left.

LkHα 198 itself is displaced to one side of Loop A. If one continues a line onwards from LkHα 198B through Knot A, eventually the curved feature B is encountered, some 39" away from LkHα 198B. Although this feature is more or less coincident with a section of Loop A, it is almost certainly not reflection nebulosity since the remainder of the loop vanishes in the difference frame.

As for LkHα 198 itself, some residual HH emission is found immediately to the south (C) which might be identified with the emission noted by Strom *et al.* (1986). That this is not an artifact of the subtraction process is confirmed by the spectra (see §4.3.3). The shape of this emission is best seen in the contour plot presented in Fig. 4.4(a) and it appears to open in a fan-shape (opening angle $\approx$ 100°) away from LkHα 198. Two additional HH objects (D and E) are seen at a position angle of 160° w.r.t. this star and these, along with possibly F, seem to define a collimated outflow. Indeed, D and E seem clearly to be portions of a jet. It is also particularly interesting that the newly-discovered HH knot by Goodrich (1993) is found along this direction (see §4.1), although it is more distant at 81" from LkHα 198 (see Fig. 4.2).

The alignment of F with the jet (C, D, E, and Goodrich's HH object) from LkHα 198, might be fortuitous, since apart from F several other HH objects are also present in the vicinity of V376 Cas. These are marked as G, H, I and J in Fig. 4.1(d). Spectroscopy, and perhaps proper motion studies, are required to determine what, if any, relationship they have to V376 Cas. Some remarks, however, can be made concerning these HH objects. First the semi-stellar Knot I contains a continuum, as well as an emission line, component. The continuum is very weak and can only just be seen in Fig. 4.1(c). Presumably the exciting star for Knot I is embedded in the HH emission. Second, one notes the bow shock-like appearance of J, the symmetry axis of which has a position angle of around 55° and which roughly points in the direction of Knot I and V376 Cas. Lastly, it is pointed out that only knot G, at a P.A. of 100° lies close to the direction (P.A. 120°) of the presumed bipolar nebula of V376 Cas.

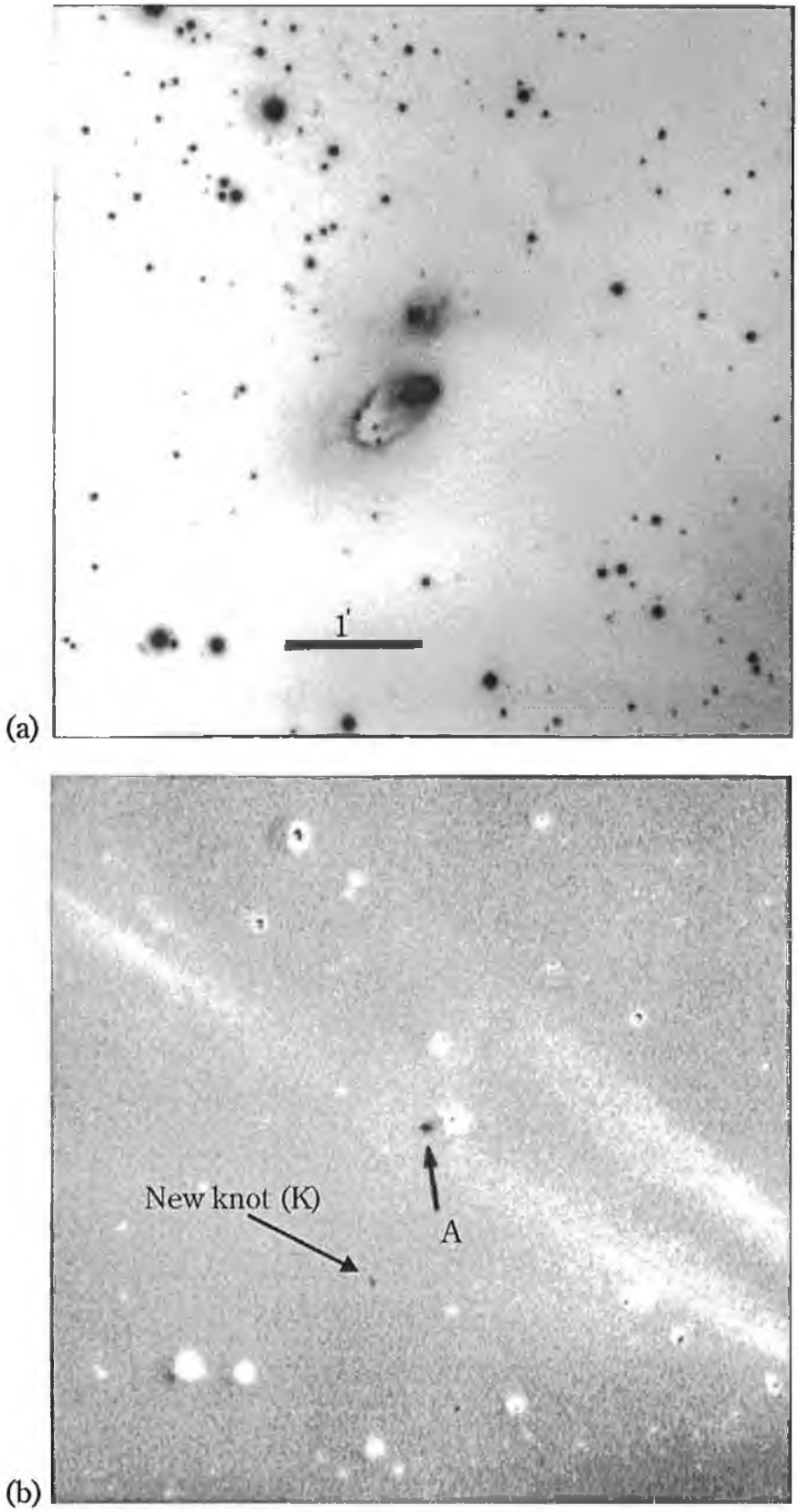

Figure 4.2: (a) A [SII] image and (b) a continuum-subtracted [SII] image of LkHα 198 taken from Goodrich (1993). Note in addition to knot A, the newly discovered emission line object at P.A. 160° w.r.t LkHα 198.

4.3.2 Infrared Imaging

In Fig. 4.3, a K band image of the region about LkHα 198 is displayed. In addition to LkHα 198, which is unfortunately saturated in this image, one can clearly see in the inset (shown at higher contrast) LkHα 198B positioned to the north. This star was also detected in J, and its apparent brightness has been determined as 13.8 mag in J and 10.3 mag in K. One other extended feature of interest is also indicated (IRS–1) in Figs. 4.1(c) and (d) by a large cross. IRS–1, is a moderately bright (m_K = 13.2 mag) peculiar non–stellar looking object which is detected solely in the K band within Loop A.

A K band image of the region about V376 Cas was also examined (not presented), and interestingly an extremely weak infra-red source (m_K = 18 mag) was detected coinciding with knot I (see Fig. 4.1(d)). Although other infra-red sources are detected in the vicinity of V376 Cas, they bear no obvious geometrical relationship to the optical HH knots and they are in general greater than 20" distant from them. One possible exception is an infrared source (m_K = 14.6), which lies about 6" west of knot F, (off the [SII]–r_n image in Fig. 4.1(d)).

4.3.3 Spectral Analysis

A long slit spectrum through LkHα 198 is shown in Fig. 4.4 for a P.A. 100° (wavelength range 6550–6750Å). The position angle was chosen such that Knot A (see §4.3.1) was contained within the slit and this choice was based on, what now appears to be the false assumption that Knot A is part of an optical outflow from LkHα 198. In Fig. 4.4 a position–velocity (PV) diagram is displayed for the [SII]$\lambda\lambda$6716,6731Å doublet in which the stellar continuum has been removed. For comparison a contour plot of the corresponding [SII]-r_n image indicating the slit position is also presented. Measurements were made of the heliocentric radial velocity (v_{rad}), electron densities (n_e), and excitation using the ratio of Hα/[SII]λ6716+6731. The line profiles however were unresolved in this spectrum, so true linewidths could not be determined.

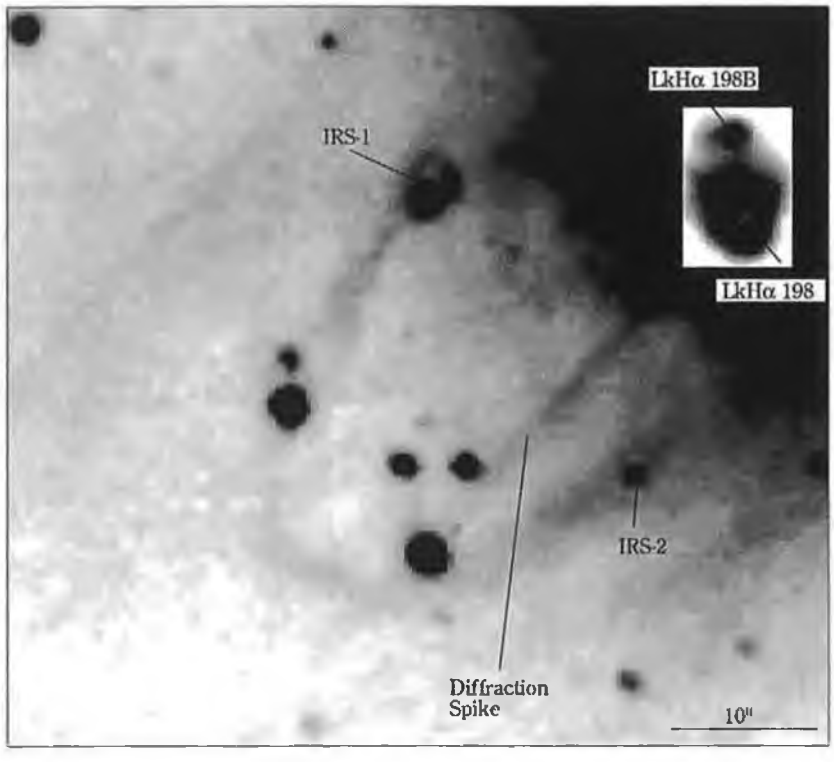

Figure 4.3: A K band mosaic of the region about LkHα 198. The inset reveals at a higher contrast the location of this star in addition to its newly discovered companion LkHα 198B. An infrared source IRS–1, is also indicated as it lies close to the axis of the optical outflow from LkHα 198 (P.A. 60°). Another noatable feature is the rather peculiar shaped IRS–2, which may in fact be H_2 emission (see text for details).

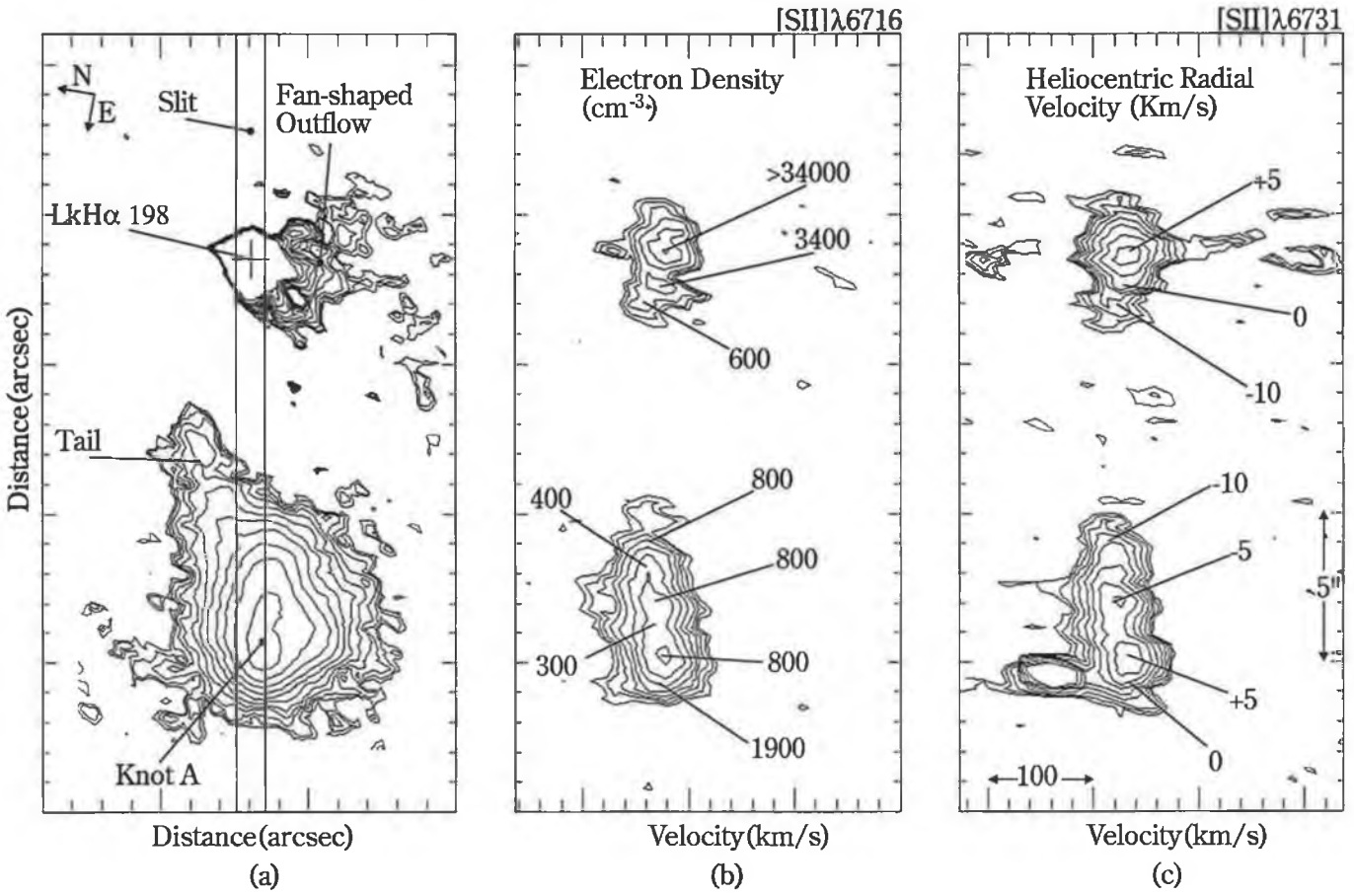

Figure 4.4: (a) A contour plot of the [SII]–r_n frame containing LkHα 198, its associated "fan-shaped" outflow, and the separate optical outflow of the "knot+tail". The slit positions and orientation of the frame are as indicated. (b) A contour plot of the [SII]λ6716 line. Electron densities at various features of interest are shown. In particular, note the decrease in electron density with increasing distance from LkHα 198. For the "knot+tail" higher electron densities are detected towards the knots and the outer edges of the feature. (c) As (b) but for the [SII]λ6731 line and with the heliocentric radial velocities shown. A marginal decrease in radial velocity is seen for the fan-shaped outflow, while the reverse is found for the "knot+tail". In both spectral lines the stellar continuum has been removed for direct comparison with (a).

Considering the almost fan-shaped HH emission (object C) extending a few arc-seconds to the south of LkHα 198 first, one notes that this emission seems to be virtually at rest with respect to the star. However, a marginal blueshifted increase in radial velocity is detected away from the star (+5 to -10 km s^{-1}). Accompanying this marginal increase in radial velocity is a steady decrease in the electron density, from >34000cm^{-3} at LkHα 198 to about 600cm^{-3} at about 2" distant. As already pointed out such a drop in electron density is typical of other optical outflows close to their source (see for example Mundt, Brugel and Bührke 1987). It is also important to note that since the radial velocities of object C are extremely low, its motion must be close to the plane of the sky. Moreover, as this object forms part of the collimated outflow associated with LkHα 198, then presumably knots D, E, F and Goodrich's HH object also have low radial velocities. With this in mind, a long slit spectrum was taken (by M. Corcoran) recently (July 1993) through LkHα 198 (P.A. 160°). Although the signal to noise is extremely weak, [SII] emission is seen to extend some 16" from the star, and the velocity of this emission remains low and constant.

Turning now to the brightest feature, i.e. Knot A and its "tail" (see §4.3.1), it is clear from the observations of Strom *et al.* (1986) that the radial velocity of Knot A is also low. The observations here show that not only is this true of Knot A but it is similarly the case for that portion of the "tail" covered by the slit. Variation in the radial velocity shows only a marginal decrease in value from -10 km s^{-1} to +0 km s^{-1}. As for electron densities, the higher densities appear to be associated with the condensations in knot A and its outer edges. In contrast, the excitation ratio Hα/λ6717+6731 is low (0.4) and varies little over the object's length.

Spectra of LkHα 198 are presented in Figs. 4.5(a) to (c). Firstly, one notes that the Hα profile (Fig. 4.5(a)) is double peaked, which is the most common shape for this emission line amongst HAEBESs (Finkenzeller and Mundt 1984). An estimate of the equivalent width of this feature is made by summing the flux above the continuum level (using a standard procedure in IRAF), and a value of -54Å is derived. This value is somewhat lower than that quoted by Cohen and Kuhi (1979) at -66Å and the lowest of the values by Nakano *et al.* (1990) at -65Å. Such variations in the Hα equivalent width are however, an expected characteristic of HAEBESs (Finkenzeller and Mundt 1984).

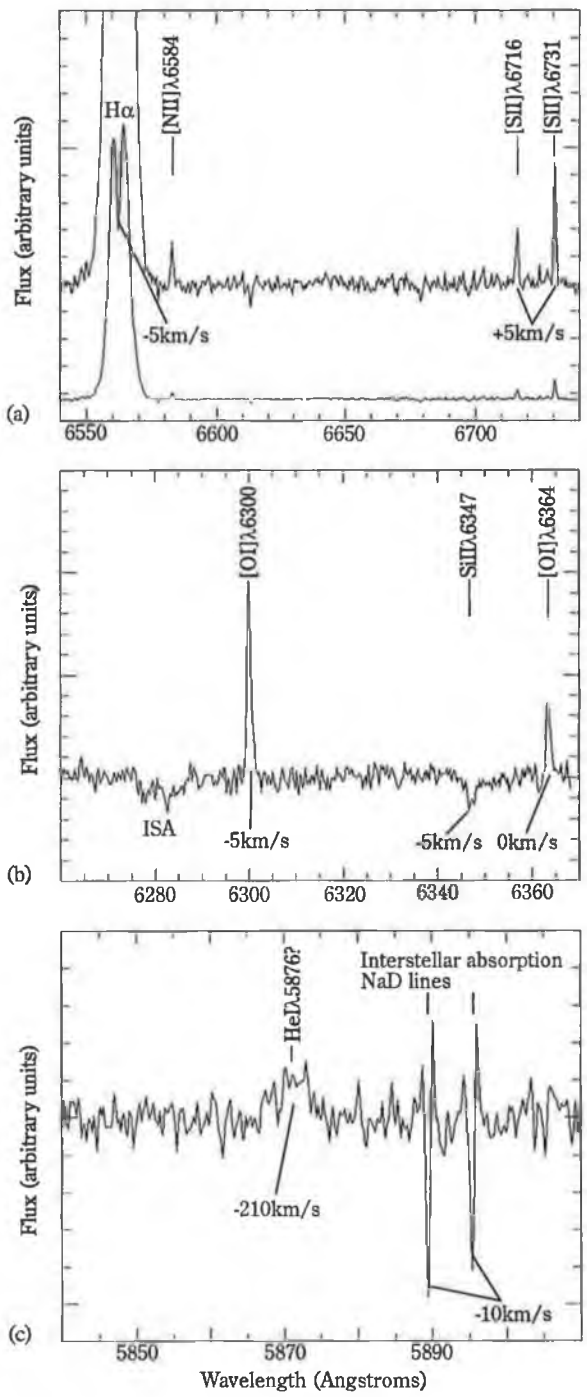

Figure 4.5: (a) A spectrum of LkHα 198 with various features and their respective heliocentric radial velocities indicated (wavelength range 6540–6750Å). In particular note the double peak profile of Hα and the presence of [SII] emission. (b) As (a) except for the wavelength range 6260–6270Å containing the well know [OI]$\lambda\lambda$6300,6364 lines. An interstellar absorption feature (ISA) is also marked. (c) As in (a) except for the wavelength range 5840–5910Å containing the NaD lines and the HeIλ5876 line. One notes that if the broad spectral feature is HeI then it is highly blushifted.

The forbidden emission lines of [SII]$\lambda\lambda$6716,6731 (Fig. 4.5(a)) and [OI]λ6300,6364 (Fig. 4.5(b)) are also detected within the spectrum of LkHα 198 and the mean heliocentric radial velocity of these lines is close to 0 km s^{-1}. It is interesting, that the equivalent width of the [OI]λ6300 line (-1.1Å) may have changed. From the observations made here it appears to be a factor of two smaller than the value previously recorded by Cohen and Kuhi (1979). Also noteworthy, is an absorption feature which is probably due to SiIIλ6347 (see Fig. 4.5(b)). The estimated equivalent width is $\approx$ 0.3Å, and its FWHM$_c$ is $\approx$ 90 km s^{-1}, a value consistent with the vsini's of other HAEBESs (see Finkenzeller 1985).

It is interesting to compare the heliocentric radial velocities of the local molecular cloud, with those of the stellar emission and absorption features. Finkenzeller and Jankovics (1984) have shown, that NaD ISA features and the local molecular cloud have similar radial velocities to the stellar emission and absorption lines. A local molecular cloud velocity of -9 km s^{-1} is determined from the observations of Cantó *et al.* (1984) after correcting for the solar motion of +20 km s^{-1} towards 18 hrs 30° (1950). This value is in excellent agreement with the radial velocities of the NaD ISA and the Hα absorption reversal in the spectrum of LkHα 198. One notes that the forbidden line emission is also close to the stellar velocity, which may be because the outflow lies close to the plane of the sky.

Finally, it can be seen in Fig. 4.5 that there is marginal evidence for NaD emission in the spectrum of LkHα 198, but most importantly the HeIλ5876 line appears quite blueshifted (the broad emission extending from approximately -90 to -450 km s^{-1}). Blueshifted HeI lines have already been noted for the luminous stars such as V645 Cyg and AFGL 4029 (Hamann and Persson 1989, Ray *et al.* 1990) and in the HAEBESs e.g. MWC 1080 (Poetzel *et al.* 1992). In these cases, however, the blueshifted feature is seen in absorption rather than emission. It is also particularly noteworthy, that the measured equivalent width of the HeIλ5876 line is only -0.7Å, which is considerably less than that inferred by Chavarría (1985); from his optical photometry, he expected a feature (either HeIλ5879 or the NaD lines) of -40Å ($\pm$ 30%).

Spectra of V376 Cas are presented in Figs. 4.6(a) and (b). A spectrum in the wavelength region containing the HeIλ5879 and NaD lines is not presented since neither feature was observed (presumably because of the poor S/N ratio). Examining the Hα line first, (see Fig. 4.6(a)), one finds that like LkHα 198 a double peak profile is evident, however, for V376 Cas the profile is a great deal more asymmetric. The equivalent width for this line is estimated at -39Å, which is only marginally greater than the value of -37Å determined by Cohen and Kuhi (1979).

Both [SII]$\lambda\lambda$6716,6731 and [OI]λ6300 forbidden lines are detected within the spectrum of V376 Cas. Although, marginally blueshifted (-20 to -30 km s^{-1}), one sees that the radial velocity of the Hα absorption dip has a similar value (-40 km s^{-1}). The latter feature, like that in the spectrum of LkHα 198 is interpreted as an absorption reversal, (its radial velocity being therefore representative of the star's systemic motion). Thus as is the case for LkHα 198, the radial velocities of the forbidden lines are similar to the rest velocity of the star. Again the explanation maybe that the outflow from V376 Cas is moving in the plane of the sky. Lastly, it is worth pointing out that the measured equivalent width of the [OI]λ6300 line is -3.2Å, which compares reasonably well to the value derived by Cohen and Kuhi (1979) of -2.8Å.

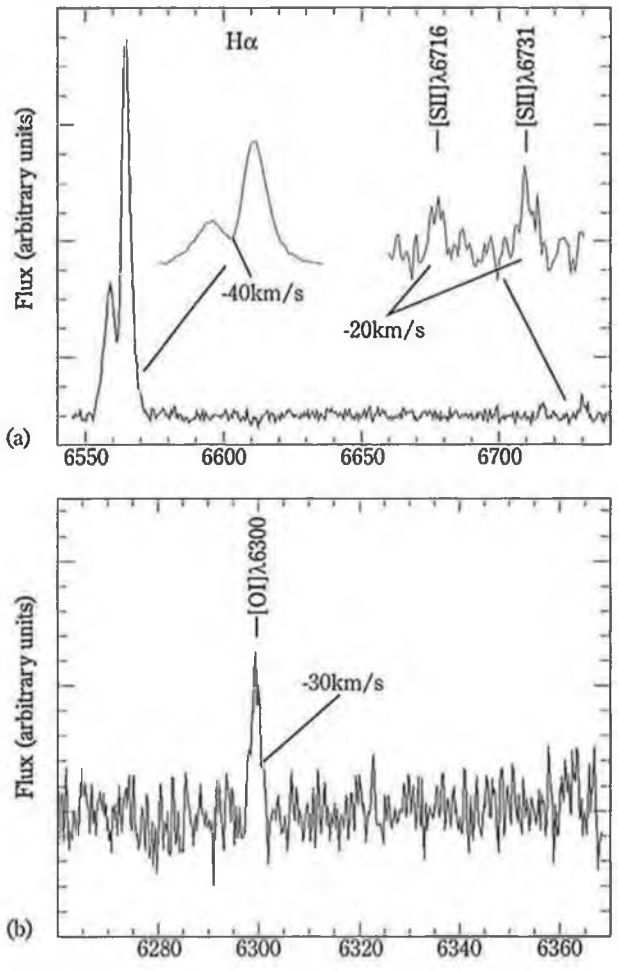

Figure 4.6: (a) A spectrum of V376 Cas with various features and their respective heliocentric radial velocities indicated (wavelength range 6540–6750Å). Note the assymetric shape of Hα, and that the aborption dip in this profile is blueshifted by a similar amount to the [SII]$\lambda\lambda$6716,6731 lines. (b) As (a) except for the wavelength range 6260–6270Å. The [OI]λ6300 line is seen and has a similar blueshift to the previous spectral features.

4.4 Discussion

4.4.1 LkHα 198 and its Companion LkHα 198B

As mentioned in the Introduction, LkHα 198 is a HAEBES and collimated optical outflows from such stars, although not unknown, are rare. Up to now it has been assumed that the bright emission knot, discovered by Strom *et al.* (1986) i.e. Knot A, traced an optical outflow from LkHα 198 at a PA 100°. Both the difference image and its spectrum confirm the HH nature of Knot A (contradicting Nakano *et al.* 1990), but the "tail" feature associated with this object, instead of pointing towards LkHα 198, points towards the newly discovered star, LkHα 198B.

4.4.2 The Optical Outflow from LkHα 198B

A more detailed picture of Knot A's morphology is seen in the contour plot of Fig. 4.4(a). It should be pointed out that the deconvolved width of Knot A and its tail is approximately the same (2") over the entire length of this object (10"). Indeed, the aspect ratio (i.e. the length to diameter ratio) is marginally within the parameter range for what one might call a jet (see Mundt 1988). However, given the widely different intensities of these two features it is perhaps more appropriately described as a "knot+tail". In comparison with other optical outflows (see, for example, Mundt *et al.* 1987) the estimated mass loss rate $\approx 10^{-8}$ $M_{\odot}$/yr is typical of a low mass outflow[1] while its low absolute radial velocities ($\leq$ -10 km/s) imply that its motion is in the plane of the sky. As pointed out previously, if one then projects this outflow to the southeast, the bow-shaped object B is encountered (see Fig. 4.1(d)). Although this is not a good example, its structure is reminiscent of other bow-shaped HH objects, e.g. the HH 34 system (Bührke, Mundt and Ray 1988), or RNO 43N (Ray 1987).

[1]The mass loss rate was calculated following the procedures of Mundt *et al.* (1987). Recently, this method has been questioned and it may well be, that the value quoted here and those in Mundt *et al.* (1987) are underestimated by one or two orders of magnitude (see Ray 1993 for details).

4.4.3 The Origin of the Reflection "Loop" Nebulae

With the presence of two stars LkHα 198 and LkHα 198B separated by only some 5" or 3000 A.U., it is necessary to address the question as to which of them illuminates Loops A and B. For example it has been claimed by LHL and more recently by Piirola *et al.* (1992) from their polarisation data, that the inner loop (Loop A) is seen in scattered light from LkHα 198. This, however, is because LkHα 198 is close to the centre of the usual circumferential pattern. LkHα 198B may thus be equally responsible. Given that LkHα 198B lies at the apex of Loop A, while LkHα 198 is displaced to one side, and that the axis of the optical outflow associated with Knots A and B, lies along the major axis (P.A. 135°) of Loop A, it would appear that LkHα 198B is the more likely illuminator of this the brightest loop. The origin of the loop structure then most probably arises from a limb brightening effect, in which one presumably sees the edge of a wind blown cavity.

The explanation of the fainter Loop B is slightly more complicated owing to the presence of IRS–1. If this feature is stellar (although its appearance does not suggest it), then the "rim " of nebulosity (see Fig. 4.1(c)), might represent part of a conical nebula with IRS–1 situated close to its apex. In this way, one could then attribute the origin of both this nebulosity and Loop B to IRS–1 rather than LkHα 198B. A more likely explanation given the non-stellar appearance and its presence in only the K band is that IRS–1 could be H_2 emission, as is the case for the rather diffuse knot seen near V380 Ori (see §2.5.1). Indeed, it is then extremely interesting that the shocked emission knots A and B, together with IRS–1, all occur at positions where Loops A and B seem to overlap (see Fig. 4.1(c)). A suggestion therefore, is that the fainter Loop B might represent an earlier outflow from LkHα 198B. After some time the dominant wind direction of this star has changed blowing a new cavity (Loop A). At regions where these cavities overlap, local density enhancements might be expected with the result that bright shocks would occur.

4.4.4 The Optical Outflow from LkHα 198

For the newly discovered optical outflow (C, D, E, Goodrich's HH object, and probably F), it is important here to check whether LkHα 198 is the only possible outflow source. An infrared source (labelled IRS–2) is seen close to the outflow axis (see Figs. 4.3 and 4.1(d)) but this star, however, has an apparent brightness considerably smaller (by nine magnitudes in J and K) than LkHα 198. Thus the star is of low luminosity and/or heavily embedded within the molecular cloud. Moreover, it is only one of many similar infrared sources within this region (see Fig. 4.3) and so, the chance coincidence of one such source with the outflow axis is high. Most importantly however, one notes that HH emission has been detected at the position of LkHα 198 while none has been detected at the position of IRS–2. It is thus almost certain, that the occurrence of IRS–2 along the outflow axis is merely a random coincidence.

The spectroscopic data on object C and that inferred from the most recent observations, clearly indicates that the optical outflow from LkHα 198 exhibits low radial velocities. Its motion therefore is most probably in the plane of the sky. Given the P.A. of this outflow is 160°, it is noteworthy that its orientation is then very similar to the outflow from LkHα 198B (P.A. 130°), the motion of which is also tangential to the line of sight. One also notes the similarity of these orientations with the axis of the bipolar nebula centered on V376 Cas (P.A. $\approx$ 120°). Such alignments are not uncommon amongst small associations of YSO's (Strom *et al.* 1986, Ray 1987, Reipurth 1989), in which the local magnetic field is thought to dictate the outflow direction. However, LHL has found that the interstellar polarisation (and hence the interstellar field) is at 67° $\pm$ 14°, i.e. approximately normal to the LkHα 198 and LkHα 198B outflow directions. It is likely therefore, that the interstellar magnetic field has been substantially disturbed in this region.

4.4.5 The Origin of the Molecular Outflow

The obvious question arises as to whether LkHα 198 or its companion LkHα 198B drives the bipolar molecular outflow in this region? Up to now, it has been generally accepted

that LkHα 198 is responsible, but, the presence of LkHα 198B complicates the picture. The optical outflows from LkHα 198 and LkHα 198B have different PAs of 130° and 160° respectively but the uncertainty in molecular outflow axis is within this range (see Strom *et al.* 1986 and LHL). Moreover, although in the near-infrared LkHα 198B is considerably fainter than LkHα 198 (about 4 mags lower in both J and K), a recent observation (Oloffson private communication 1993) reveals that at 10μm, this star is already of comparable luminosity (about 40% of the 10μm flux of LkHα 198). Given the embedded nature of LkHα 198B it is perhaps more plausible that this is the molecular outflow source[2] but an uncertainty still remains.

4.4.6 The Polarimetric Data of the LkHα 198 Region:An Explanation

Knowing the PA of the optical outflow from LkHα 198 and that a companion is present, largely explains the confusing polarimetric data of LHL (see §4.1.2). Indeed, in Fig. 1 of LHL (a polarimetric map in the I band) there are clear indications of deviations from the normal centro-symmetric pattern around LkHα 198 at the position of LkHα 198B. Close to LkHα 198, within 100 AU, LHL observed the polarisation direction to be 154° but on a larger scale (approximately 1000 AU) their model indicated a polarisation direction of 96$\pm$10°. LHL found it difficult to relate the observed geometries and polarisation directions, together with the axes of the observed CO outflow and the apparent optical outflow axis (defined by Knot A and LkHα 198).

LHL interpreted the polarisation at 154° in terms of single scattering in a disk of moderate optical thickness ($\tau_{1.6\mu m} \approx 1$) the axis of which is at this angle. Such a disk orientation is clearly consistent with the direction of the optical outflow discovered here (P.A. 160°). At greater distances (i.e. 1000 AU), it is possible that one is largely observing scattered light from this disk, perhaps mingled with a contribution from an anisotropic surrounding medium[3]. One must ask the question however, how can the

[2]Most sources of the known molecular outflows are EIRSs (e.g. Fukui 1989)

[3]This medium might be the lobes or cavity walls produced by the stellar wind, but LHL have interpreted the halo region as remnant material left over from the star formation process. This point will be considered in the next section

disk orientation derived by Piirola *et al.* (1992) at P.A 138° (± 90°) be resolved with that derived by LHL (P.A. 154°). To understand this consider that for an optically thick disk ($\tau > 1$), the polarisation angle is perpendicular to the disk axis (see Bastien 1987). Thus for LkHα 198 as the disk optical thickness increases (as might occur when one observes the disk at progressively shorter wavelengths) one expects the polarisation direction to change from P.A. 154° towards P.A. 64°. This would explain the smaller angle (P.A. 138°) found by Piirola *et al.* (1992) since their observations were made at a shorter wavelength (0.9μm) than those of LHL (1.6μm). Piirola *et al.* (1992) are presumably observing polarisation from the disk but at an optical thickness somewhere between the optically thick and optically thin limits. It is also interesting to note that on scales of around 5×10^4 A.U., Nakano *et al.* (1990), found a NE-SW disk like distribution in both CS and HCO^+ lines i.e. approximately normal to the optical outflows.

One must also address the question of whether it is likely that the disk surrounding LkHα 198 is optically thin at 1.6μm. In general the YSO disks are expected to remain optically thick well into the far infrared (e.g. see Beckwith *et al.* 1990). Since the optical outflow from LkHα 198 is almost in the plane of the sky, the disk which is normally at right angles to the outflow direction, as e.g. in HL Tau (see Appenzeller and Mundt 1989, and references therein), must be seen almost edge on. Moreover, the c.s. disk is likely to be geometrically thin (see e.g.. Bertout 1989), which at the distance to LkHα 198 would correspond to a size of only some hundreds of an arcsecond i.e. outside the range of even the LHL speckle polarimetry. Moving out of the disk plane the scattering medium would then presumably become optically thinner. Thus, in the observations of LHL one would expect to see light predominantly scattered from above and below the optically thicker parts of the disk. In this way one can associate the orientation of the polarisation vector derived by LHL (P.A. 154° within the core region of 100 A.U.), with either optically thinner parts of the disk, and/or the surrounding dust in the inner lobes of the cavity walls (both of which would be indistinguishable). On larger size scales (10^4 A.U.), the results of the multicolour polarimetry of LHL , show that the orientation of the polarisation vector is between 163° and 169° i.e. almost parallel to the optical outflow from LkHα 198. This polarisation direction is thereby consistent with single scattering in the outer lobes or cavity walls of this star.

4.4.7 Has LkHα 198 a Far-Infrared halo?

The most recent models for LkHα 198 (Hillenbrand *et al.* 1992, Natta *et al.* 1992, Natta *et al.* 1993) all propose a star/disk system surrounded by an envelope of material (see §. 4.1.3). That a disk is present seems reasonably certain (see above), however, whether there is an envelope of the type described by Natta *et al.* (1992;1993) surrounding LkHα 198, is open to question. The presence of this envelope is inferred principally from a far infrared excess found about the star (Harvey *et al.* 1979, Hillenbrand *et al.* 1992) which has been resolved by Natta *et al.* (1992) and which the authors suggest appears spherical.

The discovery of LkHα 198B, which rises from 3% of the K band luminosity of LkHα 198 to 40% at 10μm, is obviously of relevance here. One does not know a priori whether the 100μm emission (and in particular the extended component) comes from LkHα 198 or LkHα 198B. The resolution of the 100μm KAO observations described by Natta *et al.* (1992;1993) is around 30" and this obviously leads to confusion. While it is important to stress that there is good evidence in this case, as in many others, of a far–infrared halo (see Natta *et al.* 1993), there is some question here not only whether a spherical distribution is appropriate, but moreover, which star the halo is associated with. It should also be noted that published SEDs for LkHα 198 refer to both stars at least longwards of the near-infrared.

Since the excess of mid–infrared flux which has in the past been attributed to LkHα 198 may now possibly be attributed to a companion star, high resolution photometry is required to separate the SED of both stars. Only then can accurate models of the environment of LkHα 198 be made. In particular, it would be extremely interesting to know whether, the density distribution of material in the halo region of LHL (1000 A.U.), is either a remnant of the star formation process, or material driven by a stellar wind.

4.4.8 V376 Cas and its Surrounding Region

In §4.3.1, it was seen that several faint HH objects lie in the region surrounding V376 Cas. One of these, knot F, is probably a component of the outflow from LkHα 198, however, as pointed out earlier, it may alternatively be associated with a K band source located some 6" to its west. Of the other objects, J with it's bow shock-like morphology appears interesting. At a PA of 54°, it points back roughly towards V376 Cas. LHL and Piirola *et al.* (1992), have however, concluded that the "bar-like" continuum emission around this star arises in a bipolar nebula at a PA of 120°. If this interpretation is correct, it would then appear that the alignment with the bow axis is simply fortuitous. Another possible source, as has already been mentioned, may be knot I. Although largely HH emission, knot I also contains a faint optical continuum and is detected, albeit marginally, in the K band ($m_K = 18$). In other words, it may be a star. If a star is present, then the P.A. of this outflow is some 48° and by virtue of its proximity and its orientation, knot H may also be associated. Interestingly, the orientations of knots H, I and J roughly coincide with the direction of the local magnetic field. As for knot G, it is tentatively suggested that at a P.A. of 100° w.r.t. V376 Cas, it may be associated with an optical outflow from this star.

Chapter 5

Summary and Conclusions

In the following, a summary and conclusions are presented for the investigations conducted here into the optical outflows in the vicinity of four intermediate/high luminosity YSOs. Based on this work and existing studies, the nature of optical outflows from such stars is examined, in particular, the question of whether their optical outflows are more frequently poorly collimated than those from lower luminosity sources? Throughout this chapter possible work that might be carried out in the future will be indicated.

5.1 The V380 Ori Region

A remarkable emission line "loop" discovered here together with the previously known CO molecular lobe, was interpreted, as revealing a poorly collimated bipolar outflow in the vicinity of the HAEBES V380 Ori. The optical and molecular data are most easily explained if this star lies close to the edge of a molecular cloud. Although, two near infrared sources were detected close to V380 Ori, and therefore were potential outflow sources, it seemed unlikely that this was the case. One of the objects V380 Ori-B is not associated with an IRAS point source and is of inherently lower luminosity. The second source, V380 Ori-C, is owing to its diffuse morphology, its detection solely in the K band and its association with a number of HH objects, most likely H_2 shocked emission. V380 Ori is therefore the most probable source of the poorly collimated bipolar outflow.

The orientation of the bipolar outflow is an east–west direction. Moreover, it was suggested that the outflow also moved predominantly in the plane of the sky. Such an orientation would explain not only the low radial velocities of at least two HH objects namely, HH 35a and object B (components of the emission "loop"), but also the low radial velocities of the molecular outflow. Indeed, such an outflow direction also explained the observed change from a symmetric Hα spectral profile at V380 Ori, to the assymetric Hα redwing seen in the surrounding nebula. One can understand this by assuming the local dust in the nebula reflects the view from within the outflow lobes, hence a P-Cygni type wind profile. In contrast, looking directly at the star, the profile is symmetric since the wind is moving almost perpendicular to the line of sight.

To explain the poorly collimated bipolar outflow, several momentum driven models for the production of an oval shaped cavity were examined. To do this the predicted cavity shapes were compared qualitatively with the observations of the emission "loop" and it was found that for most cases they were not in agreement. The predicted cavities either ended in a bright shock, or tapered off too sharply, neither of which is seen. The best agreement was found, where the cavity was formed by the wind's ram pressure alone. Such an alternative had been explored in both the models of Cantó (1980) and Smith (1986). Not only did this relax the necessity of a bright termination shock, but it allowed for a weaker more spherical shock front at the cavity end. This model also had the benefit of explaining some of the radial velocity trends observed for the HH objects nearest V380 Ori. A supersonic flow would be expected to occur along the cavity walls nearest the source, and the observed decrease in radial velocities of the HH objects with distance from V380 Ori, could be explained by the changing flow direction along the cavity walls with respect to the line of sight. However, such a model could not explain the higher electron densities of the furthest HH objects nor could it explain their lower excitations. Moreover, it was uncertain whether the furthest parts of the emission "loop" (I, J and K) were actual HH emission, though it was clear they outlined the edges of a wind blown cavity. The conclusion drawn is that the existing models poorly explain the observed properties of the emission "loop".

An alternative model was suggested in which the bipolar outflow represented an earlier outburst in activity from V380 Ori. The emission "loop" and molecular lobe would

then simply delineate a cavity which is at present not evolving. It was demonstrated however, that the collapse of such a cavity would take of the order of a HAEBES lifetime. In such a model, the observed HH emission would simply be the result of the present wind from V380 Ori interacting with the cavity walls. Higher densities at greater distance from the source would imply that this wind is still time variable. As to the more distant components of the emission "loop" these might have been gas collected along the edge of the cavity and subject to local ionisation, i.e. they would be part of the weak HII emission which was shown to cover the entire region. As weakly ionised gas it was then possible to understand the orientation of two components I and J with the large scale magnetic field. Obviously long slit spectra would be useful here in determining whether these components are indeed, HII emission or as previously thought weak HH objects. As to the the bullet shape objects of presumably HH emission seen to the north of V380 Ori, these objects were connected by fingers of weak line emission to NGC 1999, which argued for their association not only with the nebula but presumably with its illuminating source V380 Ori. Indeed, their positional coincidence with the molecular outflow, might suggest that they are associated with the counterflow from this star.

There is ample evidence to support outburst activity, in V380 Ori. Certainly, it was noted that the Hα line of this as in many other YSOs is highly variable. Most importantly however, it is apparent owing to the presence of LiIλ6708 and various FeI absorption features that the star cannot be as previously thought an A0 star, more likely its spectral class should be later than F0 i.e. it is a T-Tauri type star. If the bolometric luminosity is as high as 300 $L_\odot$ (but see §2.5.4), then much of the luminosity must arise outside the star perhaps in an active accretion disk. A more conservative value of the bolometric luminosity has been made by Berilli *et al.* (1992) who compute this value for V380 Ori, at between 80 and 140 $L_\odot$. Even so, this is extremely high for a T-Tauri star, the luminosities of which would be usually a factor of ten times smaller. Indeed, it may well be that this large luminosity represents the latest energetic outburst from V380 Ori, and that it is this outburst which is responsible for the presently observed HH emission.

As to the region about V380 Ori, two other notable optical outflows were investigated, including one which was newly discovered here, namely HH 147. For the other, HH 130, it had previously been thought to be an isolated object but was shown here to be

part of an extended (0.7pc) outflow. In particular, it was demonstrated that this optical outflow could be well explained in terms of a "light jet" i.e. one that is less dense than its surrounding medium. The source of the outflow was not discovered and infrared imaging would be useful in determining its location. As for HH 147, it was best interpreted as arising from a poorly collimated wind observed edge on. The source of this outflow, is a T-Tauri star N^3K50 which exhibits a P-Cygni spectral profile in the Hα emission line. Owing to the rarity of such stars in particular those associated with optical outflows, HH 147 and its source are good candidates for an in-depth observing campaign.

5.2 Cep A

As with V380 Ori, an emission line "loop" was also discovered to be associated with the EIRS in Cep A. The HH "loop" to the east of this source, together with GGD 37 in the west, clearly revealed the presence of a bipolar poorly collimated wind. Moreover, by examining the existing data at various wavelengths, in particular H_2 and radio observations, it was demonstrated that the optical emission "loop" traces a presumably wind blown cavity which is seen through progressively greater extinction closer to the source. Unlike V380 Ori, it is also more apparent that the entire "loop" structure arises from shock excitation. It was uncertain however, whether the apparent differences in morphology between the east and west outflows, would be caused by either differences in the environments or whether they are due to an intrinsic asymmetry in the bipolar outflow.

The question of the outflow direction was also investigated. In particular there seemed to be considerable controversy amongst earlier studies, not only as to what this direction might be, but also on exactly how many outflows were present. Hayashi *et al.* (1988) for example had suggested that there were in fact two molecular outflows; a lower velocity flow to the northeast–southwest, and a higher velocity flow in the east-west direction. However, it was proposed here that a single East–West outflow could also produce this effect, either by a latitude dependent wind or the molecular material being driven in an expanding shell viewed almost edge on. In either case a range of velo-

cities would be expected both in the northeast–southwest and the southeast–northwest directions, but the highest velocities would always be along the outflow axis i.e. the east–west. On detailed examination of the data of Hayashi *et al.* (1988) such an effect could be observed. Furthermore, from the existing proper motion data it was deduced that the outflow appeared to move predominantly in the plane of the sky. It was concluded therefore, that the most likely cause of the apparent multiple molecular outflows was a projection effect of molecular material expanding in a shell.

The two brightest objects in the emission line "loop", namely HH-NE and HH-NE2, were shown to have both the morphology and excitations characteristic of bow shocks. As to the origin of these objects it was suggested that they might result from inhomogeneities in the poorly collimated wind but it was also noted that they both occur along the edge of the "loop" structure (a point which is discussed below). As to other objects in the emission "loop", their shock properties should be investigated in a future study.

5.3 LkHα 198 and V376 Cas

One of the most important discoveries made here was the detection of a companion star to LkHα 198, LkHα 198B at only some 5" distant. In particular, it was shown that an emission line knot previously suspected of being HH emission associated with LkHα 198, although indeed HH emission, was in fact part of an outflow from the companion star. This star was also proposed as a more likely source of the observed reflection "loops", being better positioned geometrically at the apex of these nebula. Furthermore, it was clear that the observed optical outflow from LkHα 198B, lay directly along the central axis of the inner reflection "loop".

A K band source (IRS–1) brought into question, the source of the outermost reflection "loop", however, it was concluded, that IRS–1 was not sellar but most likely shocked H_2 emission. Certainly, this source should be considered for H_2 imaging and near infrared spectroscopy. It was further noted that the location of IRS–1 and the optical outflow from LkHα 198B seemed to coincide with possible overlap positions of the inner and

outer reflection "loops". It was proposed therefore that these "loops" delineated separate cavities blown at different times from LkHα 198B. Where these cavities overlapped local density enhancements together with the new wind, would give rise to the observed shocks.

A separate optical outflow was also detected from LkHα 198. The HH object closest to this source was found to be fan–like (opening angle $\approx$ 100°), thus obviously showing evidence of poor collimation. At greater distances however, several objects were found to be almost collinear with a P.A. of 160° with respect to LkHα 198. The similarity of the outflow direction with that of the outflow from LkHα 198B (P.A. 130°) and the bipolar nebula of V376 Cas (P.A. 120°), suggested some form of local alignment of the outflows in the region. Indeed, low radial velocities were found for both optical outflows, and also for V376 Cas as indicated by [SII] line emission of that star. Such a characteristic implies that the orientations of the outflows in the plane of the sky, reflects their true spatial directions. Importantly, however, the alignment was not with the magnetic field (P.A. 64°) as might be expected (Strom *et al.* 1986, Reipurth 1989b), but approximately normal to this direction. In this context, one also notes that many of the optical outflows in the vicinity of V380 Ori, are also orientated at right angles to the expected magnetic field direction e.g. HH 147 (see also Chapter 2 and Fig. 2.12). The question of outflow orientation with magnetic field obviously warrants further investigation, not just for the regions observed here but also in existing and any further studies.

The detection of outflows from both LkHα 198 and LkHα 198B allowed the re-interpretation of existing polarimetric studies, the results of which had previously been confusing. In particular, it was found that the polarisation direction within 100 A.U. of LkHα 198 (P.A. 154°), was consistent with the interpretation of light scattered either in the optically thinner parts of a c.s disk viewed edge on, or in the lobes or cavity walls close to the star. The proximity of LkHα 198B to LkHα 198 also raised some questions. For example, it is now uncertain to which of these stars the molecular outflow in the region can be attributed to. Given that most molecular outflow sources are deeply embedded like LkHα 198B, the latter may well be the more likely candidate. Furthermore, since the SED of LkHα 198B appears to be rising steeply towards the far infrared, it is probable that this star dominates the extended emission observed at these wavelengths. The existence of a far infrared halo around LkHα 198 is therefore drawn into question.

For V376 Cas, although several possible HH objects were detected in its near vicinity most of these are probably associated with a separate embedded star. Only one object (Knot G) was close to the presumed outflow axis of V376 Cas (P.A. 120°), and this was tentatively suggested as being associated. Spectroscopy and perhaps proper motion studies are required to verify the relationships proposed here. Indeed, such studies should also be carried out in the future for the optical outflows from both LkHα 198 and LkHα 198B.

5.4 The Question of Poorly collimated Optical Outflows from Intermediate/High Luminosity Sources?

Excluding V376 Cas, for which the evidence of any associated outflow is only tentative, the remaining three high luminosity sources examined here, clearly possess poorly collimated optical outflows. Of course the best examples are the HAEBESs, V380 Ori, and the EIRS, Cep A, but the rather broad fan shaped HH object nearest LkHα 198 is also indicative of poor collimation. In the following the question of whether such a phenomenon is *frequently* seen amongst higher luminosity sources is examined.

From previous studies, there are approximately ten good examples of optical outflows associated with high luminosity sources (see Table 1.1). In at least three cases, these outflows are regarded as being definitely poorly collimated, namely V645 Cyg, MWC 1080 and Cep A (see §1.4.3). Obviously, V380 Ori also belongs to this sample, (which will be henceforth referred to as type I outflows) but the morphology of LkHα 198 is strikingly different. Indeed, if one excludes the HH object coincident with the star, the appearance of the optical outflow is jet like. In at least one other HAEBES a somewhat similar outflow is observed namely, LkHα 234 (see Ray *et al.* 1990 ibid. Fig. 1). In addition to one of the best examples of a jet, Ray *et al.* (1990) describe a spur like feature close to the star and this has been determined here to subtend an angle of approximately 35° w.r.t. the jet axis. It is clear therefore that both this star and LkHα 198 possess in addition to their jets poorly collimated components close to their source (henceforth these objects will be referred to as type II outflows). Moreover, if one also relaxes the

definition of poorly collimated optical outflows to include those from "high luminosity sources associated with poorly collimated shocked emission", it is also possible to include AFGL 2591 in this sample. Shocked molecular H_2 emission, is seen to cover a wide range of opening angles with respect to this star (see Poetzel *et al.* 1992 ibid Fig. 6). Justification for broadening the definition is to be found for example, from the studies presented here on the poorly collimated outflow to the east of Cep A. One recalls that the shocked H_2 emission provided a near continuation of the optical emission "loop" closer to the source (see also Fig. 3.6). Unfortunately, such 2.1μm observations are only available for a few of these objects at present. Nevertheless, from the total sample of twelve high luminosity sources, over half possess poorly collimated shocked emission.

It is also worth considering two other YSOs namely, L1551–IRS5 and SVS 13. Some similarities can be drawn between the HH emission east of Cep A (see Chapter 2) and that of L1551 IRS 5. A faint parabolic cavity was detected to the southwest of L1551 IRS 5 and this was seen to contain a large number of HH emission knots (Strom *et al.* 1986 and Stocke *et al.* 1988). Recent observations by Graham and Heyer (1990), in which a difference image has been produced from their direct imaging in Hα and continuum filters, reveals that this cavity is almost entirely filled with shocked emission, and that the envelope of this emission has the shape of a partial ellipse i.e. a type I outflow. The second source SVS 13 was brought to my attention by Dr. Mundt and a [SII] image of this and its well–known optical outflow HH 7–11 is presented in Fig. 5.1(a). Based on the observations supplied by Dr. Mundt, a [SII]–r_n difference image has been produced here and is displayed at high contrast in Fig. 5.1 (b). Of great interest, is that HH 7–11 appears in fact to be the brightest part of an extended ellipse of poorly collimated HH emission (i.e. again a type I outflow). In addition a counterflow[1] can be observed towards the northwest, which is also poorly collimated and is comprised of several condensations reminiscent perhaps of GGD 37 (see Chapter 3).

The bolometric luminosity of SVS 13 was calculated by Cohen and Schwartz (1987) to be 115 $L_\odot$ and recently Eislöffel *et al.* (1991) has found that this star is highly variable. Eislöffel *et al.* (1991) detected an increase in its visual magnitude by about 2.5 mag

[1]This counterflow will be discussed at length in a forthcoming paper by Eislöffel *et al.* (1993).

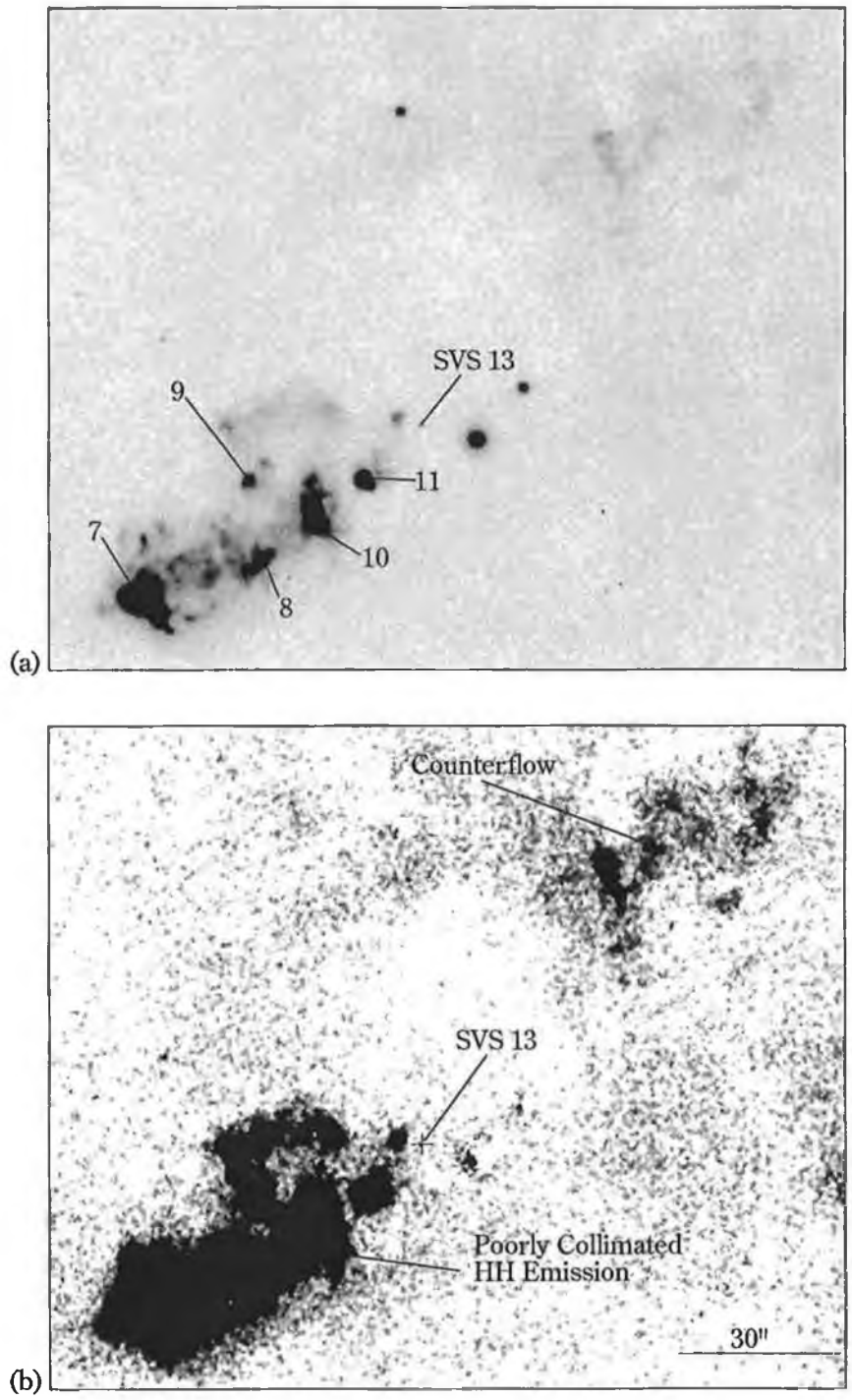

Figure 5.1: (a) A [SII] image of the well known optical outflow HH 7–11, with the individual HH objects and the source SVS 13 marked. (b) A [SII]–r_n difference image at high contrast of the same region as in (a). Note that HH 7–11 is only the brightest part of an ellipse of poorly collimated HH emission, and that a counterflow which is also poorly collimated can be seen to the northeast of SVS 13.

(from December 1988 to September 1990), and suggest the star is an example of what is termed an EXor, named after the original star to exhibit such a property EX Lupi (see Herbig 1989). As such, the quoted luminosity of $115\,L_{\odot}$ which was calculated in the star's quiescent period, should be regarded as a lower limit. Thus, one can include the SVS 13/HH7–11 outflow within the sample of optical outflows associated with high luminosity sources. Indeed, one notes that its luminosity is comparable to V380 Ori (see above).

As regards L1551–IRS5, which also possesses a "type I" outflow, its inclusion as a high luminosity source may at first appear questionable: Cohen and Schwartz (1987) have calculated its bolometric luminosity as $36\,L_{\odot}$. One notes however, that like ZCMa, L1551–IRS5 is probably an FU Orionis type star (see Mundt *et al.* 1985, Stocke *et al.* 1988). Such stars are known to undergo significant increases in the visual magnitude of 5–6 mag in $\leq$ 1yr, possibly every 10^3 years (see Hartmann and Kenyon 1985, Herbig 1989). It is possible therefore that the present low luminosity of L1551–IRS5 is due to a quiescent period. If it is not, then it is one of the relatively few low luminosity sources known to be associated with a poorly collimated optical outflow. Another example, may be HH 147 which was discovered here (see Chapter 2), and the source of which, N^3K50, has a bolometric luminosity of $30\,L_{\odot}$ (Strom *et al.* 1989). In general however, inspection of existing HH outflow catalogues (see e.g. Strom *et al.* 1986, Mundt *et al.* 1987, Reipurth 1989), reveals that almost all optical outflows from low luminosity sources are well collimated, and that the number of "type I" outflows are negligible.

Thus, although the sample is still statistically small, it appears that over half (7/13) of the optical outflows (including SVS 13 and L1551–IRS5), are poorly collimated. One can then remark, that *it is becoming increasingly more apparent that poorly collimated optical outflows are more frequently observed for intermediate/high luminosity YSOs than for their lower luminosity counterparts.*

One now asks, what determines the type of optical outflow produced by an intermediate/high luminosity YSO? Although the answer is still unclear, one might expect there to be two dominant factors, namely variability of the source and the presence of a poorly collimated wind. Consider the variability of the source. Certainly, this has been invoked

to explain not only the HH objects nearest V380 Ori and the emission line "loop" (see §2.5.3), but also HH 7 for SVS 13 (e.g. Hartigan *et al.* 1989), and numerous HH objects about L1551–IRS5, including HH 28 and HH 29 (Stocke *et al.* 1988). In this respect, it is also noteworthy that both L1551–IRS5 and SVS 13 are examples of highly variable YSOs, namely FU Orionis and EXor type stars. For both, the increase in luminosity has been attributed to changes in mass accretion through a circumstellar disk (see Hartmann and Kenyon 1985 and Eislöffel *et al.* 1991). Furthermore, the sudden release of energy from this change is thought to be a possible source of the optical outflows, not only from FU Orionis type stars but also CTTSs (see Reipurth 1989 for a discussion). At present however, one can only speculate to whether such a release in energy is responsible for poorly collimated HH emission. Moreover, even if energetic outbursts are responsible, why are some optical outflows poorly collimated (e.g. V380 Ori) and others highly collimated (e.g. LkHα 234) ? These questions are as yet unanswered but the most likely explanation is the presence of a poorly collimated wind component.

It is now well known that SVS 13, drives a poorly collimated atomic wind, with velocities up to 170 km s^{-1}, which decrease with either distance from the source, or with changing angle from the outflow axis (Lizano *et al.* 1988). Thus HH 8, HH 10 (see above) and indeed, the distribution of shocked emission seen in the blueshifted lobe to the southeast of SVS 13 (see Fig. 5.1) are explained. It is also noteworthy that the Lizano *et al.* (1988) have detected a possible atomic wind emanating from L1551–IRS5, which was invoked by Stocke *et al.* (1988) to drive drive such objects as HH 28 and HH 29. Furthermore, as suggested by Stocke *et al.* (1988), the interaction of this poorly collimated wind with a higher velocity and more tightly collimated component, would also explain the jet seen to emanate from L1551–IRS5. Thus, poorly collimated HH emission and the presence of jets seem to find a natural explanation in a two component wind. However, both the highly collimated and poorly collimated components are clumpy in some sense: HH knots are seen in both (e.g. Cep A, LkHα 234, V380 Ori). Ultimately, both components must have inhomogeneities in velocity and density which may require the presence of an intermittent flow. Obviously, radio observations of HI for the outflows of other higher luminosity sources, are required to support the hypothesis given here, that a two component wind is also applicable to them.

One important question remains, why does one apparently see more poorly collimated HH emission from higher luminosity sources. To answer this, one recalls that the jet mass loss rate scales with the stellar bolometric luminosity over several decades ($L_{BOL}^{-0.6}$) (Edwards *et al.* 1993). One might intuitively expect the poorly collimated wind component to do likewise, as is indicated by the momentum required to drive the associated molecular outflows (Levreault 1988).

As such, one would be more likely to see the interaction of this wind with the cavity walls, through shocks *that are optically visible* for high rather than low luminosity sources. That it is not seen in all cases probably reflects conditions in the surrounding environment. By the same token, one might also expect to see poorly collimated emission for low luminosity sources by using a lower shock velocity tracer such as H_2. As yet however, extensive H_2 imaging and spectroscopic studies *do not* exist for either low or high luminosity sources, but this must be addressed in the future.

Finally, one considers the observation that the brightest HH objects always appear to occur along the edges of the cavity structure i.e. HH 35 (V380 Ori), HH–NE, HH–NE2 (Cep A), HH 8, HH 10 (SVS 13), HH 28, HH 29 (L1551–IRS5) and HH 147B (N^3K50). Since many of these objects can be interpreted as bow shocks, it seems unlikely that this results from an optical edge effect as seen for e.g. in planetary nebulae. Could it be that they may be confined within a plane? This suggests perhaps oddly that the "loop" structures to which they belong may be exactly that!

Acknowledgments

The layout of the acknowledgments is as follows, after reviewing those people who have most helped me, I will concentrate on those friends who have bought the most beer and told the best jokes, but seriously! It has been both my pleasure and my good fortune to work under the continual guidance of Tom Ray. Without his help, patience, and quick thinking, particularly on a sailing trip that will never be forgotten, this thesis could not have been completed. Thank you Tom! Thanks are also due to Danny Heffernan, without whom I would not have found this position in the first place and to Reinhard Mundt for his continual interest and his helpful discussions on Cepheus A. I would also like to acknowledge Alan Moorehouse, who arrived in Ireland as a lonely astronomer became a good friend, answered thousands of my questions and left as a family. I'd like to think I had a part in that, if only because I wasn't there one Saturday night. I also cannot fail to mention a lunatic of a chinese man, Wai Ming Tai. On occasion he has at my request, not only arrived in the middle of the night to fix the computer system (while I pulled out my hair), but he has always lent a listening ear.

I am extremely grateful to the Governing Board of the Institute for funding this thesis, in particular Luke Drury. I would like to acknowledge everybody at the Institute, not only for their help but their friendship over the four years. I apologize if I don't mention everyone's name, but instead single out those who deserve particular attention. I would like to mention Eimhear Clifton, who re-typed a substantial amount of the text after a computer failure and I cannot but acknowledge Susan and Geraldine, who allowed me a place to smoke and listened to the occasional ravings of a tired student. Special thanks are also due to Ivan O' Brien for his help in the preparation of the figures, and to both Ivan and Myles Corcoran, for their perpetual good humour and scientific consultations.

As to friends that have remained good friends even though they have seen little of me during the past year, I would like to acknowledge, Brian Finnegan, Marcus Davey, and Fintan Moore (they'll be seeing too much of me too soon!). Finally, I owe so very much to my family, they have been a constant source of strength over the past four years. During these years I have not only completed a thesis but seen both my brothers

get married. I cannot forget them nor my sister for the breaks, not to mention the occasional backhanders of money and food. In particular, I have to mention three very special people, my Mam, my Dad and Goretti, their support, their kindness and of course *the prayers* have seen me through to the end and I dedicate this thesis to them (patience is definitely their virtue!).

References

Allen, D.A., Burton, M.G.: 1993, *Nature* **363**, 54

Adams, F.C., Lada, C.J., Shu, F.H.: 1987, *Astrophys. J.* **312**, 788

Appenzeller, I ., Reitermann, A ., Stahl, O.: 1988, *Publ. Astr. Soc. Pacific* **100**, 815

Appenzeller, I., Jankovics, I., Jetter, R.: 1986, *Astron. Astrophys. Suppl. Ser.* **64**, 65

Appenzeller, I., Mundt, R.: 1989, *Astron. Astrophys. Rev.* **1**, 291

Axon, D.J., Taylor, K.: 1984, *Mon. Not. R. astr. Soc.* **207**, 241

Bachiller, R., Gómez-González, J.: 1992, *Astron. Astrophys. Rev.* **3**, 257

Bally, J., Lada, C.: 1983, *Astrophys. J.* **265**, 824

Bally, J., Lane, A.P.: 1982, *Astrophys. J.* **257**, 612

Bally, J., Langer, W.D., Stark, A.A., Wilson, R.W.: 1987, *Astrophys. J. (Lett.)* **312**, L45

Barral, J.F., Cantó, J.: 1981, *Rev. Mex. Astron. Astrof.* **5**, 101

Basri, G., Bertout, C.: 1989, *Astrophys. J.* **341**, 340

Basri, G., Bertout, C.: 1993, in *Protostars and Planets III*, eds. E. Levy and J. Lunine (University of Arizona Press), p. 543

Bastien, P.: 1987, *Astrophys. J.* **317**, 231

Bastien, P., Ménard, F.: 1988, *Astrophys. J.* **326**, 334

Bastien, P., Ménard, F., Asselin, L., Turbide, L.: 1988, in *Modelling the Stellar Environment: How and Why ?*, eds. Delache, P., Laloe, S., Magnan, C., Tran Thanh Van,

J., (Editions Frontières, Paris), p.185

Beckwith, S.V.W., Sargent, A.J., Chini, R.S., Güsten, R.: 1990, *Astron. J.* **99**, 924

Beichman, C.A., Becklin, E.E., Wynn-Williams, C.G.: 1979, *Astrophys. J. (Lett.)* **232**, L47

Berrilli, F., Corciulo, G., Ingresso, G., Lorenzetti, D., Nisini, B., Strafella, F.: 1992, *Astrophys. J.* **398**, 254

Bertout, C.: 1989, *Ann. Rev. Astron. Astrophys.* **27**, 351

Bertout, C., Basri, G., Bouvier, J.: 1988, *Astrophys. J.* **330**, 350

Blandford, R., Rees, M.J.: 1974, *Mon. Not. R. astr. Soc.* **169**, 395

Blondin, J.M., Fryxell, B.A., Königl, A.: 1990, *Astrophys. J.* **360**, 370

Blondin, J.M., Königl, A., Fryxell, B.A.: 1989, *Astrophys. J. (Lett.)* **337**, L37

Brück, M.T.: 1974, *Mon. Not. R. astr. Soc.* **166**, 123

Brügel, E.W., Mundt, R., Bührke, T.: 1984, *Astrophys. J. (Lett.)* **287**, L73

Bührke, T., Mundt, R., Ray, T.: 1988, *Astron. Astrophys.* **200**, 99

Cabrit, S.: 1989, in Proceedings of the ESO Workshop on*Low Mass Star Formation and Pre-Main Sequence Objects*, ed. B. Reipurth, (ESO, Garching) p.119

Cabrit, S., Edwards, S., Strom, S.E., Strom, K.M.: 1990, *Astrophys. J.* **354**, 687

Cantó. J.: 1980, *Astron. Astrophys.* **86**, 327

Cantó, J., Rodríguez, L.F., Calvet, N., Levreault, R.M.: 1984, *Astrophys. J.* **282**, 631

Cantó, J. Tenorio-Tagle, G., Różyczka, M.: 1988, *Astron. Astrophys.* **192**, 287

Catala, C.: 1989, in Proceedings of the ESO Workshop on *Low Mass Star Formation and Pre-Main Sequence Objects*, ed. B. Reipurth, (ESO Garching) p.471

Catala, C., Czarny, J., Felenbok, P., Talavera, A., Thé, P.S.: 1991, *Astron. Astrophys.* **244**, 166

Catala, C., Kunasz, P.B., Praderie, F.: 1984, *Astron. Astrophys.* **134**, 402

Catala, C., Kunasz, P.B.: 1987, *Astron. Astrophys.* **174**, 158

Catala, C., Simon, T., Praderie, F., Talavera, A., Thé, P.S., Tjin A. Djie, H.R.E.: 1989, *Astron. Astrophys.* **221**, 273

Chavrria-K.C.: 1985, *Astron. Astrophys.* **148**, 317

Cohen, M.: 1973, *Mon. Not. R. astr. Soc.* **161**, 105

Cohen, M.: 1975, *Mon. Not. R. astr. Soc.* **173**, 279

Cohen, M.: 1980, *Mon. Not. R. astr. Soc.* **191**, 499

Cohen, M., Emerson, J.P., Beichman, C.A.: 1989, *Astrophys. J.* **339**, 455

Cohen, M., Kuhi, L.V.: 1979, *Astrophys. J. Suppl.* **41**, 743

Cohen, M., Schwartz, R.D.: 1979, *Astrophys. J. (Lett.)* **233**, L77

Cohen, M., Schwartz, R.D.: 1987, *Astrophys. J.* **316**, 311

Cohen, R.J., Rowland, P.R., Blair, M.M.: 1984, *Mon. Not. R. astr. Soc.* **210**, 425

Cohn, H.: 1983, *Astrophys. J.* **269**, 500

Collins, G.W., Sonneborn, G.H.: 1977, *Astrophys. J. Suppl.* **41**, 734

DeCampli, W.M.: 1981, *Astrophys. J.* **244**, 124

Dopita, M.A.: 1978, *Astron. Astrophys.* **63**, 237

Doyon, R., Nadeau, D.: 1988, *Astrophys. J.* **334**, 883

Edwards, S., Ray, T., Mundt, R.: 1993, in *Protostars and Planets III*, eds. E. Levy and J. Lunine University of Arizona Press, p. 567

Edwards, S., Snell, R.L.: 1983, *Astrophys. J.* **270**, 605

Edwards, S., Snell, R.L.: 1984, *Astrophys. J.* **281**, 237

Eichler, D.: 1982, *Astrophys. J.* **263**, 571

Eislöffel, J., Günther, G., Hessman, F.V., Mundt, R., Poetzel, R., Carr, J.S., Beckwith, S., Ray, T.P.: 1991, *Astrophys. J. (Lett.)* **383**, L19

Eislöffel, J. Mundt, R.: 1992, *Astron. Astrophys.* **263**, 292

Eislöffel, J. Mundt, R.: 1993, in preparation

Eislöffel, J *et al.*: 1993, in preparation

Evans II, N.J., Becklin, E.E., Beichman, C., Gatley, I., Hildebrand, R.H., Keene, J., Slovak, M.H., Werner, M.W., Whitcomb, S.E.: 1981, *Astrophys. J.* **244**, 115

Evans II, N.J., Levreault, R.M., Beckwith, S., Skrutskie, M.: 1987, *Astrophys. J.* **320**, 364

Falle, S.A.E.G., Innes, D.E., Wilson, M.J.: 1987, *Mon. Not. R. astr. Soc.* **225**, 741

Falle, S.A.E.G., Raga, A.C.: 1992, *Mon. Not. R. astr. Soc.*, in press

Finkenzeller, U.: 1985, *Astron. Astrophys.* **151**, 340

Finkenzeller, U., Jankovics, I.: 1984, *Astron. Astrophys. Suppl. Ser.* **57**, 285

Finkenzeller, U., Mundt, R.: 1984, *Astron. Astrophys. Suppl. Ser.* **55**, 109

Fuente, A., Martín-Pintado, J., Cernicharo, Brouillet, N., Duvert, G.: 1992, *Astron. Astrophys.* **260**, 341

Fuente, A., Martín-Pintado, J., Cernicharo, J., Bachiller, R.: 1990, *Astron. Astrophys.* **237**, 471

Fukui, Y.: 1989, in Proceedings of the ESO Workshop on *Low Mass Star Formation and Pre-Main Sequence Objects*, ed. B. Reipurth, (ESO Garching) p.95

Garmany, C.: 1973, *Astron. J.* **78**, 185

Garrison, L.: 1978, *Astrophys. J.* **224**, 535

Goodrich, R.W.: 1986, *Astrophys. J.* **311**, 882

Goodrich, R.W.: 1993, *Astrophys. J. Suppl.* **86**, 499

Graham, J.A., Heyer, M.H.: 1990, *Publ. Astr. Soc. Pacific* **102**, 972

Güdel, M., Benz, A.O., Catala, C., Praderie, F.: 1989, *Astron. Astrophys. (Lett.)* **217**, L9

Gyulbudaghian, A.L., Glushov, Yu.I., Denisyuk, E.K.: 1978, *Astrophys. J. (Lett.)* **224**, L137

Hamann, F., Persson, S.E.: 1989, *Astrophys. J.* **339**, 1078

Hamann, F., Persson, S.E.: 1992a, *Astrophys. J. Suppl.* **82**, 285 : **(HPa)**

Hamann, F., Persson, S.E.: 1992b, *Astrophys. J. Suppl.* **82**, 247 : **(HPb)**

Hamann, F., Persson, S.E.: 1992c, *Astrophys. J.* **394**, 628 : **(HPc)**

Haro, G.: 1952, *Astrophys. J.* **115**, 572

Hartigan, P.: 1989, *Astrophys. J.* **399**, 987

Hartigan, P., Curiel, S., Raymond, J.: 1989, *Astrophys. J. (Lett.)* **347**, L31

Hartigan, P., Lada, C.J.: 1985, *Astrophys. J. Suppl.* **59**, 383

Hartigan, P., Lada, C.J., Stocke, J., Tapia, S.: 1986, *Astron. J.* **92**, 1155

Hartigan, P. Raymond, J.C., Hartmann, L.: 1987, *Astrophys. J.* **316**, 323

Hartmann, L., Kenyon, S.J.: 1985, *Astrophys. J.* **299**, 462

Hartmann, L., Kenyon, S.J., Calvet, N.: 1993, *Astrophys. J.* **407**, 219

Hartmann, L., Kenyon, S.J., Hewett, R., Edwards, S., Strom, K.M., Strom, S.E., Stauffer, J.R.: 1989, *Astrophys. J.* **338**, 1001

Harvey, P.M., Thronson Jr, H. A., Gatley, I.: 1979, *Astrophys. J.* **231**, 115

Hayashi, C.: 1966, *Ann. Rev. Astron. Astrophys.* **4**, 171

Hayashi, S.S., Hasegawa, T., Kaifu, N.: 1988, *Astrophys. J.* **332**, 354

Herbig, G.: 1989, in Proceedings of the ESO Workshop on *Low Mass StarFormation and Pre-Main Sequence Objects*, ed. B. Reipurth, (ESO Garching) p.233

Herbig, G.H.: 1951, *Astrophys. J.* **113**, 697

Herbig, G.H.: 1960, *Astrophys. J. Suppl.* **4**, 337

Herbig, G.H.: 1960, *Astrophys. J. Suppl.* **44**, 369

Herbig, G.H.: 1974, *Lick Observatory Bulletin*, No. 658

Herbig, G.H.: 1990, *Astrophys. J.* **360**, 639

Herbig, G.H., Bell, K.R.: 1988, *Lick Observatory Bulletin*, No. 1111

Herbig, G.H., Jones, B.F.: 1981, *Astron. J.* **86**, 1232

Herbig, G.H., Jones, B.F.: 1983, *Astron. J.* **88**, 1040

Herbst, W., Miller, D.E., Warner, J.W., Herzog, A.: 1982, *Astron. J.* **87**, 98

Hillenbrand, L., Strom, S.E., Vrba, F., Keene, J.: 1992, *Astrophys. J.* **397**, 613 : **(HSVK)**

Ho, P.T.P., Moran, J.M., Rodríquez, L.F.: 1982, *Astrophys. J.* **262**, 619

Hu, J.Y., Thé, P.S. de Winter, D.: 1989, *Astron. Astrophys.* **208**, 213

Hughes, V.A.: 1982, *Astron. Astrophys.* **106**, 171

Hughes, V.A.: 1985, *Astrophys. J.* **298**, 830

Hughes, V.A.: 1988, *Astrophys. J.* **333**, 788

Hughes, V.A.: 1993, *Astron. J.* **105**, 331

Hughes, V.A., Wouterloot, J.G.A.: 1984, *Astrophys. J.* **276**, 204

Iben, I.: 1965, *Astrophys. J.* **141**, 993

Joyce, R.R., Simon, T.: 1986, *Astron. J.* **91**, 113

Kenyon, S.J., Hartmann, L.: 1987, *Astrophys. J.* **323**, 714

Königl, A.: 1982, *Astrophys. J.* **261**, 115

Königl, A., Ruden, S.P.: 1993, in *Protostars and Planets III*, eds. E. Levy and J. Lunine (University of Arizona Press), p. 641

Kuhi, L.V.: 1964, *Astrophys. J.* **140**, 1409

Lada, C.J., Blitz, L., Reid, M.J., Moran, J.M.: 1981, *Astrophys. J.* **243**, 769

Lago, M.T.V.T.: 1984, *Mon. Not. R. astr. Soc.* **210**, 323

Lane, A.: 1989, in Proceedings of the ESO Workshop on*Low Mass Star Formation and Pre-Main Sequence Objects*, ed. B. Reipurth, (ESO, Garching) p.331

Lane, A., Bally, J.: 1993, in preparation

Larson, R.B.: 1969, *Mon. Not. R. astr. Soc.* **145**, 271

Larson, R.B.: 1972, *Mon. Not. R. astr. Soc.* **157**, 121

Leinert, Ch., Haas, M., Lenzen, R.: 1991 *Astron. Astrophys.* **246**, 180 : **(LHL)**

Lenzen, R.: 1988, *Astron. Astrophys.* **190**, 269

Lenzen, R., Hodapp, K.-W., Solf, J.: 1984, *Astron. Astrophys.* **137**, 202

Levreault, R.M.: 1988, *Astrophys. J. Suppl.* **67**, 283

Lind, K.R., Payne, D.G., Meier, D.L., Blandford, R.D.: 1989, *Astrophys. J.* **344**, 89

Lynden-Bell, D., Pringle, J.E.: 1974, *Mon. Not. R. astr. Soc.* **168**, 603

Lizano, S., Heiles, C., Rodríguez, L.F., Koo, B.C., Shu, F., Hasegawa, T., Hayashi, S.S., Mirabel, I.F.: 1988, *Astrophys. J.* **328**, 763

Loren, R.B.: 1977, *Astrophys. J.* **218**, 716

Lorenzetti, D., Saraceno, P., Stratfella, F.: 1983, *Astrophys. J.* **264**, 554

Marcaide, J.M., Torrelles, J.M., Güsten, R., Menten, K.M., Ho, P.T.P., Moran, J.M., Rodríquez, L.F.: 1988, *Astron. Astrophys.* **197**, 235

Mereghetti, S., Garilli, B.: 1987, *Astron. J.* **94**, 1616

Moore, T.J.T., Chandler, C.J.: 1989, *Mon. Not. R. astr. Soc.* **241**, 19P

Morgan, J.A., Schloerb, F.P., Snell, R.L., Bally, J.: 1991, *Astrophys. J.* **376**, 618

Moriarty-Schieven, G.H., Snell, R.L., Hughes, V.A.: 1991 *Astrophys. J.* **374**, 169

Morse, J.A., Hartigan, P., Cecil, G., Raymond, J.C., Heathcote, S.: 1992, *Astrophys. J.* **399**, 231

Morwood, A.: 1990 in *ESO newsletter* **61**, 51

Mundt, R.: 1985, *Can. J. Phys.* **64**, 407

Mundt, R.: 1988, in *Formation and Evolution of Low Mass Stars*, eds. A.K. Dupree, M.T.V.T. Lago, (Dordrecht, Reidel), p.257

Mundt, R., Brugel, E.W., Bührke, T.: 1987, *Astrophys. J.* **319**, 275

Mundt, R., Bührke, T., Fried, J.W., Neckel, T., Sarcander, M., Stocke, J.: 1984, *Astron. Astrophys.* **140**, 17

Mundt, R., Fried, J.W.: 1983, *Astrophys. J. (Lett.)* **274**, L83

Mundt, R., Ray, T.P., Bührke, T.: 1988, *Astrophys. J. (Lett.)* **333**, L69

Mundt, R., Ray, T.P., Bürke, T., Raga, A., Solf, J.: 1990, *Astron. Astrophys.* **232**, 37

Mundt, R., Ray, T.P., Raga, A.C.: 1991, *Astron. Astrophys.* **252**, 740

Mundt, R., Stocke, J., Strom, S., Strom, K., Anderson, E.: 1985, *Astrophys. J. (Lett.)* **297**, L41

Myers, P.C., Fuller, G.A., Mathieu, R.D., Beichman, C.A., Benson, P.J.*et al.*: 1987, *Astrophys. J.* **319**, 340

Nakajima, T., Nagata, T., Nishida, M., Sato, S., Kawara, K.: 1986, *Mon. Not. R. astr. Soc.* **221**, 483

Nakano, M., Kogure, T., Yoshida, S., Tatematsu, K.: 1990, *Publ. Astron. Soc. Japan* **42**, 567

Natta, A., Palla, F., Butner, H.M., Evans II, N.J., Harvey, P.M.: 1992, *Astrophys. J.* **391**, 805

Natta, A., Palla, F., Butner, H.M., Evans II, N.J., Harvey, P.M.: 1993, *Astrophys. J.* **406**, 674 : **(NPBEH)**

Neckel, T., Staude, H.J.: 1990, *Reviews in Modern Astronomy* **3** 266

Neckel, T., Staude, H.J., Sarcander, M., Birkle, K.: 1987, *Astron. Astrophys.* **175**, 231

Norris, R.P.: 1980, *Mon. Not. R. astr. Soc.* **193**, 39P

Norman, C.A., Silk, J.: 1979, *Astrophys. J.* **228**, 197

Norman, M.L., Smarr, L., Winkler, K.-H., Smith, M.D.: 1982, *Astron. Astrophys.* **113**, 285

Norman, M., Winkler, K.H., Smarr, L.: 1984, in *Physics of Energy Transport in Extragalactic Radio Sources*, eds. A. Bridle, J. Eilek (NRAO Greenbank Workshop No.9), P.150

Ogura, K., Walsh, J.R.: 1991, *Astron. J.* **101**, 285

Palla, P., Stahler, S.W.: 1990, *Astrophys. J. (Lett.)* **360**, L47

Palla, P., Stahler, S.W.: 1991, *Astrophys. J.* **375**, 288

Palla, P., Stahler, S.W.: 1992, *Astrophys. J.* **392**, 667

Palla, P., Stahler, S.W.: 1993, *Astrophys. J.* in press

Payne, D.G., Cohn, H.: 1985 *Astrophys. J.* **291**, 655

Piirola, V., Scaltriti, F., Coyne, G.V.: 1992, *Nature* **359**, 399

Poetzel, R., Mundt, R., Ray, T.P.: 1989, *Astron. Astrophys. (Lett.)* **224**, L13

Poetzel, R., Mundt, R., Ray, T.P.: 1992, *Astron. Astrophys.* **262**, 229

Praderie, F., Simon, T., Catala, C., Bosegaard, A.M.: 1986, *Astrophys. J.* **303**, 311

Pravdo, S.H., Rodríquez, L.F., Curiel, S., Cantó, J., Torrelles, J.M., Becker, R.H., Sellgren, K.: 1985, *Astrophys. J. (Lett.)* **293**, L35

Pringle, J.E.: 1989 *Mon. Not. R. astr. Soc.* **236**, 107

Racine, R.: 1968, *Astron. J.* **73**, 233

Raga, A.C.: 1989, in Proceedings of the ESO Workshop on *Low Mass Star Formation and Pre-Main Sequence Objects*, ed. B. Reipurth, (ESO Garching) p.281

Raga, A.C., Böhm, K.H.: 1985, *Astrophys. J. Suppl.* **58**, 201

Raga, A.C., Böhm, K.H.: 1986, *Astrophys. J.* **308**, 829

Raga, A.C., Böhm, K.H.: 1987, *Astrophys. J.* **323**, 193

Raga, A.C., Cantó, J., Binette, L., Calvet, N.: 1990, *Astrophys. J.* **364**, 601

Raga, A.C., Mateo, M.: 1987, *Astron. J.* **94**, 684

Raga, A.C., Mundt, R., Ray, T.P.: 1991, *Astron. Astrophys.* **252**, 733

Ray, T.P.: 1981, *Mon. Not. R. astr. Soc.* **198**, 617

Ray, T.P.: 1987, *Astron. Astrophys.* **171**, 145

Ray, T.P.: 1993, in *Stellar Jets and Bipolar Outflows*: Proceedings of the 6^{th} International Workshop of the OAC, eds. L. Errico and A. Vittone (Dordrecht, Kluwer), in press

Ray, T.P., Mundt, R.: 1993, in *Astrophysical Jets*, Cambridge University Press, eds. M. Fall, C. O'Dea, M. Livio and D. Burgarella, in press

Ray, T.P., Poetzel, R., Mundt, R.: 1991, in *Molecular Clouds*, eds. R.A. James, T.J. Millar (Cambridge University Press), p. 145

Ray, T.P., Poetzel, R., Solf, J., Mundt, R.: 1990 *Astrophys. J. (Lett.)* **357**, L, 45

Raymond, J.C.: 1979, *Astrophys. J. Suppl.* **39**, 1

Raymond, J.C., Hartigan, P., Hartmann, L.:1988, *Astrophys. J.* **326**, 323

Reipurth, B.: 1985, *Astron. Astrophys. Suppl. Ser.* **61**, 319

Reipurth, B.: 1989a, *Astron. Astrophys.* **220**, 249

Reipurth, B.: 1989b, in Proceedings of the ESO Workshop on*Low Mass Star Formation and Pre-Main Sequence Objects*, ed. B. Reipurth, (ESO, Garching) p.247

Reipurth, B., Graham, J.A.: 1988, *Astron. Astrophys.* **202**, 219

Reipurth, B., Heathcote, M.R., Roth, M., Noriega-Crespo, A., Raga, A.C.: 1993, *Astrophys. J. (Lett.)* **408**, L49

Reipurth, B., Heathcote, S.: 1991, *Astron. Astrophys.* **246**, 511

Richardson, K.J., White, G.J., Avery, L.W., Woodsworth, A.W.: 1987, *Astron. Astrophys.* **174**, 197

Rodríguez, L.F., Cantó, J.: 1983, *Rev. Mex. Astron. Astrof.* **8**, 163

Rodríguez, L.F., Reipurth, B.: 1989, *Rev. Mex. Astron. Astrof.* **17**, 59

Rodríquez, L.F., Ho, P.T.P., Moran, J.M.: 1980, *Astrophys. J. (Lett.)* **240**, L149

Rodríquez, L.F., Ho, P.T.P., Torrelles, J.M., Curiel, S., Cantó, J.: 1990, *Astrophys. J.* **352**, 645

Rolph, C.D., Scarrott, S.M., Wolstencroft, R.D.: 1990, *Mon. Not. R. astr. Soc.* **242**, 109

Safier, P.N., Königl, A.: 1992, *Astrophys. J.*, submitted

Sargent, A.I.: 1977, *Astrophys. J.* **218**, 736

Sato, S., Nagata, T., Nakajima, T., Nishida, M., Tanaka, M., Yamashita, T.: 1985, *Astrophys. J.* **291**, 708

Schwartz, P.R., Buhl, D.: 1975, *Astrophys. J. (Lett.)* **201**, L27

Schwartz, R.D.: 1975, *Astrophys. J.* **195**, 631

Schwartz, R.D.: 1978, *Astrophys. J.* **223**, 884

Schwartz, R.D.: 1983, *Ann. Rev. Astron. Astrophys.* **21**, 209

Shevchenko, V.S., Yakubov, S.D.: 1989, *Sov. Astron.* **33**, 370

Skinner, S.L., Brown, A., Stewart, R.T.: 1993, *Astrophys. J. Suppl.*, submitted

Smith, M.: 1991, *Mon. Not. R. astr. Soc.* **253**, 175

Smith, M.D.: 1986, *Mon. Not. R. astr. Soc.* **223**, 57

Solf, J., Böhm, K.H.: 1991, *Astrophys. J.* ,, 375 618

Solf, J., Raga, A.C., Böhm, K.H., Noriega-Crespo, A.: 1991, *Astron. J.* **102**, 1147

Stahler, S.W., Shu, F.H., Taam, R.E.: 1980, *Astrophys. J.* **241**, 637

Stahler, S.W., Walter, F.M.: 1993, in *Protostars and Planets III*, eds. E. Levy and J. Lunine (University of Arizona Press), p. 405

Staley, S.B., Kastner, J.H., Weintraub, D.A.: 1992, *Bull. Amer. Astron. Soc.* **24**, 1141

Stocke, J.T., Hartigan, P.M., Strom, S.E., Strom, K.M., Anderson, E.R., Hartmann, L.W., Kenyon, S.J.: 1988, *Astrophys. J. Suppl.* **68**, 229

Strom, K., Strom, S., Wolff, S., Morgan, J., Wenz, M.: 1986, *Astrophys. J. Suppl.* **62**, 39

Strom, K.M, Newton, G., Strom, S.E., Seaman, R.L., Carrasco, L., Cruz-Gonzalez, I., Serrano, A., Grasdalen, G.: 1989, *Astrophys. J. Suppl.* **71**, 183

Strom, K.M., Strom, S.E., Wolff, S.C., Morgan, J., Wenz, M.: 1986, *Astrophys. J. Suppl.* **62**, 39

Strom, S.E., Strom, K.M., Grasdalen, G.L., Sellgren, K., Wolff, S., Morgan, J., Stocke, J., Mundt, R.: 1985, *Astron. J.* **90**, 2281

Strom, S.E., Strom, K.M., Yost, J., Carrasco, L., Grasdalen, G.: 1972, *Astrophys. J.* **173**, 353

Torbett, M.V.: 1984, *Astrophys. J.* **278**, 318

Torrelles, J.M., Cantó, J., Rodríquez, L.F., Ho, P.T.P., Moran. J.M.: 1985, *Astrophys. J. (Lett.)* **294**, L117

Uchida, Y., Schibata, K.: 1985, *Publ. Astron. Soc. Japan* **37**, 515

Von Hippel, T.,Bell Burnell, S.J., Williams, P.M.: 1988, *Astron. Astrophys. Suppl. Ser.* **74**, 431

Warren-Smith, R.F.: 1983, *Mon. Not. R. astr. Soc.* **205**, 349

Warren-Smith, R.F., Scarrot, S.M., King, D.J., Taylor, K.N.R., Bingham, R.G., Murdin, P.: 1980, *Mon. Not. R. astr. Soc.* **192**, 339

Weliachew, L., Emerson, D.T., Forveille, T., Bieging, J.H., Wright, M.C.H., Ellder, J.: 1985, *Astron. Astrophys.* **153**, 139

Wouterloot, J.G.A., Brand, J.: 1992, *Astron. Astrophys.* **265**, 144

Zou, H.: 1989, Ph.D. Thesis, University of Heidelberg